Ph.D. Dissertation

Development of Drug Customized Polymeric Carriers for Improved Therapeutic Efficiency

Mohamed Mahmoud Ahmed Abdelghafour

Supervisor:

Dr. László Janovák

Assistant Professor

DOCTORAL SCHOOL OF CHEMISTRY

University of Szeged
Faculty of Science and Informatics
Department of Physical Chemistry and Materials Science

Szeged
2023

Table of Contents

List of abbreviations

Abbreviation	Definition
^{1}H-NMR	Proton nuclear magnetic resonance Spectroscopy
GPC	Gel permeation chromatography
FTIR	Fourier transform infrared spectroscopy
GC	Gas chromatography
DLS	Dynamic light scattering
NPs	Nanoparticles
PBS	Phosphate-buffered saline (pH = 7.4 and 0.9 wt% NaCl content)
SEM	Scanning electron microscopy
TEM	Transmission electron microscopy
TGA	Thermogravimetric analysis
DSC	Differential scanning calorimetry
UV-VIS	Ultraviolet-visible spectroscopy
EDS	Energy dispersive spectroscopy
XRD	X-ray diffraction
DDS	Drug delivery system
SA	Succinic anhydride
PVA	Polyvinyl alcohol
CYS	Cysteamine
MMC	Mitomycin C
PVA-SA	Succinated PVA
PVA-SA-CYS	Conjugated particles of succinated PVA with cysteamine
PVA-SA-CYS-MMC	Polymeric prodrug of Mitomycin C
PVA-CHO	Aldehyde (4-Formylbenzoate) modified PVA
CHIT	Chitosan
CHIT-SH	Thiolated (3-Mercaptopropinate) chitosan
PVA-CHO/CHIT-SH	Crosslinking hydrogel between PVA-CHO and CHIT-SH
PES	Poly(ethylene succinate)
PBSu	Poly(butylene succinate)
M_n	Number average molecular weight
M_w	Weight average molecular weight
NIMO	Nimodipine

NIMO-loaded PES	Encapsulation of NIMO into PES
Θ	Contact angle (°)
Φ	Volume fraction
MRSA	Methicillin-resistant *Staphylococcus aureus* bacterial strains
MRC-5	Human embryonic lung fibroblasts cells
Hep-2c	Human carcinoma cells
RI detector	Refractive index detector
IC_{50}	The half-maximal inhibitory concentration (mg/L)
$[\eta]$	Intrinsic viscosity (mL/g)
G'	Storage modulus (Pa)
G"	Loss modulus (Pa)
G*	Complex modulus (Pa)
EE%	Drug encapsulation efficiency (%)
NTU	Nephelometric Turbidity unit
ζ	zeta potential (mV)
DS%	Degree of substitution (%)
DMSO	Dimethyl sulfoxide
THF	Tetrahydrofuran
DMF	Dimethylformamide
MTT	3-(4,5-dimethylthiazol-2-yl)-2,5-diphenyltetrazolium bromide
$\bar{X}_n$	Degree of polymerization (%)
δ	Chemical shift
P%	Conversion percent of monomers
OD	Optical density
hrs	Hours
MEC	Minimum effective concentration
MTD	Minimum toxic concentration
RES	Reticuloendothelial system
EPR	Enhanced permeability and retention effect
BMP	Bone morphogenetic protein
KMH	Kuhn-Mark-Houwink

List of Figures and Tables

1. Introduction

The low bioavailability and unpredictable plasma drug levels of conventional drug delivery methods (e.g., tablets, capsules, syrups, ointments, etc.) prevent them from achieving sustained release and the desired therapeutic effects. The entire therapy procedure may be ineffective without a reliable delivery system. To achieve optimal efficacy and safety, the drug must also be administered at a precise regulated rate and at the target site. Problems with traditional drug delivery are addressed by the development of controlled drug delivery systems. Over the past two decades, controlled drug delivery systems have seen significant evolution, moving from large-scale to the nanoscale to intelligent targeted. The hydrophobic structure of many effective drugs (e.g., Nimodipine, a Ca^{+2} channel blocker) makes them difficult to solubilize in a physiological medium, making it challenging to generate a suitable pharmaceutical form for drug administration utilizing traditional delivery approaches. Additionally, hydrophilic drugs (e.g., Mitomycin C, as an anticancer agent, and Tilorone dihydrochloride, as an anti-muscular atrophy agent) require frequent administration due to their high rate of excretion from the human body. To address these and other obstacles, innovative, polymer-based drug delivery systems for more convenient, controlled, and targeted distribution have been developed.

Polymeric drug delivery is a rapidly growing field of research that has the potential to revolutionize the way drugs are administered to patients. This technology involves the use of polymers to encapsulate and deliver drugs to target sites in the body, protecting them from the body's immune system and allowing them to be more effectively absorbed into the bloodstream. Polymers are versatile materials that can be tailored to meet specific drug delivery requirements, such as controlled release, targeted delivery, and sustained release. Polymeric drug delivery systems have many advantages over traditional drug delivery methods, including improved bioavailability, increased stability, and reduced toxicity. Additionally, they can be used to target specific areas of the body, allowing for more precise delivery of drugs. This can result in improved efficacy and fewer side effects.

In this dissertation, we will explore the potential of polymers for drug delivery applications, focusing on their design, synthesis, and characterization. We also will design novel types of polymer-based controlled drug delivery systems for the three applied drugs (Mitomycin C, Tilorone dihydrochloride, and Nimodipine). We will discuss the advantages and limitations of prepared polymer-based drug delivery systems, and evaluate their potential for improving drug efficacy and patient compliance.

2. Literature Background

2.1. Polymers

Polymers are a type of material that has become increasingly popular in recent years due to their versatility and durability. Polymers are made up of long chains of molecules that are linked together, forming a strong and flexible material. They can be used in a variety of applications, ranging from medical devices to consumer products [1–5]. Polymers are extremely versatile and can be used to create a wide range of products. For example, polymers are used to create medical devices such as prosthetics, implants, and artificial organs [5–7]. They are also used to create consumer products such as packaging, automotive parts, and sporting goods [8–10]. Polymers are also used in the construction industry, where they are used to create strong and durable building materials [11]. Polymers are also incredibly durable and can withstand a wide range of temperatures and environmental conditions. This makes them ideal for use in a variety of applications, from medical devices to consumer products. Polymers are also resistant to corrosion, making them ideal for use in outdoor applications [12]. Polymers are also incredibly lightweight, making them ideal for use in products that require a lightweight material. This makes them ideal for use in products such as aircraft and spacecraft [13,14]. Polymers are also incredibly strong, making them ideal for use in products that require a strong material [15]. Polymers are also incredibly cost-effective and easy to work with, making them ideal for use in a variety of applications as shown in **Figure 1**. Overall, polymers are an incredibly versatile and durable material that can be used in a variety of applications. They are incredibly strong, lightweight, easy to work with, and cost-effective. Thus, they are suitable for a wide range of applications.

Based on the source of availability (origin), polymers are classified into three categories: natural polymers, synthetic polymers, and semi-synthetic polymers. Natural polymers are large molecules composed of repeating structural units connected by covalent chemical bonds. They are found in all living organisms and are essential for life. Natural polymers are the building blocks of life, providing structure and function to cells, tissues, and organs. Examples of natural polymers include proteins, carbohydrates, nucleic acids, and lipids [16,17]. Proteins are the most abundant and diverse type of natural polymer. They are composed of amino acids and are responsible for many essential functions in the body, such as catalyzing biochemical reactions, transporting molecules, and providing structural support [18]. Proteins are also involved in the regulation of gene expression and the formation of antibodies [18]. Carbohydrates are the

second most abundant type of natural polymer. They are composed of monosaccharides and are the main source of energy for the body. Carbohydrates are also important for the formation of cell walls, the storage of energy, and the synthesis of other molecules [19]. Nucleic acids are the third type of natural polymer. They are composed of nucleotides and are responsible for the storage and transmission of genetic information [20]. Nucleic acids are also involved in the regulation of gene expression and the formation of proteins [20]. Finally, lipids are the fourth type of natural polymer. They are composed of fatty acids and are important for the formation of cell membranes, the storage of energy, and the synthesis of hormones [21]. Lipids are also involved in the regulation of gene expression and the formation of proteins [21]. Natural polymers are essential for life and are involved in many essential functions. They provide structure and function to cells, tissues, and organs, and are involved in the regulation of gene expression and the formation of proteins. Without natural polymers, life as we know it would not exist.

Figure 1. Applications of polymers

Synthetic polymers are a type of material that is created through chemical synthesis [17]. Synthetic polymers are used in a variety of applications, ranging from medical and industrial to consumer products [1,3,22]. Synthetic polymers are made up of long chains of molecules called monomers. These monomers are linked together to form a polymer chain. Synthetic polymers have many advantages over natural polymers. They are more durable and resistant to environmental factors such as heat, light, and chemicals. They are also more cost-effective and easier to manufacture. Synthetic polymers can also be tailored to meet specific needs, such as

being able to withstand extreme temperatures or being able to resist certain chemicals [23]. Synthetic polymers are used in a variety of products, such as packaging materials, medical devices, and automotive parts [9,10,24,25]. They are also used in the production of synthetic fabrics, such as nylon and polyester. Synthetic polymers are also used in the production of plastics, adhesives, and coatings. Synthetic polymers have a variety of benefits, but they also have some drawbacks. They are not biodegradable and can be difficult to recycle. They can also be toxic if not handled properly. Additionally, synthetic polymers can be expensive to produce and are not always as durable as natural polymers [23]. Despite their drawbacks, synthetic polymers are an important part of modern society. They are used in a variety of applications and can be tailored to meet specific needs. They are also cost-effective and easier to manufacture than natural polymers. Synthetic polymers are an important part of our everyday lives and will continue to be used in many different ways.

Natural polymers that have undergone chemical modification, like cellulose and vulcanized rubber, make up the majority of semi-synthetic polymers. The two primary classes of cellulose derivatives are cellulose ethers and cellulose esters, which have various physicochemical and mechanical characteristics. The derivatives of cellulose exhibit qualities including surface activity, viscosity in solution, stability against heat, biodegradation, oxidation, and hydrolysis. The cellulose ethers such as sodium carboxymethyl cellulose, carboxymethyl cellulose, methylcellulose, hydroxyethyl cellulose, and ethyl cellulose are water-soluble polymers, whereas water-insoluble cellulose esters include hydroxypropyl methylcellulose phthalate, cellulose acetate phthalate, and cellulose acetate polymers with good film-forming properties [26]. In cosmetic products such as shampoos, creams, gels, and lotions, these polymers are extensively utilized as bioadhesives, gelling agents, thickening, and stabilizing agents. Also, semisynthetic polymers have been used for drug delivery applications [26]. Compared to natural gelling agents including gelatin, sodium alginate, pectin, agar, and starch, they are less susceptible to microbial contamination [27].

2.2. Polymers in drug delivery

Due to the drawbacks of traditional drugs, the topic of drug delivery systems has recently attracted more interest. For instance, clinicians may decide to reduce the dosage given, postpone treatment, or even stop the chemotherapy program due to the harmful side effects of anticancer medications on healthy tissues. Drugs that are widely absorbed by the body may have an adverse impact on healthy organs, which might have dose-limiting adverse effects (for example, heart toxicity of doxorubicin). Also, low drug concentrations in the target tissues result in

subpar therapeutic effects that need to be administered more frequently [28–30]. The hydrophobic structure of many effective drugs makes them difficult to solubilize in a physiological medium, making it challenging to generate a suitable pharmaceutical form for drug administration utilizing traditional delivery approaches [29]. Additionally, hydrophilic drugs require frequent administration due to their high rate of excretion from the human body. To address these and other obstacles, innovative drug delivery systems for more convenient, controlled, and targeted distribution have been developed.

The drug delivery systems could be materials or devices that are internal or exterior that assist a patient take their medications. Drug delivery systems that are administered internally, may be made of a wide range of substances that have been functionalized with medicines, including polymers, metalloids, and lipids [28,29,31]. These systems have the following benefits: (1) improving the soluble properties of poorly water-soluble drugs, (2) prolonging drug release at a minimal systemic quantity, or directing drug delivery to the appropriate cells to reduce the undesirable side effects of drugs that are administered, (3) enhancing the bioavailability of drugs and bioactive agents via protecting them from various mechanisms of inactivation and degradation within the human body, (4) enhancing pharmaceutical effectiveness and lowering the dosage of the drug for specific therapeutic benefits to minimize the cost of therapy, (5) enhancing patient compliance by decreasing administration frequency and the likelihood that dosage would be missed or administered incorrectly [28–31]. From the business side, many pharmaceutical companies recognize the benefits that new drug delivery technologies bring to enhance the value of their current products. They are implementing these technologies to reformulate their off-patent drugs in order to compete with generic versions of those drugs. Substantial pharmaceutical companies have also abandoned a large number of potentially useful medicinal medicines due to extreme toxicity during preclinical or clinical testing. With the use of innovative drug delivery techniques, it may be possible to reformulate these medications and recoup the enormous sums that were expended on their creation and research.

Drug formulations, such as tablets, capsules, ointments, or solutions, are referred to as a "drug delivery system". When a formulation includes a technology built in to manage the drug release kinetics over time, it is referred to as having a "controlled release drug delivery system" or a "controlled drug delivery system". Unlike traditional formulations, which release the majority or the entirety of the loaded drug(s) instantly and uncontrolled, controlled-release drug delivery methods allow for regulated drug release. Therefore, "immediate release" formulations are the common names for traditional formulations. The main goal of a controlled delivery system is

to release drugs at the intended anatomical region and to keep drug concentrations within a therapeutic range for the desired duration of time (**Figure 2**). Ineffective therapy or toxicity comes from drug concentrations that are below the minimum effective concentration (MEC) or over the minimum toxic concentration (MTD), respectively. For the purpose of successful disease treatment, a prolonged release mechanism could keep the therapeutic dosage constant over extended periods, reducing the potential of underexposure as well as the toxicity associated with overexposure.

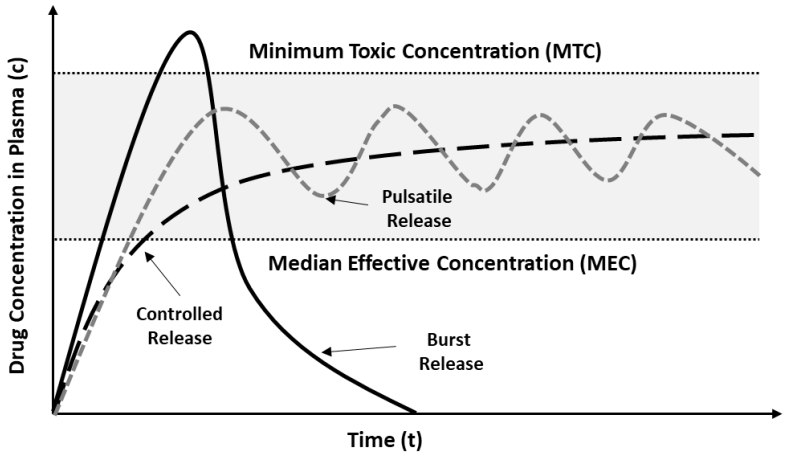

Figure 2. Therapeutic band illustrating the effects of controlled, pulsatile, and burst releases concerning effective and toxic concentrations [32].

The use of polymers-based drug delivery systems has become increasingly important in the pharmaceutical industry for a long time due to their ability to improve drug efficacy, reduce side effects, and increase patient compliance [32]. Polymers are versatile materials that can be tailored to meet specific drug delivery requirements, such as controlled release, targeted delivery, and sustained release. This has enabled the development of novel drug delivery systems that can improve the therapeutic efficacy of drugs, reduce their toxicity, and increase patient compliance. Practically, polymers are often utilized in all popular dosage forms, such as tablets, capsules, films, semi-solids, gels, suspensions, and transdermal patches. They are also frequently used in specialty delivery methods, such as long-acting injections and biodegradable implants [33]. The use of polymers in drug delivery systems can be divided into two main categories: non-degradable and degradable polymers. Non-degradable polymer systems are composed of polymers that remain intact in the body and slowly release drugs over a long time. These systems are typically used for sustained-release formulations, such as those used to treat chronic diseases. Degradable polymers, on the other hand, are designed to break down in the body over time, allowing for the release of drugs in a more controlled manner.

These systems are typically used for targeted drug delivery, such as those used to treat cancer [34].

Nowadays, polymers-based drug delivery is one of the most widespread methods for controlling drug delivery. In these systems, polymers are used to surround the drug core, the release rate of the encapsulated drug (core) is governed by the polymer (shell) characteristics (e.g., polymer composition and molecular weight), the thickness of the coating layer, and the physicochemical properties of the encapsulated drug, like drug particle size, solubility, and molecular weight [30,35]. Polymers can also be used to improve the safety and efficacy of drugs. For example, polymers can be used to encapsulate drugs, protecting them from the body's immune system and allowing them to be more effectively absorbed into the bloodstream. Polymers can also be used to modify the surface of drugs, making them more soluble and allowing them to be more easily absorbed by the body. One of the following two applications is where these systems perform best: (1) a localized drug that is administered over a prolonged time to a specific area (i.e., organ, body cavity, etc.). This is often done if the target location (such as the eye or ear) is difficult to treat with systemic medication and/or the medications used are toxic and may need to be taken over an extended time (i.e., cancer treatments). (2) A medication depot for systemic delivery over an extended period. Typically, an intramuscular, subcutaneous, or implantable injection is used to give this. Polymeric drug delivery systems based on the morphology are classified as shown in **Figure 3** into three types: colloidal carriers (Nano/or micro-particles, polymeric micelles, nano/micro-gels), implantable/ injectable hydrogels or networks, and polymer-drug conjugates.

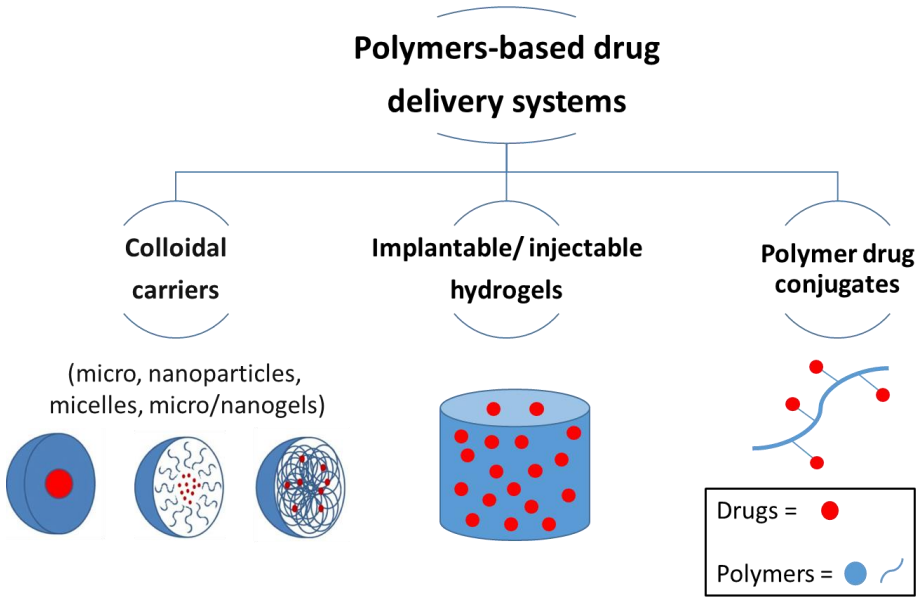

Figure 3. Classification of polymeric drug delivery system

2.2.1. Colloidal carriers

Because of their tiny sizes and ability to deliver drugs directly to specific sites in the body, micro- and/or nano-spheres are among the most attractive forms of parenteral delivery systems. These nanocarriers can be designed to release drugs in a controlled manner, allowing for more targeted delivery of drugs. Micro and/or nanospheres involve coating small drug particles with various polymer materials, which can be routinely injected using narrow-gauge needles or given orally [28,35]. After administration, the drug is released from the polymer through diffusion or breakdown of the polymer matrix in a rate-controlled manner. The molecular weight and composition of the polymer, the particle size, and the shape all affect how quickly drugs are released in these systems. The route of administration of the injected nanospheres and microspheres may be constrained by their size. For instance, to prevent getting stuck in the body's circulatory system during intravenous (I.V.) injection, the injected stable particles must be significantly less than the diameter of the capillaries (5 – 10 μm) [36]. For injection into cavities, intramuscularly, subcutaneously, or both, larger particles (>10 μm) are useful.

Both the polymerization of monomers and the synthesis of linear or cross- linked polymers may be used to prepare micro- and nanospheres. Emulsion, dispersion, and suspension are three of the strategies that may be used to polymerize monomers. The emulsion is frequently used to create homogeneous nanometer-sized particles (10 to 1000 nm). A water-soluble initiator and a monomer are commonly dispersed in water as part of the process. Uniform micelles are created using a surfactant, and polymerization occurs within these micelles. Micrometer-scale (0.5–10 μm) particle size is produced using dispersion polymerization. In this method, the monomer, initiator, and stabilizer—a hydrophobic and hydrophilic organic polymer—are dissolved in an organic solvent, and polymerization occurs inside the monomer droplets. The organic solvent precipitates the polymer beads out. Typically, suspension polymerization is used to create particles between 50 and 500 μm in size. In the suspension polymerization process, a stabilizer, an initiator that is soluble in the monomer phase, and the monomer are all dispersed in an aqueous phase. The monomer phase is where polymerization takes place. In addition to the aforementioned polymerization methods, a lot of research has also been done on dispersion polymerization in supercritical CO_2, which does not need the use of hazardous solvents and may be useful for medical purposes [35]. A simple and low-energy method for creating polymeric nanoparticles is nanoprecipitation. Due to the displacement of a solvent with a non-solvent, it is based on interfacial deposition. Nanoprecipitation requires the miscibility of the solvents and the diluted polymer solutions [37]. In a conventional nanoprecipitation

procedure, a polymer and hydrophobic drug are dissolved in a solvent that is miscible with water. Under continuous stirring, the polymer-drug solution is dropped into an aqueous solution for the small-scale preparation of nanoparticles. The chemical characteristics of the medicine, the polymers employed, and the process used to create the micro- and nanospheres all affect how the drug is incorporated.

Moreover, spray drying and solvent evaporation are two other methods used often in the preparation of micro- and nanospheres (1–100 μm). These techniques are beneficial for polymers like polyglycolide (PGA) and polylactic acid (PLA) that cannot be created by the emulsion process. Additionally, they can be useful for some natural polymers like chitin, cellulose, and chitosan. The double emulsion (or solvent evaporation) method includes the dissolving of the drug in water followed by dispersion in the polymer phase that is dissolved in an organic solvent (often methylene chloride, chloroform, or ethyl acetate) to generate the first emulsion. The second emulsion (w/o/w) is created by dispersing the first emulsion in an aqueous stabilizing media (often polyvinyl alcohol, PVA). As the polymer solidifies and the methylene chloride evaporates, micro- or nanospheres are created with encapsulation of the drug [38]. While in the case of the spray drying method, the drug is either dissolved or dispersed in the polymer solution before being sprayed dry. Plasticizers, such as citric acid, which encourage polymer particles coalescence/ aggregation on the drug particles and hence enhance the development of spherical and smooth surfaced microspheres (1–10 μm), can be added to spray-dried microspheres to increase their quality. The spraying rate, the feed rate of the polymer-drug solution, the size of the nozzle, and the drying temperature can all be used to regulate the size of the microspheres. This straightforward, reproducible, and scaleable approach of microencapsulation is especially less dependent on the solubility properties of the medication and polymer [39].

The first controlled-release drug approved by the Food and Drug Administration (FDA) was Lupron Depot, an injectable microsphere made of leuprolide acetate and lactic acid-glycolic acid copolymer. This system, which released the drugs over a 30-day period to treat prostate cancer, was introduced in 1989 [30]. Other FDA-approved micro- or nanosphere drug delivery systems include AmBisome (amphotericin B liposomal for the treatment of fungal infections) [40], Adagen (Polyethylene glycol PEG-modified adenosine deaminase ADA as in the treatment of severe combined immunodeficiency) [41], Doxil/Caelyx (PEG-stabilized liposomal doxorubicin/pegylated liposomal Doxorubicin for treatment of metastatic ovarian and breast cancer) [42], DepoCyt (Lymphomatous meningitis treatment using liposomal

cytosine arabinoside) [43], Denileukin diftitox (trade name Ontak as an antineoplastic agent for cutaneous T-cell lymphoma) [44], PEG-Intron (Peginterferon Alfa-2b for hepatitis C) [45], Mylotarg (Gemtuzumab ozogamicin for CD33-positive acute myeloid leukemia) [46], and Pegfilgrastim (Neulasta for the treatment of chemotherapy-related febrile neutropenia) [47].

2.2.2. Hydrogel systems

Three-dimensional, cross-linked networks of water-soluble polymers make up hydrogels. Hydrogels are produced from synthetic or natural polymers and are extremely absorbent (up to 99.9% water). Due to their biocompatibility and inertness to a variety of medicines, particularly proteins, biodegradable hydrogels have attracted particular interest as controlled drug delivery systems. Additionally, hydrogels might be created as slabs, micro- and nanoparticles, films, and various other physical shapes. Because hydrogels are very porous, the drug release rate is greatly influenced by the ability of drug molecules to diffuse through the gel network. By adjusting the degree of cross-linking, it is simple to adjust the porosity of hydrogels, which will impact how quickly the drug particles are released from their entrapment [48–50].

Hydrogels can be created through both chemical and physical cross-linking. The formation of the physical cross-linking hydrogel can be through using intermolecular interactions, including van der Waals forces, hydrogen bonds, π interactions, hydrophobic interactions, ionic bonds, and host–guest interactions [51]. Changes in pH, temperature, and ionic strength, as well as a range of physicochemical interactions, can affect the physical crosslinking of hydrogels. Thus, they usually have extremely limited mechanical strength, and external stimuli can modify their shape and properties very quickly [51]. Relatively high mechanical strength and stability have been shown by hydrogels that have undergone chemical cross-linking, which entails introducing extra cross-linking entities to covalently attach to hydrogels [51]. Diels-Alder reactions, enzyme mediations, Michael additions, photopolymerizations, or Schiff-base reactions can all form a covalent bond [51]. Hoare and Kohane reported two major in situ covalent cross-linking binding strategies namely small-molecule and polymer-polymer cross-linking and discussed their advantages and disadvantages [49]. Injectable hydrogels have several benefits over their prefabricated counterparts, including simple syringe delivery, minimum surgical incisions, facile synthesis, adaptability, a high drug-loading capacity, and controlled drug-release capability [51,52]. Various bioactive compounds, such as vaccinations, immune cells, cytokines, antibodies, and immunotherapeutic and chemotherapeutic drugs, can be incorporated into injectable hydrogels [51–54].

Although employing hydrogel systems for drug delivery has many benefits, it also has certain drawbacks. Rapid swelling of hydrogels with water can cause the loaded medicine to release quickly and the polymer to degrade quickly. Hydrophilic medications administered by hydrogel systems generally have a release period of hours to days, which is significantly less time than that of hydrophilic pharmaceuticals delivered by micro- or nanospheres based on hydrophobic polymers. Several approaches have been developed to increase the efficacy of hydrogels for drug delivery, including implementing covalent bonds between hydrogels and drugs, improving hydrogel-drug bonding via physical interactions (such as copolymerization or ionic interaction), and changing the microstructure of hydrogels (as raising the cross-linking density/percentage, creating a hydrogel surface layer with limited permeability, second hydrogel network formation, and co-forming hydrogel matrix with particulate systems) [49,50].

Hydrogel drug delivery systems are designed for a variety of uses. For instance, biodegradable hydrogels have demonstrated enhanced ectopic bone growth when bone morphogenetic protein-2 is released under controlled conditions [55]. Ibuprofen-containing solid lipid nanoparticles have been added to dextran hydrogels, and it has been demonstrated that these formulations are acceptable for oral administration [56]. Many injectable hydrogels have been created to address ear issues. These include gelatin hydrogels that provide insulin-like growth factors, which have been shown to enhance hearing in individuals with abrupt sensorineural hearing loss [57], and poloxamer hydrogels that contain dexamethasone [58–60]. In addition to their usage in drug delivery systems [61], hydrogels have further uses in tissue engineering and wound management [62,63].

2.2.3. Drug-polymer conjugate

A polymeric carrier with covalently bonded drug molecules is known as a drug-polymer conjugate, also known as polymeric prodrugs [64,65]. The polymer-drug conjugation technique enhances therapeutic qualities and has several benefits, such as a longer half-life, improved water solubility, enhanced stability, and reduced antigenicity and immunogenicity to the original parent drugs. Polymeric drug conjugates are a unique drug delivery system that not only protects the medication from early degradation but also enables it to be selectively targeted to different bodily cells and tissues. This approach was first introduced by Helmut Ringsdorf in 1975 when he postulated that a polymer covalently bonded to a drug molecule enhances not only the water solubility of the drug but also its bioavailability [64]. Increased drug circulation times are offered by these polymer-drug conjugates, which also enable medications to be released gradually and under control. When there are variations in temperature, enzyme

concentration, or pH, they offer targeted and controlled drug release at the intended site of therapeutic need [66,67]. The carrier polymer can transport a lot of covalently attached drug molecules because of its macromolecular structure and numerous available functional groups. The concept is appealing because it enables the attachment of many drug agents with either the polymer backbone or functional side groups, together with a targeting moiety, an imaging agent, and other relevant agents. The conjugation occasionally contains a targeted moiety or a solubility enhancer to increase pharmacokinetic behavior and medicinal effectiveness [64]. The encapsulating effect of the drug conjugate reduces macrophages and reticuloendothelial system (RES) uptake. These conjugates prolong the period that blood circulates through tumor tissues, taking advantage of their leaky vasculature and poor lymphatic drainage, and increasing the therapeutic index of the drug in those tissues. The enhanced permeability and retention effect (EPR) is the name given to this phenomenon [68,69].

One of three methods is frequently used for the synthesis of polymer-drug conjugates; 1) conjugation/coupling of a drug with an existing polymer, 2) conjugation/coupling of a drug with monomers, and polymerizing by ring-opening metathesis polymerization (ROMP), reversible addition-fragmentation transfer (RAFT) polymerization, or ring-opening polymerization (ROP), as well as 3) employing a drug with two or maybe more functional moieties as a monomer for drug-polymer polymerization [70,71]. Depending on the size and type of the polymer structure, the first technique may result in poor control over drug conjugation and little drug loading. Drug-monomer conjugates, however, often offer significant control over drug loading and desired outcomes [71,72]. Although the linker must be carefully chosen to show the best *in vivo* drug release rates for the desired therapeutic use, drugs are frequently conjugated to polymers using biodegradable linkers that can adjust the site and rate of drug release [73]. However, it's crucial to remember that the physicochemical characteristics of the polymer might affect the *in vivo* release of drugs connected through "biodegradable" linkages, especially if enzyme availability is necessary [74–76].

The major area of concern in the drug development process is the safety of the polymer-drug conjugates. Several drug-polymer conjugates have succeeded through certain clinical studies and are already being utilized commercially [77–80]. Cancer treatment using drug-polymer conjugates demonstrated promising results [81–84]. The toxicity studies for polymeric drug conjugates must be carefully taken into account since they commonly display distinct pharmacokinetic characteristics and occasionally even demonstrate altered biodistribution. The main element exhibiting the pharmacological impact in a drug-polymer conjugate is the drug

release from the polymer [85,86]. The drug often does not release during systemic transport, but if it does, it may have unintended adverse consequences and the polymeric drug combination will have a poor overall effectiveness and safety profile [87]. As a result, the optimal drug-polymer conjugate should display a perfect balance between the stability of the drug conjugate and drug release to achieve the necessary efficacy and safety in usage.

2.3. Modification of biopolymers for drug delivery system

Recent trends in formulation development have expanded the usage of biodegradable polymer-based formulations from controlled drug delivery to complex systems including targeted, pulsatile, environment-sensitive, and intelligent/smart drug delivery systems [88,89]. Research to date has shown that in order to create an efficient drug delivery system, various pharmaceutical formulations call for the optimization of different and specific combinations of polymeric and structural properties. Additionally, depending on the physicochemical and pharmacological nature of each drug, varied demands are made for production conditions and release characteristics. As a result, when formulating the design, it is important to consider the required qualities of the biodegradable polymers, which vary between different formulations [89–91]. According to reports, the physical and chemical properties of polymers, such as their solubility, degradation, chemical structure, crystallinity, and hydrophilicity, have a significant influence on the method of preparation, polymer-drug compatibility, zeta potential (ζ), surface morphology, and the release of drugs from prepared formulations [92,93]. Other considerations, such as formulation type and objective, administration route, drug characteristics, etc., impact the choice of polymer in addition to polymeric properties (see **Figure 4**) [94]. Therefore, choosing the right polymer is an essential step in creating a successful drug delivery system.

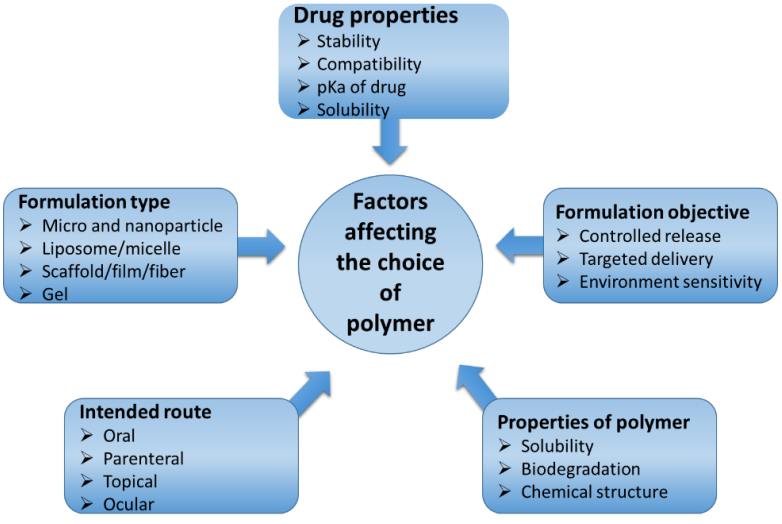

Figure 4. The factors that influence polymer choice [94].

Several biodegradable polymers have been described so far as having less-than-ideal properties for medicinal formulations. Their varied features make it easier for them to preferentially achieve particular goals [95,96]. Biodegradable polymers offer benefits and drawbacks of their own, regardless of the origin (natural or synthetic). Natural polymers for drug administration and tissue engineering, for example, have acceptable compatibility but their use is constrained by the absence of adequate physical qualities like solubility, mechanical strength, or stability. However, although having excellent qualities for processing formulations, the majority of synthetic polymers cannot be used in pharmaceutical formulations and devices because they lack a biological recognition signal [91]. To achieve a predesigned set of characteristics without moving between polymers, a modification technique is used. The numerous ways to modify the characteristics of polymers are shown in **Figure 5**.

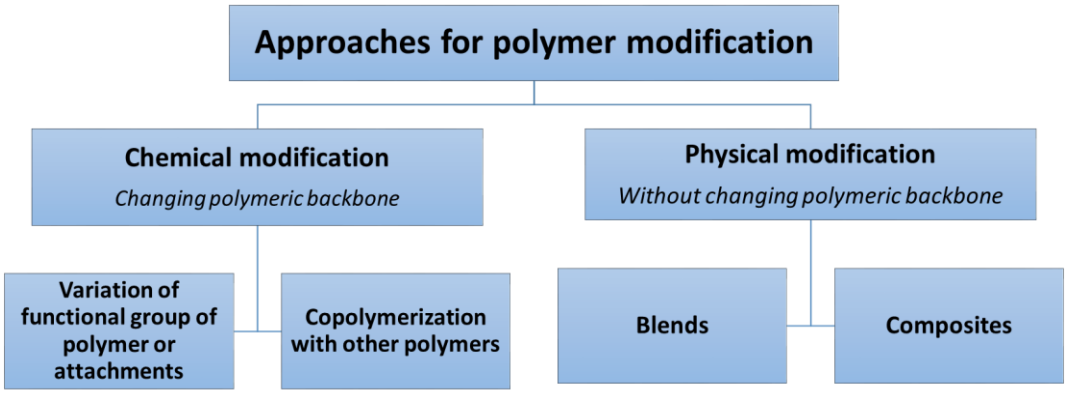

Figure 5. Several polymeric modifications are used for tissue engineering and drug delivery [94].

Although polymeric modification is not a particularly novel strategy, it has recently been widely used to modify polymeric characteristics that reduce degradation, alter drug release patterns, or change mechanical characteristics to produce a polymer that is more biocompatible or suitable for multiple formulations. Additionally, sophisticated polymer modification and design produced materials with targeting properties, P-glycoprotein inhibitory action, environmental sensitivities, and improved pharmacokinetic profiles of many hydrophobic medicines [97]. In order to overcome biological (poor selectivity and bioavailability, shorter half-life, etc.) and pharmaceutical (physicochemical characteristics for formulation processing) limits, it is expected that polymeric qualities will function as the determinant for formulation design or development. During this present assortment, we specifically highlight the modifications of polymers and their function in drug delivery with particular reference to PVA and chitosan.

Polyvinyl alcohol (PVA), a water-soluble, nontoxic, inert, and biocompatible synthetic polymer, has been extensively employed for drug delivery systems due to its beneficial

characteristics including high hydrophilicity, solvent resistance, high mechanical behavior, and biocompatibility [98,99]. Using potassium hydroxide to hydrolyze polyvinyl acetate in ethanol, Hermann and Haehnel produced PVA for the first time in 1924 [100]. Nowadays, PVA is industrially synthesized from polyvinyl acetate. PVA has already been approved by the Food and Drug Administration (FDA) for its clinical usage in the human body and is currently employed for implanted devices such as catheters, occlusive agents, eyedrops, tissue adhesion barriers, nerve routers, and cartilage replacements [99]. It is also commonly used for biomedical applications, either alone or in copolymers [101,102]. PVA shows biocompatible with different cell lines, according to an *in vitro* test [103]. However, the bioelimination and/or biodegradability of PVA in animals is still up for debate even after the hopeful findings of Yamaoka et al., concerning the body distribution of PVA with different molecular weights which demonstrated that the low quantity of accumulated PVA in the organs to impact their biological fate and always minimally interacted with distinct cells [104]. Furthermore, Kaneo et al. investigated the elimination of PVA after intravenous (IV) administration and proposed that PVA is removed only through mechanisms that do not require saturable transport pathways [105]. The elimination pathways and biological fate of poly(vinyl alcohol) microparticles were *in vivo* tested by Cerroni et al. in mice, and the investigation supported the conclusion that no harmful (cytotoxic) effects were seen [106]. Modification of PVA with the terminal COOH groups can provide a good modified polymer candidate which can form an ester and/or amide linkage with amino and/or carboxyl and/or hydroxyl groups of biologically active compounds such as proteins, peptides, synthetic chemical, or natural products compounds (e.g. mitomycin C as an antitumor agent and antifibrotic drug). Moreover, PVA with terminal CHO groups is a promising candidate for hydrogel formation with another polymer with NH_2 groups (e.g. chitosan) based on the Schiff-base linkage and the resulting hydrogel can be employed for controlled drug delivery applications.

Chitosan, a polycationic biopolymer, is typically derived from the alkaline deacetylation of chitin, the major component of arthropod exoskeletons and fungal cell walls. In comparison to the annual output of synthetic polyethylene of 80 million tons [107], the biosphere has over 10 gigatonnes of chitin. As a result, chitosan is regarded as one of the most essential green and renewable materials [108]. Chitosan is typically biocompatible, nontoxic, and biodegradable polymer which has been utilized for a variety of biomedical applications, including topical ophthalmic treatments [109], implant and periodontal surgeries [110,111], and injections [112]. Dynamic chitosan-based hydrogels may be exploited as vehicles for controlled drug release

since physiological systems frequently contain certain chitosan-digesting enzymes (such as pepsin and lipase). However, application of the chitosan is constrained by several disadvantages, including poor mechanical and thermal properties, high cost, low surface area, and dissolution under highly acidic environments. Chitosan has to be modified to improve its solubility and mucoadhesion to be used more frequently in physiological conditions and increase its applications. Chen et al. reported on the advancements in chemical modification techniques of chitosan and their pharmaceuticals and textiles applications [113]. Thiolated chitosan is one approach for increasing chitosan's solubility and mucoadhesive characteristics, Namdar and Mourya reported on the preparation, characteristics, and applications of thiolated chitosan [114].

2.4. Polyesters for pharmaceutical and biomedical applications

In addition to the synthetic and natural biocompatible polymers discussed above aliphatic polyesters have gained recent a great deal of attention in studies for biomedical and pharmaceutical applications including drug delivery systems [115,116], functional materials [117], and artificial implants in tissue engineering [118]. This is because they have also favorable biocompatibility and biodegradability characteristics and belong to the most significant groups of synthetic biodegradable polymers [119,120]. Their biocompatibility and strong capability for hydrolysis in the human body are key benefits of these aliphatic polyesters [121]. The field of drug delivery benefits greatly from the use of biocompatible and biodegradable polymers, particularly when creating nanoparticles that can be used as a carrier to protect the drug or bioactive substance from *in vivo* or *in vitro* degradation. This increases therapeutic efficacy, controls and prolongs the drug release process, and decreases side effects and frequency of drug administration [122,123].

Besides PLA and PLGA, one of the most promising biodegradable polyesters, poly(ethylene succinate) (PES), has great biocompatibility and particularly outstanding biodegradability [119,124]. PES is appropriate for biomedical applications as a drug delivery since its biocompatibility is comparable to the highest biocompatibility polymers like polylactic acid (PLA) and polycaprolactone (PCL) which are currently widely employed [119]. PES exhibits mechanical qualities that are equal to those of polypropylene and polyethylene, also several studies are investigating the biodegradation of PES under different conditions and environments [125–132]. PES, for instance, degrades hydrolytically considerably more quickly than poly(butylene succinate) (PBSu), which makes it an ideal base for drug release systems.

According to Carothers and Dorough (1930), aliphatic polyesters were first synthesized by the condensation polymerization of diols and dicarboxylic acids [133]. Nowadays, the two-stage melt polycondensation method (esterification and polycondensation) is used for the synthesis of PES with a relatively high molecular weight, however, it needs to use relatively toxic catalysts, such as tetrabutoxy titanium, and also the formation of polyester with a relatively low molecular weight [134–136]. It is possible to eliminate the need for toxic catalysts and synthesis polyester using a simple process called direct polycondensation. In this approach, only monomers are needed to form a relatively long polyester chain at the appropriate temperature to avoid monomer and polymer decomposition and to sustain further chain formation.

2.5. Drug release and mechanism for polymeric drug delivery systems

"Drug release" for polymeric systems often refers to the way a drug compound is transferred from its start point in a polymer matrix towards the exterior of the polymeric matrix, and then how it is delivered to the external environment [137].

By diffusion through the water-filled pores, drugs can be released from their drug delivery systems. This process is controlled by random drug movements and driven by gradients in their chemical potential and convection that is brought on by osmotic pressure. Erosion is another method for releasing drugs from the polymer matrices in addition to diffusion. Erosion causes pore creation and erosion effects, which can be seen after the time of the drug release process [138]. Conventional drug release processes are based on the degradation of polymer, erosion, and drug diffusion, as well as drug release based on exogenous and endogenous stimuli are covered in this section as shown in **Figure 6**.

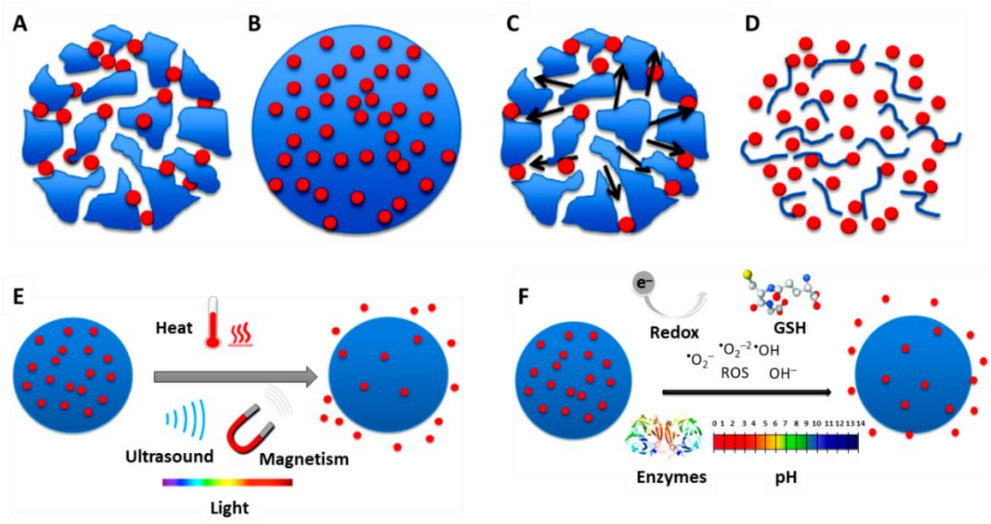

Figure 6. Mechanisms of drug release from polymeric systems: (**A**) diffusion through pores filled with water, (**B**) diffusion through the polymeric matrices, (**C**) osmotic pumping, (**D**) erosion, (**E**) release of drugs in response to external stimuli, and (**F**) release of drugs in response to internal stimuli [138].

2.5.1. Diffusion of the drugs through water-filled pores

This process explains how the drug compounds are moving randomly as a result of a concentration gradient-approximated chemical potential gradient. Drug release in degradable polymeric systems is regulated by diffusion via a porous network with changing topologies as the polymer matrix breaks down. Polymeric materials instantly absorb water, which is a quicker procedure than medication release. Over time, the water that is present in the polymer matrix creates pores that are filled with water, growing in size and quantity until they are finally large enough to allow for drug release [139,140].

2.5.2. Diffusion of the drugs through the polymer matrix

Herein, drug compounds just diffuse out of the matrix of the polymer. Diffusion is the prime reason for releasing the drug from a non-degradable drug delivery system, and its rate is constant, unaffected by concentration gradients, but rather by the characteristics of the polymeric membrane (thickness and permeability) [141].

2.5.3. The osmotic pumping

Convection-driven drug delivery through pores filled with water is another method. Osmotic pressure, which results in the influx of water into a non-swelling system, is what causes drug transport; this force is also known as osmotic pumping. An in-depth discussion of the design and construction of osmotically driven DDS employing osmogens and semipermeable membranes may be found elsewhere [142].

2.5.4. Erosion

Surface (or heterogenous) erosion.

Surface erosion happens when the rate of erosion outpaces the rate of water uptake in the bulk polymer [143], and it happens when polymers begin to degrade at the matrix/scaffold surface, gradually shrinking the size of the scaffold/matrix from the outside into the inside [144]. Numerous drug delivery systems benefit greatly from surface erosion since it is simple to control and repeat the kinetics of erosion, which in turn results in predictable drug release. In addition, since water-sensitive drugs are protected, the modest water permeability rate is appropriate for drug administration [143].

Bulk (or homogenous) erosion.

As water penetrates the polymer's bulk, it causes bulk erosion, which occurs throughout the polymer material and causes the entire matrix to degrade uniformly [145,146]. The polymer chains inside the bulk of a matrix are usually able to be hydrolyzed because the rate of water permeation is higher than the rate of erosion [143]. Bulk erosion is a less efficient strategy for controlled drug delivery because it is unpredictable and is unable to protect drug molecules from the environment [143].

2.5.5. Exogeneously stimuli-responsive drug release

Exogenous or external stimuli are those produced by stimulation from outside the body (including heat, electrical, ultrasonic, or light induction) as shown in **Figure 6E**. The therapeutic load can then be released into a specific biological environment as a result of this induced release, which can often affect the chemistry or structure of the drug delivery system. Drugs that are covalently conjugated to the polymer backbone can be released by rupturing the linkage bonds; however, when the drug is trapped inside polymeric nanoparticles, release can be initiated by inducing structural changes such as polymer degradation, conformational changes, de-shedding of surface layers, and charge switching. Numerous literature reviews have described using external stimuli to adjust the release of drugs [147–150].

2.5.6. Endogenously stimuli-responsive drug release

The production of chemically induced drug release from polymeric NPs can take advantage of a variety of internal triggers, including shifts in pH, redox status, and ionic content within cells and tissues (**Figure 6F**) [147,148,150–155]. For instance, the acidic pH conditions seen in solid tumors (pH 6–7) can be utilized to cause chemical alterations in polymer bonds that promote drug release [147,148,154]. The varied low-pH conditions that subcellular compartments (such as the cytosol, lysosome, endosome, etc.) provide after absorption of the drug delivery system might result in the shedding of the surface layer of polymeric drug delivery or conformational changes that promote site-specific and enhance drug release [147,148,154].

2.6. Mathematical models of polymeric drug release

The goal of mathematical modeling of the release of the drug is to predict the rates of drug release and diffusion patterns of the drug from the drug delivery system. By correlating experimental results with mathematical models, this knowledge helps to optimize the release

kinetics and establish the physical mechanisms that govern drug transport. The overall therapeutic effectiveness and drug safety profiles can be enhanced by precise drug release prediction. In the conclusion, it is envisioned that the systematic use of mathematical models to forecast drug release rates and behavior will save costs and experimentation times, resulting in more precise drug formulations and dosage regimens [138]. The results of *in vitro* drug release were fit to the following mathematical release kinetics models (**Equation 1-5**) to evaluate the mechanism of the drug release [156]:

Zero-order model:	$D_t = D_0 + k_0 t$	(**1**)
First-order model:	$\log D_t = \log D_0 + k_1 t/2.303$	(**2**)
Higuchi model:	$D_t = D_0 + k_H t^{1/2}$	(**3**)
Hixon-Crowell model:	$D_t^{1/3} = D_0^{1/3} - k_{HC} t$	(**4**)
Korsmeyer–Peppas model:	$M_t/M_\infty = k_{KP} t^n$	(**5**)

where D_0 is the initial drug amount released, D_t is the drug amount released at time t, M_t/M_∞ is the fraction of drug released at time t, k_0 is the zero-order release rate constant, k_1 is the first-order release rate constant, k_{HC} is the Hixson–Crowell release rate constant, k_H is the Higuchi release rate constant, n is the release exponent, and k_{KP} is the Korsmeyer-Peppas release rate constant. These models have been discussed in detail in several publications [156–159].

2.7. Description of drugs used in the thesis

2.7.1. Mitomycin C (MMC)

Mitomycin C was first discovered by Wakaki et al. (1958) from fermentation cultures of the *Streptomyces caespitosus* after discovering Mitomycin A and B by Hata et al. (1956) and they were initially described as new antibiotics [l60,161]. The most potent of the fractions, mitomycin C, was discovered to have a wide range of efficacy toward transplanted tumors [162]. Historically, glaucoma patients have been treated with mitomycin C (MMC) to minimize fibroblast proliferation and the risk of unwanted trabecular meshwork blockage [163]. Mitomycin C (MMC) has long been used as an antifibrotic, antibiotic, and antineoplastic agent, and also the antiproliferative (antitumor) mechanism of MMC is based on using it as a bifunctional alkylating agent that causes DNA synthesis to be inhibited by binding to DNA chains, but its undesirable side-effects minimize the dose in chemotherapy [164–166]. MMC has severe side effects such as renal damage, gastrointestinal damage, and bone marrow

depression [164,167,168]. MMC with a relatively good water solubility (~0.9 mg/mL) administered as a free form was rapidly excreted from the body and could not be detected in the urine samples after 1 day [169,170]. MMC is usually administered into a vein (intravenous) but the leakage of mitomycin (extravasation) from the vein into which it is administered can cause significant damage to the surrounding tissue [171,172]. MMC can be orally administrated and absorbed by all mucus membranes. However, it is required around 8 times compared to intravenous (I.V.) and intraperitoneal (I.P.) administration in addition to LD_{50} for oral administration of MMC was 3 to 12 times the LD_{50} for injection administration [166]. As a result, many efforts have therefore been made to reduce the toxic impact and enhance the efficacy of MMC using different methods of delivery. The most common types of MMC delivery is drug encapsulating in micro- or nano-particles by the use of various polymers, like N-succinyl-chitosan [173], dextran [174,175], poly(butyl cyanoacrylate) [176], albumin [177], hydrogels [178], estradiol [179], and poly-epsilon-caprolactone [180]. Unfortunately, these methods have shown considerable difficulties in the local administration of MMC because of the quick degradation of these drug carriers in the body.

2.7.2. Tilorone dihydrochloride

Tilorone dihydrochloride, whose full name is 2,7-Bis(2-(dimethylamino)ethoxy)-9H-fluoren-9-one dihydrochloride, is one of the promising drugs used clinically as broader spectrum antivirals (for influenza, viral hepatitis, acute respiratory viral infection, myelitis, viral encephalitis, SARS-CoV-2, and others) [181,182]. It is a synthetic, low molecular weight (M_w = 483.47 g/mol) compound that can be oral or intraperitoneal injection administration. The Tilorone drug, which is yellow/orange in color, has generally been utilized in the salt form of dihydrochloride (water solubility ≥ 28 mg/mL). Initial synthesis and development of Tilorone took place at Marion Merrell Dow (pharmaceutical company), which is currently a part of Sanofi [183]. In recent years, the synthesis has been enhanced [184,185].

Following denervation, the skeletal muscles exhibit focal atrophy, which poses treatment difficulties in the case of various muscular dystrophies. In addition to being a potentially fatal disease, acquired laryngeal-tracheal muscular atrophy is a very difficult and challenging issue in laryngology. The most significant symptom in addition to hoarseness in situations of vocal fold palsy (particularly bilateral) brought on by muscle atrophy and determined by repeated nerve damage is dyspnea, which can even result in severe asphyxia [186,187]. Injectable laryngoplasty (steroid, lipoaugmentation, bFGF, and stem cell treatment) and laryngeal

framework surgery (medialization thyroplasty) have all been investigated as possible therapeutic approaches, although their efficacy has been inconsistent [188–190]. Notably, increasing muscle size can treat laryngotracheal muscular atrophy without innervation repair. In contrast to myostatin/TGF-beta signaling, the BMP (bone morphogenetic protein)-Smad1/5/8 signaling axis (**Figure 7**) is a key positive regulator of adult myofibers [191], as well as the claim that muscle hypertrophy is induced by increased BMP7 expression [192]. Remarkably, Tilorone increases BMP-7 expression and activates BMP signaling [193]. In a mouse model of silica-induced lung fibrosis, Tilorone was also shown to have antifibrotic effects [193], recommending that it may be a novel therapy for the treatment of cardiac fibrosis related to heart failure [194]. Importantly, Tilorone injections dramatically increase muscle mass in cancer cachectic patients [195,196]. The effectiveness and safety of systemic administration of myostatin inhibitors in treating sarcopenia, muscle dystrophies, and muscle wasting after hip fracture surgery are the subjects of numerous ongoing clinical studies [197–200]; however, the local administration of these drugs in cases of local muscle atrophy has not yet been examined.

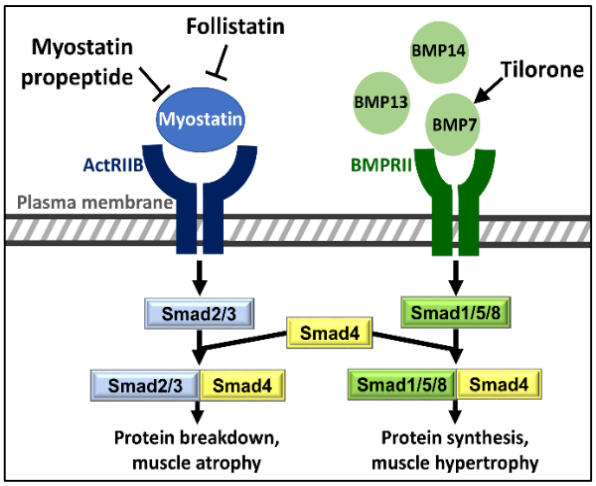

Figure 7. Signaling of myostatin and BMPs.

2.7.3. Nimodipine

Nimodipine (NIMO), a dihydropyridine calcium antagonist, a poorly water-soluble (0.653 µg/mL) drug is used to treat cerebrovascular spasms, Alzheimer's disease, hypertension, and stroke [201–204]. It could be administered intravenously or orally, although each has advantages and disadvantages [205]. NIMO is taken orally in the form of soft gelatin capsules and tablets for clinical usage, however, there are several drawbacks, including large dosages, poor oral bioavailability, and numerous side effects, which limit the therapeutic efficacy [206–208]. After oral administration, NIMO is quickly absorbed in humans, and peak concentrations are often reached within an hour [209]. Due to substantial first-pass metabolism, bioavailability is only 3–30% after an oral dose and 100% after an intravenous injection [203,209–212]. NIMO, however, needs the use of organic solvents during IV administration because of its poor water solubility. Commercially available Nimotop injection from Bayer contains 24% *v/v* ethanol as a solubilizer [213]. However, the evident high amount of organic solvent irritates

blood vessels, resulting in discomfort and inflammation at the injection site. According to the suggested NIMO dose, phlebitis and poor compliance might occur during the infusion as a result of regular exposure to organic solvents (like ethanol) [214–217]. Additionally, after Nimotop injection has been diluted with glucose or saline solutions due to its poor water solubility, drug crystallization might form, providing a health risk to patients [205]. Additionally, NIMO is rapidly decomposed by light, losing its pharmacological action [203,218]. As a result, there is an urgent need for a novel approach to producing effective and safe NIMO formulations with enhanced solubility and bioavailability. In our prior study, the biological activity of NIMO release from polymeric drug carriers (pH-sensitive chitosan nanoparticles) has been described and contrasted with pure NIMO [219]. This result unambiguously shows that NIMO released by polymeric particles can have a biological impact.

3. Objectives

During my doctoral work, we aspire to produce different polymer-based controlled drug delivery systems for three drugs (Mitomycin C, Tilorone dihydrochloride, and Nimodipine) with very different structures and material properties, by modifying and synthesizing biocompatible polymers to introduce novel drug delivery systems and solving the associated problems related to the use of conventional drug delivery methods.

[i] Development of mucoadhesive polymeric prodrug for Mitomycin C

To reduce the severe side effects of Mitomycin C and provide a suitable localized drug delivery system for treating throat cancer and preventing scar tissue formation in the area of head and neck surgery, we planned to synthesize a MMC loaded mucoadhesive polymeric prodrug (**Objective#1** in **Figure 8**) which has various advantages including a prolonged and controlled drug release process, protecting the drug and decreasing its cytotoxicity. To achieve this goal, the synthesis of a partially succinylated PVA-based polymeric prodrug was presented (**Figure 8**) that can spontaneously self-assemble into nanoparticles and conjugate (covalent bonding) drugs with amino, hydroxyl, and/or carboxyl groups via ester or amide linkages. Additionally, the crosslinking density (varied by the OH/ COOH ratio) of polymeric prodrugs can be used to control and adjust the drug release process. Therefore, I planned to systematically increase the crosslinking density of succinated PVA by increasing the COOH content and evaluating the impact on the drug release process and morphology of polymeric prodrugs. I also planned to use CYS to increase the mucoadhesive properties of the polymeric prodrug. Also, I planned to study in detail the physicochemical properties of potential polymeric prodrugs as well as the relevant antibacterial and anticancer activities in addition to the *in vitro* drug release measurements to assess their applicability. The developed drug delivery system provides a safe drug administration method, reducing frequent administration of the drug, and increasing the residence time to increase the bioavailability and efficiency of MMC.

[ii] Mucoadhesive self-assemble injectable hydrogel of Tilorone dihydrochloride

The goal of this part is to introduce a novel potential therapeutic approach for the local treatment of muscle atrophy (laryngotracheal atrophy) by developing a dynamic injectable mucoadhesive hydrogel incorporating Tilorone, a BMP inducer. Thus, we present the synthesis of the dynamic injectable hydrogel (**Objective#2** in **Figure 8**) based on evolving Schiff-base (-CH=N-) bonds between the 4-formylbenzoic acid modified PVA (PVA-CHO) and 3-mercaptopropionic acid

modified chitosan (CHIT-SH). Moreover, the presence of thiolated chitosan improved the mucoadhesive properties of the hydrogel, as well. Also, I planned to increase the crosslinking density by systematically increasing the concentration of the precursor polymer solutions to provide a controlled method for the drug release process. The newly developed hydrogel, which has mucoadhesive, self-assembling, and self-healing capabilities, is a promising candidate for protecting the Tilorone drug during the injection through thin needles and retention at target sites. Tilorone injection-based self-healing hydrogel for controlled release offers several benefits, such as a decreased dosage, fewer side effects, enhanced bioavailability, easy delivery by syringe, high drug-loading capacity, minimal surgical wounds for patient comfort, controlled drug release capability, and improved therapeutic effectiveness. Also, the concentration/crosslinking density of PVA-CHO/CHIT-SH hydrogel can be used to control the Tilorone release from the hydrogel matrix (**Figure 8**). Moreover, I planned to study in detail the biocompatibility and the physicochemical properties of the hydrogel system as well as the *in vitro* and kinetic drug release measurements, to assess its applicability.

[iii] Nimodipine-loaded poly(ethylene succinate) (PES) nanoparticles

Related to this part my objective is to develop a unique controlled drug delivery system for NIMO to overcome poor water solubility and enhance drug bioavailability as well as introduce safe and efficient NIMO formulations (**Objective#3** in **Figure 8**). Encapsulating NIMO in biocompatible and biodegradable PES polyester reduces the crystallinity of the drug while also increasing the stability of the encapsulated form in an aqueous media, resulting in an improved bioavailability of poor water-soluble NIMO. Furthermore, the molecular weight of the polymer shell for the encapsulated drug can be exploited to control drug release (**Figure 8**). Therefore, I planned to synthesize a promising biocompatible and biodegradable poly(ethylene succinate) PES (**Figure 8**) with varied molecular weights based on the changing of the polymerization time, and study its solubility and precipitation properties in detail due to the little information available in the literature. Following that, I intended to develop an appropriate precipitation technique for encapsulating NIMO in PES polyester (**Figure 8**), as well as to thoroughly investigate the stability and physicochemical characteristics of the produced encapsulated form, as well as the *in vitro* and kinetics of drug release, to assess its applicability.

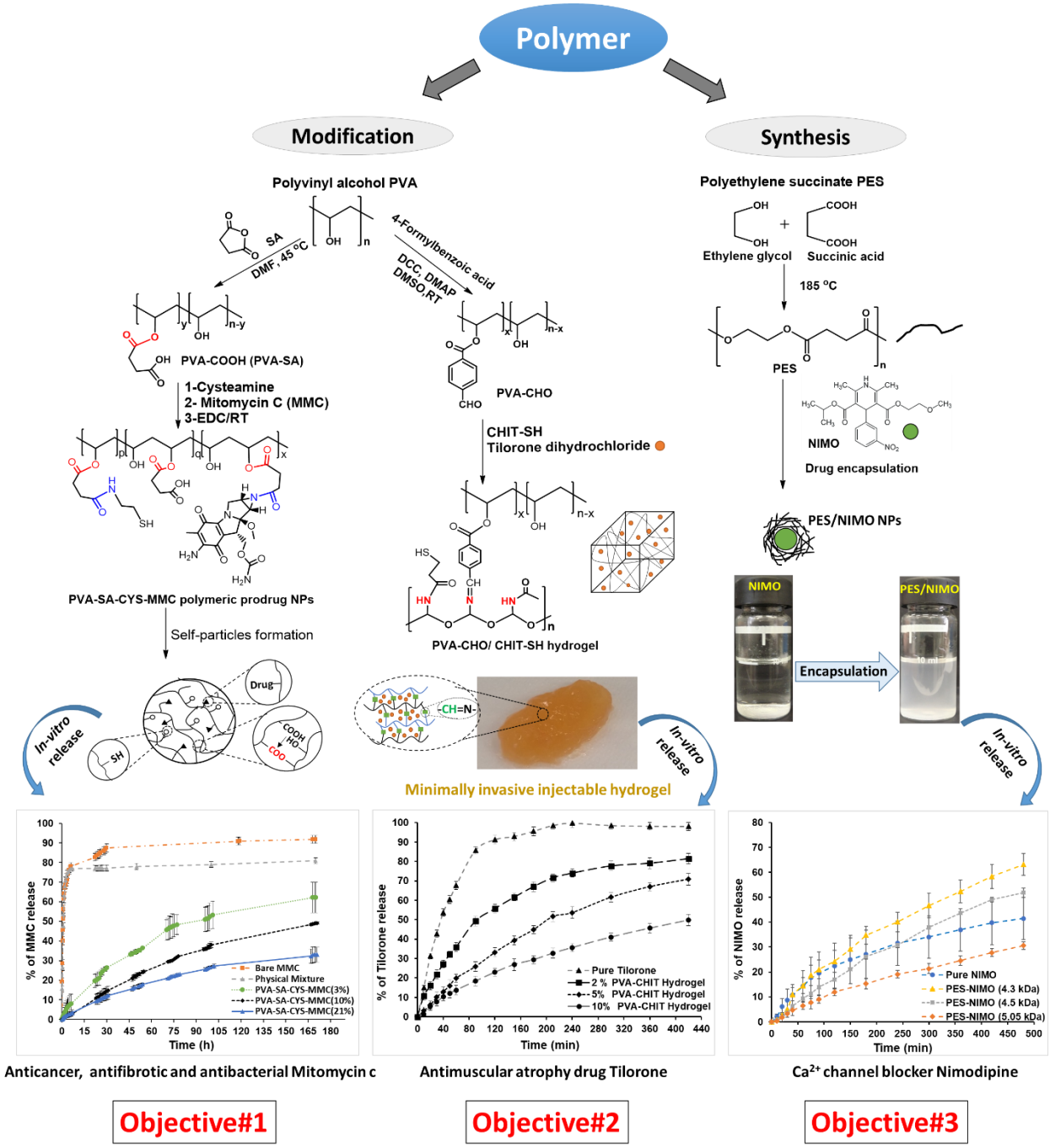

Figure 8. Schematic representation of doctoral work goals.

4. Experimental

4.1. Materials

4.1.1. Modification of PVA

Materials used for synthesis and characterization of PVA-SA-CYS-MMC NPs

- Polyvinyl alcohol (PVA), 86-89% hydrolyzed, Nagart Kft.
- Mitomycin C, Medac GmbH, and [1]Pluschem LLC.
- Succinic acid ($C_4H_6O_4$), Molar Chemicals Kft.
- Acetic anhydride ($C_4H_6O_3$), Molar Chemicals Kft.
- Sodium acetate ($C_2H_3NaO_2$), Molar Chemicals Kft.
- Sodium hydroxide (NaOH), Molar Chemicals Kft.
- Acetone (C_3H_6O), Molar Chemicals Kft.
- 1-(3-Dimethylaminopropyl)-3-ethylcarbodiimide hydrochloride (EDC, $C_8H_{17}N_3 \cdot HCl$), 98+%, Thermo Fisher GmbH.
- 3-(4,5-dimethylthiazol-2-yl)-2,5-diphenyltetrazolium bromide (MTT), Sigma Aldrich.
- Sodium dodecyl sulfate (SDS, $NaC_{12}H_{25}SO_4$), Sigma-Aldrich
- Silver nitrate ($AgNO_3$), Merck KGaA.
- Potassium thiocyanate (KSCN), Sigma-Aldrich
- Dimethylformamide (DMF), Fluka Chemicals.
- Diethyl ether, VWR Chemicals BDH®.
- Mucin from the porcine stomach (type III), Sigma Aldrich.

Materials used for synthesis and characterization of PVA-CHO/CHIT-SH Hydrogels

- Polyvinyl alcohol (PVA), 86-89% hydrolyzed, Nagart Kft.
- Low molecular weight (50–190 kDa) chitosan (CHIT, $C_{12}H_{24}N_2O_9$), ≥ 75 % deacetylation, Merck Ltd.
- Tilorone dihydrochloride ($C_{25}H_{34}N_2O_3 \cdot 2HCl$), Merck KGaA.
- 1-(3-Dimethylaminopropyl)-3-ethylcarbodiimide hydrochloride (EDC, $C_8H_{17}N_3 \cdot HCl$), 98+%, Thermo Fisher GmbH.
- 3-Mercaptopropionic acid ($C_3H_6O_2S$), Fluka Analytical.
- 4-Formylbenzoic acid (FBA, $C_8H_6O_3$, 97%), Sigma-Aldrich.
- N, N′-dicyclohexylcarbodiimide (DCC, $C_{13}H_{22}N_2$, 99%), Sigma-Aldrich.
- 4-(dimethylamino)pyridine (DMAP, $C_7H_{10}N_2$, ≥99%), Sigma-Aldrich.

- Ethylenediaminetetraacetic acid tetrasodium salt dihydrate (EDTA), Sigma-Aldrich.
- 5,5′-dithio-bis-(2-nitrobenzoic acid) (Ellman's reagent, $C_{14}H_8N_2O_8S_2$), Thermo Fisher Inc.
- 3-(4,5-dimethylthiazol-2-yl)-2,5-diphenyltetrazolium bromide (MTT), Sigma Aldrich.
- Sodium dodecyl sulfate (SDS, $NaC_{12}H_{25}SO_4$), Sigma-Aldrich
- Dimethyl sulfoxide (DMSO), Merck KGaA.
- Lysozyme from chicken egg, Sigma-Aldrich.

All chemicals were used as received without further purification.

4.1.2. Synthesis of poly(ethylene succinate) PES

Materials used for synthesis and characterization of Poly(ethylene succinate) PES.

- Succinic acid ($C_4H_6O_4$, SA), 99%, Molar Chemicals Kft.
- Ethylene glycol ($C_2H_6O_2$), 99.99%, Molar Chemicals Kft.
- Nimodipine (NIMO) ($C_{21}H_{26}N_2O_7$), 98+%, Alpha Aesar.
- Sodium hydroxide (NaOH), Merck KGaA.
- Dimethyl sulfoxide (DMSO), Merck KGaA.
- Tetrahydrofuran (THF), Sigma-Aldrich.
- Methanol, Sigma-Aldrich.
- Sodium dodecyl sulfate (SDS, $NaC_{12}H_{25}SO_4$), Sigma-Aldrich.

All chemicals were used as received without further purification.

Materials used to prepare phosphate-buffered saline (PBS, pH ~ 7.4) solution.

- Sodium dihydrogen phosphate monohydrate ($NaH_2PO_4 \cdot H_2O$), Sigma-Aldrich.
- Di-sodium hydrogen phosphate dodecahydrate ($Na_2HPO_4 \cdot 12H_2O$), Molar Chemicals Kft.
- Sodium chloride (NaCl), Molar Chemicals Kft.

4.2. PVA-SA-CYS-MMC polymeric prodrug

4.2.1. Synthesis of succinic anhydride precursor

The succinic anhydride was produced using the following protocol [220]. Under a nitrogen atmosphere, 15 g of succinic acid was mixed thoroughly with 25 mL of acetic anhydride in a 100 mL round-bottom flask fitted with an anhydrous calcium chloride tube closed reflux condenser. The reaction mixture was gently heated on the steam bath with frequent shaking till a clear solution was formed, then left under the same condition for 1 hr to guarantee the

completion of the reaction. The flask was cooled to ambient temperature before being placed in an ice bath; the resulting white crystals were filtered and washed with a low amount of diethyl ether, and then dried under a vacuum. The collected product weighed 10.3 g, with a yield of 81.1%.

4.2.2. Synthesis of PVA-SA with different COOH content

Succinated PVA (PVA-SA) with various COOH contents was prepared by the modification of PVA with succinic anhydride in accordance with the modified protocol reported [221]. Briefly, 1 g of PVA was dissolved in 8.6 ml of DMF followed by adding the succinic anhydride with different molar ratios (8, 16, 24, 32, 63.3, 95, and 126.6 molar% for OH content of PVA which correspond to 0.126, 0.25, 0.38, 0.5, 1, 1.5, 2 g, respectively) and then added 0.05 g of anhydrous sodium acetate as catalyst. The reaction mixture was continuously magnetically stirred at 45 °C for up to 24 hrs. An excess of diethyl ether was then used to precipitate the reaction product. The resultant crude product was then purified using repeated DMF dissolving and excess ether precipitation, followed by ether washing and drying under a vacuum.

4.2.3. Synthesis of PVA-SA-CYS-MMC polymeric prodrug NPs

The following protocol was used to produce polymeric prodrug of MMC as shown in **Figure 10**: 10 mL of 1% *w/v* aqueous PVA-SA solution with different carboxylic contents (0.5, 1.65, and 3.4 mmol/g of the COOH group; which correspond to 3.1, 10.4, and 21.5% substitution degrees, respectively) was prepared followed by adding 4 mg of MMC and 1 equivalent of cysteamine to COOH content (3.9, 7.3, and 9.6 mg; 0.05, 0.165, and 0.34 mmol, respectively) to the polymer solution, and then 1.5 equivalent of EDC to COOH content (14.4, 47.4, and 97.8 mg; 0.075, 0.248, and 0.51 mmol, respectively) was added. The reaction mixture was continuously magnetically stirred (~250 rpm) for 3 hrs at room temperature. Following the reaction period, the reaction mixture was added to an excess of ethanol to precipitate the polymeric prodrug, then centrifuged (5000 rpm, 20 min) to collect the product and washed with a 3:1 acetone-water system, and then the collected product was dried under the vacuum. The percent of MMC binding (**Equation 6**) was determined by measuring the absorbance of the supernatant to determine the unbound MMC using UV-VIS spectroscopy and the predetermined calibration curve of MMC.

$$\text{Percent of binding (\%)} = \frac{\text{Total MMC-unbound MMC}}{\text{Total MMC}} \times 100 \qquad (6)$$

4.3. PVA-CHO/CHIT-SH hydrogel

4.3.1. Synthesis of 4-formylbenzoate PVA (PVA-CHO)

The PVA containing CHO pendant groups (**PVA-CHO**, **Figure 20**) was synthesized by using the Steglich esterification process [222], as follows: 1 g of PVA was dissolved in 15 mL of DMSO, followed by adding 0.6 g of 4-formylbenzoic acid and 0.45 g of DMAP, which was then mixed for 5 min before the addition 0.62 g of DCC. The reaction was continuously magnetically stirred at room temperature for 24 hrs. Following the reaction time, to remove the insoluble byproduct of the coupling agent (N, N-dicyclohexyl urea), the reaction mixture was filtered through a 0.1 μm Whatman syringe filter, and then the excess amount of ethanol (~150 mL) was added to the filtrate for precipitating the crude product that was collected via centrifugation (5000 rpm, 20 min), followed by washing three times with ethanol, and finally dried under vacuum. The degree of functionalization (**Equation 7**) of PVA with CHO was determined using the acid-base titration method: the reaction mixture was titrated before and after the reaction with 0.1 N NaOH to determine the reacted COOH amount and then using:

$$\text{Functionalization degree (mol\%)} = \frac{\text{no. of mmol reacted COOH}}{\text{no. of mmol available OH in PVA}} \times 100 \quad (7)$$

4.3.2. Synthesis of 3-mercaptopropionate chitosan (CHIT-SH)

The modification of chitosan was carried out through the conjugation reaction between 3-mercaptopropionic acid and chitosan to produce the thiolated chitosan (CHIT-SH). In brief, 1.2 mL of 3-mercaptopropionic acid (13.7 mmol) was added to 25 mL of 2% *w/v* aqueous chitosan solution (using 2.5% *v/v* aqueous acetic acid), followed by adding 2.68 g of EDC (13.7 mmol) to the reaction mixture. The reaction was continuously magnetically stirred at room temperature for 6 hrs. Following the reaction time, an excess amount of ethanol was added to the reaction mixture to precipitate the crude product that was collected via centrifugation, followed by washing it several times with ethanol, and eventually drying under a vacuum.

4.3.3. Preparation of PVA-CHO/CHIT-SH hydrogel with Tilorone-loading

The PVA-CHO/CHIT-SH hydrogel was formed by combining the (2, 5, and 10% *w/v*) PVA-CHO solution in a 1:1 ethanol-water system with (2, 5, and 10% *w/v*) CHIT-SH solution in distilled H_2O. Thus, the same concentration ratio of polymer solutions was used to produce self-assembled hydrogel at room temperature. Tilorone was encapsulated into the hydrogel network by dissolving 2.3 mg in 1 mL of a PVA-CHO solution and then adding to 1 mL of CHIT-SH solution to produce Tilorone hydrogel with 1.15 mg/mL Tilorone content as aforementioned.

4.4. Poly(ethylene succinate) (PES) polyester

4.4.1. Synthesis of PES with different molecular weights

The direct melt polycondensation method was used to produce poly(ethylene succinate) (PES) as follows; 2.1 g of succinic acid (17.78 mmol) and 1 mL of ethylene glycol (17.78 mmol) with an equimolar ratio of monomers were heated in the oil bath at about 185 °C under continuous magnetic stirring (300 rpm). The polymerization process was quenched at predetermined time intervals (40, 50, 60, 70, 80, and 100 min) by rapidly cooling the reaction solution by placing the reaction flask in an ice bath. The crude product was then dissolved in THF, followed by precipitation with >15-fold methanol, centrifugation, and methanol washing twice. The obtained purified polyester was dried at 40 °C for 24 hrs.

4.4.2. Preparation of NIMO-loaded PES nanoparticles

The precipitation method (see **Figure 8**) was used to prepare the encapsulated form of NIMO into PES. The preparation was as the following; 22.5 mg of NIMO (5% w/w nominal NIMO content) and 450 mg of polyester were dissolved in 5 mL of DMSO, followed by dropwise addition of the obtained solution to 5 mL of distilled H_2O under strong magnetic stirring to produce the encapsulated form NIMO-loaded PES NPs. Centrifugation (Hermle centrifuge Z 36 HK, 5000 rpm×10 min) was used to collect the product, which was subsequently washed with distilled H_2O and lyophilized. To get bare NIMO microparticles without a PES polyester shell as a reference, the same method was done without utilizing polyester. The encapsulation efficiency of NIMO loaded to PES was determined by using **Equation 8:**

$$\text{Encapsulation efficiency (\%)} = \frac{\text{amount of drug in nanoparticles}}{\text{the total amount of drug added}} \times 100 \quad (8)$$

where the free drug concentration in the supernatant, as determined by UV-VIS spectroscopy, was used to calculate the amount of the drug in nanoparticles.

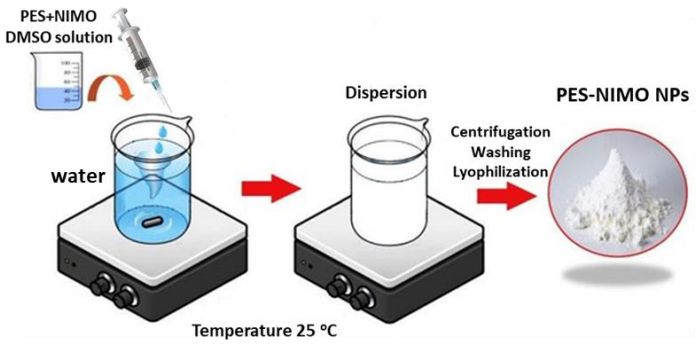

Figure 9. The schematic diagram for the precipitation method producing NIMO-loaded PES nanoparticles.

4.5. Methods of characterization

4.5.1. Fourier transform infrared spectroscopy (FTIR)

FTIR measurements were carried out to determine the chemical structure of modified and synthetic polymers to confirm the success of the polymerization and modification process via using a BioRad FTS-60A FT-IR spectrometer and also Avatar 330 FTIR spectrometer (Thermo Nicolet, Unicam Hungary Ltd., Budapest, Hungary). The spectra were recorded by the accumulation of 128 scans between 4000 and 500 cm^{-1} at a resolution of 2 cm^{-1}. The sample was used in dry solid form.

4.5.2. Proton nuclear magnetic resonance (^{1}H-NMR)

^{1}H-NMR spectroscopy measurements were carried out to study the chemical structure of polymers. NMR spectra were recorded with a Bruker DRX 500 spectrometer (Bruker BioSpin, Karlsruhe, Germany) instrument at 500 (1H) MHz at room temperature in D_2O and DMSO-d^6 using tetramethylsilane (TMS) as an internal standard. Chemical shifts are recorded in ppm (δ scale). In the case of PES samples, the number of repeating units (n) and the number average polymer molecular weights (M_n) were determined by the method reported by Izunobi and Higginbotham [223].

4.5.3. Gel permeation chromatography (GPC)

GPC measurements were used to determine the average molecular weight and its distribution of polyester (PES) samples using the Waters 2414 GPC system with an RI detector (Ultrastyragel 1000 Å, 500 Å, 100 Å). A 0.2 μm Millipore (Millex filter) membrane was used to filter the polyester samples after they had been dissolved in tetrahydrofuran. 100 μL of the 0.1% sample solution was injected while the eluent flow rate was set at 1.0 mL/min. A third-order polynomial calibration curve was described, and the polystyrene standards were employed for the calibration.

4.5.4. A transmission electron microscope (TEM)

TEM measurements were utilized to investigate the particle size and the morphology of prepared particles. The measurements were carried out with a Tecnai G^2 20 X-TWIN instrument (FEI, Hillsboro, Oregon, USA) with a 200 kV acceleration voltage and a Philips CM-10 transmission electron microscope with a 100 kV acceleration voltage. The sample preparation was carried out by dispersing samples in a suitable solvent and drying them on a carbon film on copper grids (200 mesh).

4.5.5. Differential scanning calorimetry (DSC)

DSC measurements were performed to investigate the thermal behavior of the modified and synthetic polymers. The measurements were carried out by utilized using a Mettler-Toledo 822^e instrument. In the case of initial PVA and its modified derivatives for the polymeric prodrug part, measurements were carried out on dry samples heated at a rate of 5 °C/min from 25 to 500 °C. In addition to these data, DSC was used to determine the water desorption enthalpy values for the swollen PVA-based hydrogels. To prepare 2 wt% hydrogels, the polymer samples were swollen in distilled H_2O, and the swelling/dissolution equilibrium was reached overnight. The obtained solutions were centrifuged at 14500 rpm for 10 min with an Eppendorf miniSpin device, the supernatant was eliminated, and the concentrated polymer gel (sediment) was measured. These experiments were carried out in the 25–200 °C temperature range with a heating rate of 5 °C/min.

While in the case of the initial monomers and the synthetic polyesters, samples were heated from 25 to 500 °C at a rate of 5 °C/min. To determine the crystallization temperature of PES-80 min, the heating and cooling curves of PES-80 min were also recorded; the sample was heated at a heating rate of 5 °C/min from 25 to 120°C (first heating stage), then cooled to 25°C at a heating rate of -5 °C/min (cooling stage). Using a Mettler-Toledo TGA/SDTA 851^e equipment, thermogravimetric (TGA) analysis was conducted to examine the heat degradation and thermal behavior of PES-80 min. The sample was heated at a rate of 5 °C/min from 25 to 500 °C.

4.5.6. Energy dispersive X-ray (EDX)

For the elemental composition study of modified polymers, EDX measurements were done using the Röntec EDS detector at 20 keV, and morphology was studied using field emission scanning electron microscopy (SEM, Hitachi S-4700 microscope) at 20 kV acceleration voltage. For this measurement, dried powder samples were put in the sample holder.

4.5.7. X-ray diffraction (XRD) measurements

Using a Philips X-ray diffractometer (XRD), which had an applied range of 2-35° (2Θ) and a step size of 0.02° (2Θ), the X-ray diffraction (XRD) measurements of the NIMO, PES, and NIMO loaded PES was investigated.

4.5.8. Dynamic light scattering (DLS)

Dynamic light scattering (DLS) was used to measure the zeta potential values and particle sizes of the PES and PES-NIMO particles dispersion in sterilized distilled H_2O and PBS buffer solution (pH 7.4) via using DLS (SZ-100 HORIBA Scientific, HORIBA, Ltd., Kyoto, Japan) system. To calculate the standard deviation, the measurements were carried out five times at 25 ± 0.1 °C.

As we shall see later, DLS was also employed to determine the PVA-SA particle size during the self-assembly particle formation measurement.

DLS was also used to measure the molecular weight (M_w) of the initial PVA. The experiments were carried out with various polymer concentrations (1–10 mg/mL) at a fixed scattering angle (90°) and using 0.22 μm Millipore membrane filters to filter all prepared PVA solutions prior to measurement. To determine the absolute scattering light intensity, toluene was utilized as a standard. The M_w may be computed using the angle (θ) and concentration (C) dependence of $KC/\Delta R_\theta$ according to the Debye plot formulation (**Equation** (**9**))

$$\frac{KC}{R_\theta} = \left(\frac{1}{M} + 2A_2C\right) \qquad (9)$$

where *K* stands for an optical constant, *C* for the concentration, R for the Rayleigh ratio, M for the molecular weight, and A_2 for the second virial coefficient.

4.5.9. Viscosity measurements

The viscosity measurements were conducted using a Physica MCR 301 rheometer (Anton Paar, Graz, Austria) fitted with a roller geometry cylinder type (DG 26.7) for PVA-SA samples and PES samples, while with a plate-plate type (PP20-SN13684; d = 4.5 mm) for hydrogel samples.

In the case of the PVA-SA samples, we attempt to verify an appropriate concentration for particle formation. At varying concentrations (1, 2, 3, and 4 wt%), aqueous PVA-SA solutions (with 21.5% nominal cross-linking density according to the OH/COOH ratio) were prepared. Then, 1.5 equivalents of EDC to COOH content were added to the prepared solutions, and the change in viscosity was recorded at a temperature of 25 °C.

For the hydrogel samples, we attempt to investigate the pH-dependent of the dynamic hydrogels. Using buffer solutions for the CHIT-SH polymer solution, aqueous CHIT-SH and PVA-CHO solutions were prepared at different concentrations (2 and 3 wt%) and pH ranges (3–8), and then the same volume ratios of the two solutions were mixed and left for 5 minutes for complete gel formation, then the viscosity of the obtained hydrogel was measured.

Furthermore, the viscosities of two separated solutions containing 2% *w/v* PVA-CHO and 2% *w/v* CHIT-SH separately were compared to the viscosity of a 2% *w/v* PVA-CHO/CHIT-SH hydrogel at 37 °C to indicate PVA-CHO crosslinking with CHIT-SH via the Schiff-base mechanism.

In the case of PES samples, we are trying to investigate the liquefaction/solidification temperature, so the change in viscosity as a function of temperature was measured in a temperature range of 30 to 150 °C. For this measurement, PES-40 min and PES-80 min were both used. The sample was heated to around 160 °C in an oil bath, melted, and then quickly transferred to the preheated instrument, where it was thermostated at 150 °C before being measured for viscosity. As the relevant viscosity values were recorded, the temperature of measurement was gradually reduced until it reached roughly 30 °C.

Viscometric measurements of the PES samples were also performed using an Ostwald viscometer to estimate the coefficient (K_η) and exponent α based on the Kuhn-Mark-Houwink-(KMH) equation (**Equation** (**10**)) by using a series of PES samples with various molecular weights and measuring the relevant intrinsic viscosity [η] values. Using an Ostwald viscometer, the specific viscosity (η_{sp}) (**Equation** (**11**)) of each PES solution (in DMSO) with a concentration range of 0.1–0.3 g/mL was measured at room temperature. The reduced viscosity (η_{red}) that was calculated using **Equation** (**12**) was then plotted against the concentration (g/mL), and the intrinsic viscosity [η] was calculated from the intercept value. Plotting the logarithm of intrinsic viscosity [η] for three distinct PES against the logarithm of relative molecular weights allowed for the determination of the K_η and exponent (α), which were both obtained from the intercept value and slope, respectively [224].

$$[\eta] = KM^{\alpha} \quad (10)$$

$$\eta_{sp} = \frac{t\text{-}t_o}{t_o} \quad (11)$$

$$\eta_{red} = \frac{\eta_{sp}}{c} \quad (12)$$

where t_o is the flow time of pure DMSO solvent, t is the flow time of the PES solution (in DMSO), c is the concentration of PES solution, K_η is the KMH coefficient appropriate for a particular polymer-solvent system, and α is the KMH exponent that describes the conformation of macromolecules in a solvent [224].

4.5.10. Mucoadhesive measurements

For mucoadhesive polymeric prodrug particles

PVA-SA-CYS mucoadhesive characteristics were assessed using oscillatory rheology measurements on a Physica MCR 301 rheometer (Anton Paar, Graz, Austria) with a cone/plate type (cone angle 0.99°, gap height in the middle of the cone 0.054 mm, and diameter 11.95 mm) system. 1% *w/v* PVA-SA-CYS and 1% *w/v* mucin aqueous solutions were prepared for the measurement, the solutions were combined in identical amounts, and after overnight, the gelation was determined. The gelation of the PVA-SA-CYS, mucin, and mixture was monitored at 25 °C at an angular frequency of 10 Hz, and the storage modulus (G') and loss modulus (G") were calculated throughout a strain range of 0.1 to 10%.

A simple adsorption experiment was also used to demonstrate the mucoadhesive characteristics of the polymeric particles. From the polymeric particles (PVA-SA and PVA-SA-CYS), 10 mL of 1 wt% aqueous solution was made, and a 7 cm long pig intestine purchased from a local slaughterhouse was immersed in these turbid dispersions. The produced dispersion was stirred at a speed of 200 rpm, and the turbidity decrease caused by particle surface adsorption on the intestinal membrane was evaluated as a function of time using an ISO Portable Turbidity Meter - HI98703 (Hanna instruments, Cluj-Napoca, Romania).

For mucoadhesive self-assemble hydrogel

Using a TA.XT plus Texture Analyzer (Metrohm, Budapest) and a 1 kg load cell, the mucoadhesive characteristics of the 2% *w/v* PVA-CHO/CHIT-SH hydrogel were examined. To simulate an *in vivo* mucosal surface, a pig intestinal membrane obtained from a nearby slaughterhouse was brought into contact with the hydrogel, which was attached to a cylinder probe with a 1 cm diameter using double-sided adhesive tape. The results of five parallel measurements were provided as mean SD. The disk was removed from the real mucosal surface by pushing up on the cylinder probe at a predefined speed of 2.5 mm per minute after providing a 2500 mN preload for 3 minutes. Based on the area under the "force vs. distance" curve, the work of adhesion (mN/mm) value was calculated to evaluate the mucoadhesive behavior.

4.5.11. Water contact angle (Θ) measurements

The drop shape analysis equipment (Easy Drop, Krüss GmbH, Hamburg, Germany) was used to measure the water contact angle (Θ) at 25.0 ± 0.5 °C. The device was equipped with a steel syringe needle (0.5 mm in diameter), and the test liquid was distilled H_2O. The Young - Laplace equation was employed with the CCD camera goniometer to mathematically define the drop

contour of the acquired photo using DSA100 software, and the Θ was characterized as the slope of the contour line at the point of contact of three phases. Five parallel measurements were carried out with determining the average and stander deviation values. The films preparation was performed by using of spray-drying technique in the case of modified PVA samples and the solvent-casting technique for hydrogel samples, while by melting PES over the surface of a glass sheet and then cooling to room temperature, polyester films with varying molecular weights were formed.

4.5.12. Characterization methods for polymeric prodrug of MMC

Carboxyl content determination

Acid-base titration was used to assess the available carboxyl group in the succinate polymer (PVA-SA) by dissolving 0.1 g of PVA-SA in 10 mL of distilled H_2O with magnetic stirring and warming at 45 °C to achieve a transparent solution. At room temperature, the produced solution was titrated against 0.1 M NaOH in the presence of a phenolphthalein indicator. The titration technique was done three times to calculate the standard deviation (presented as error bars).

Thiol content determination by Volhard's silver nitrate method

Volhard's silver nitrate method was used for determining thiol content. In 25 mL of 0.01 M silver nitrate solution, 100 mg of cysteamine thiolated PVA with mucoadhesive characteristics (PVA-SA-CYS) was added. Before titration, the reaction mixture was carefully covered to avoid light and stirred for 4 hrs. After that, unreacted silver nitrate was detected using ferric nitrate as an indicator in a titration with standardized 0.01 M KSCN. The titration ended when the red color complex $[Fe(SCN)_6^{3-}]$ was formed from an excess of thiocyanate anion (SCN) and the ferric ion (Fe^{3+}) of the indicator [225]. According to **Equation (13)**, the quantity of polymer thiol content (mol/g) was determined from the volume (V) of added KSCN solution and concentration (C) of the KSCN solution.

$$\text{Thiol content (mol/g)} = \frac{0.25 - (C \times V)}{\text{wt of PVA}} \qquad (13)$$

Characterization of self-assembled particles formation

Based on the turbidity measurement carried out using an ISO Portable Turbidity Meter—HI98703 (Hanna instruments, Cluj-Napoca, Romania), liner macromolecule self-assembled particle formation through ester linkages was investigated. A 1.5 molar equivalent of EDC to COOH content was introduced to a 2 % *w/v* of PVA-SA (with 21.5% cross-linking density)

aqueous solution, which was then monitored for changes in turbidity over time while also evaluating particle size by DLS (SZ-100 HORIBA Scientific, HORIBA, Ltd., Kyoto, Japan).

Anticancer and antibacterial activity measurements

The anticancer characteristics of MMC and encapsulated forms of MMC were measured by cytotoxicity test. During these tests, 3 mg of MMC (free or encapsulated form) was placed in a cellulose membrane (Sigma-Aldrich, avg. flat width 10 mm (0.4 in.)) and immersed in 10 mL of PBS (pH 7.4, 37°C) buffer solution under gently stirring. After 1, 3, 5, and 7 days, 0.5 mL of the releasing medium was collected, and the IC_{50} values were evaluated using the 3-(4,5-dimethylthiazol-2-yl)-2,5-diphenyltetrazolium bromide (MTT) assay in 96-well cell culture microplates. Human (Hep-2c) carcinoma cells were seeded at a density of 1×10^4 cells/well and cultured at 37°C for 24 hrs. The tested MMC and encapsulated forms were serially half diluted in EMEM medium in microtiter plates after 24 hrs. The compounds were diluted in 100 µl of the medium. MMC concentration was also determined spectrophotometrically in parallel. Except for the medium control wells, compounds were diluted in the medium and added to Hep-2c cells in each well after dilution. Following a 24-hour incubation at 37°C, each well was injected with 20 µl of (5 mg/ mL) MTT solution (Sigma-Aldrich, Germany). After a 4-hour incubation at 37°C, 100 µl of 10% sodium dodecyl sulfate (SDS, Sigma-Aldrich) was added into each well to dissolve the generated formazan, and the optical density (OD) was measured after 24 hrs. Cell growth was calculated by measuring the OD at 540 nm (ref. 630 nm) with a Multiscan EX ELISA reader (Thermo Lab systems, Cheshire, WA, USA). The solvent did not affect cell growth in the experiment at the doses used for IC_{50} estimations. The IC_{50} values and standard deviations of triplicate trials were calculated using GraphPad Prism software (GraphPad Software, San Diego, USA) version 5.00 for Windows with nonlinear regression curve fitting.

The antibacterial activity of the MMC against Methicillin-resistant *Staphylococcus aureus* (MRSA) bacterial strains was also *in vitro* assessed by measuring their inhibition zones using the conventional disk diffusion technique [226]. The sterile filter paper (D = 6 mm) discs wet with the MMC releasing solutions (10 µl of solutions) were placed on Tryptic Soy Agar plates (Sigma) and inoculated with the applicable bacterial suspensions (inocula of 0.5 McFarland's standard). Another plate was inoculated with no disks as a bacterial growth control. The disks were placed within 15 minutes of inoculating the plates, and incubation commenced within 15 minutes of the disks being applied (according to EUCAST regulations) [226]. The plates were incubated at 37°C for 24 hrs. The diameters of the inhibition zones (Minimum Inhibitory

Concentrations - MICs) caused by the examined drugs were measured (including disc diameter). A chemical was considered inactive when the diameter of the inhibition zones in the observed concentrations was less than 10 mm. All experiments were conducted in triplicate.

4.5.13. Characterization methods for PVA-CHO/ CHIT-SH hydrogel

Solubility measurement of initial and modified chitosan

The solubility of chitosan and CHIT-SH was assessed by combining 50 mg of polymer with 10 mL of PBS solution (with pH values ranging from 6.1 to 8.1) while vigorously stirring for 24 hrs at room temperature. The resulting suspension was then centrifuged for 30 minutes at 10,000 rpm. To calculate the amount of polymer that is soluble, the supernatant was removed, and the recovered polymer was dried in an oven overnight at 50 °C before being weighed.

Thiol content determination by Ellman Method

The thiol content of CHIT-SH was determined using Ellman's reagent. An Ellman's reagent solution was prepared by dissolving 4 mg of Ellman's reagent in 1 mL of pH = 8 phosphate buffer with 1 mM EDTA (reaction buffer). In 0.1 N HCl solution (pH = 3.8), CHIT-SH was dissolved in the range of 0.5–1.5% *w/v*. The reaction was then allowed to run for 2 hrs after being mixed with 2.50 mL of reaction buffer, 250 µL of CHIT-SH solution, and 50 µL of Ellman's reagent solution. Following the reaction period, the reaction mixture was filtered using a 0.22 µm-pore PVDF membrane filter (Teknokroma, Barcelona, Spain), and the absorbance of the filtrate was determined using a Jasco V-740 UV/Vis Spectrophotometer (ABL&E-JASCO, Vienna, Austria) at 412 nm. Using L-cysteine standards in the concentration range of 0.044–0.22 mg/mL, thiol group content was calibrated. Data were provided as mean ±SD, and each measurement was done in triplicate.

Determination of substitution degree of thiolated Chitosan

The degree of substitution (DS%) of CHIT with 3-mercaptopropionic acid was determined using the following (**Equation** (**14**)) based on the total number of accessible reaction sites in the chitosan chains before functionalization and the results of Ellman's approach:

$$DS\% = \frac{N_{Ellman} \times 161}{W_{CHIT} \times DD} \times 100 \qquad (\mathbf{14})$$

where N_{Ellman} is the number of thiols (SH) groups (mol) acquired by Ellman's technique, 161 is the average molar mass of 2-amino-2-deoxy-D-glucose units of chitosan ($g \cdot mol^{-1}$), W_{CHIT} is

the used chitosan mass (g), DD is the degree of deacetylation of CHIT that can be determined via the ^{1}H-NMR spectrum of CHIT and using **Equation** (**15**):

$$DD(\%) = 100 - \left[\frac{[\frac{A_{CH_3}}{3}]}{A_{H_2}} \times 100\right] \quad (15)$$

where A_{CH3} is the methyl hydrogen area of the acetyl (acetamide) group at 2.01 ppm and A_{H2} is the methyl hydrogen area of the C-2 carbon of glucosamine ring at 3.1 ppm [227].

Swelling measurements

Gravimetric measurements were used to examine the swelling of lyophilized PVA-CHO/CHIT-SH hydrogels at various concentrations. Around 50 mg of lyophilized dry xerogel was added to 10 mL of PBS buffer solution at 37°C, and the weight difference between the swelled and nonswollen hydrogel was tracked by drying the hydrogel's surface with filter paper and measuring it using an analytical scale at various intervals. Using **Equation** (**16**), the swelling ratio (g/g) was determined during 5 hrs of the measurements:

$$\text{Swelling ratio (g/g)} = \frac{m_t - m_o}{m_o} \quad (16)$$

where m_o is the initial weight of dry xerogel and m_t is the weight of swollen hydrogel at a different time.

In-vitro degradation measurements

Gravimetric measurements were used to examine the in vitro degradation of PVA-CHO/CHIT-SH hydrogel. The weight of the swollen hydrogel was calculated after swelling about 50 mg of lyophilized xerogel in 10 mL of PBS solution for 24 hrs. The hydrogel was then incubated at 37°C in 0.15% lysozyme (in PBS) solution, and its weight was measured at various intervals using a filter paper to dry the hydrogel's surface water prior to the weighting procedure. **Equation** (**17**) was used to compute the degradation percentage:

$$\text{Degredation (\%)} = \frac{m_i - m_t}{m_i} \times 100 \quad (17)$$

where m_i is the weight of the initial swollen hydrogel and m_t is the remaining weight of the hydrogel at a different degradation time.

Self-healing ability measurements

In order to conduct the self-healing experiment, a 2% *w/v* PVA-CHO/CHIT-SH hydrogel in two distinct colors—blue from methylene blue dye and bright red from rhodamine B dye—was first prepared. Then, the two hydrogels were simply contacted, and the healing process was observed by taking digital photos at various intervals (t = 0, 15, and 60 min).

Using the continuous step strain technique, which involves applying a low shear strain of 1.0% at 10 rad/s, a high strain of 500% for 60 s, and a low strain of 1% for hydrogel recovery for 60 s, the healing properties of the gels were also evaluated by rheology. Three cycles of the step strain sweep were performed. Physica MCR 302 Modular Compact Rheometer (Anton Paar, Graz, Austria) was used to examine the healing characteristics and the rheological properties of the hydrogels to identify the high strain that can break down the hydrogel's network structure. At a temperature of 37 °C, measurements were made using parallel plate-type measuring equipment (diameter: 25 mm, gap height: 0.30 mm).

Injectability test of hydrogel

The injectability of PVA-CHO/CHIT-SH hydrogel was examined by transferring both 7% *w/v* PVA-CHO (in ethanol-water) and 7% *w/v* CHIT-SH (in distilled H_2O) solutions to the dual syringe. By depressing the syringe and immersing it in a PBS solution (pH 7.4) at 37°C, the hydrogel was prepared.

Biocompatibility of the hydrogel

The cytotoxicity test was carried out using the 3-(4,5-dimethylthiazol-2-yl)-2,5-diphenyltetrazolium bromide (MTT) assay in 96-well cell culture microplates. 1×10^4 cells/well of MRC-5 (human embryonic lung fibroblasts) cells were seeded and incubated for 24 hrs at 37°C. Then, the disc-shaped hydrogel samples (5 and 10% *w/v*) were placed in the cell solution, with the exception of the medium control (MC) wells. Each well received 20 µL of a (5 mg/mL) MTT solution (Sigma–Aldrich, Germany) injection following a 24-hour incubation period at 37°C. After a 4-hour incubation at 37°C, 100 µL of 10% sodium dodecyl sulfate (SDS, Sigma-Aldrich) was added to each well to dissolve the formazan that had formed. After 24 hrs, the optical density (OD) was measured. When compared to the cell control, the solvent in the experiment did not affect the proliferation (cell growth) of the cells at the concentrations used in the cytotoxicity test (CC).

4.5.14. Characterization methods for synthesized PES samples

Determination of polycondensation yield

By measuring the unreacted COOH group of succinic acid using the acid-base titration method, the degree of polymerization was determined. To do this, 100 mg of the unpurified polymers were thoroughly dispersed in 10 mL of distilled H_2O, and the resulting solution was then titrated with 0.1 M NaOH in the presence of a phenolphthalein indicator. The same procedure was then repeated using the initial reaction mixture (0 min of reaction time) as a reference. **Equation** (**18**) was used to calculate the polymerization conversion, and the Carothers equation (**Equation** (**19**)) was used to determine the degree of polymerization ($\overline{X}_n$) based on monomer conversion (P, the extent of reaction):

$$\text{Percent of polymerization (\%)} = \frac{\text{Initial COOH- Unreacted COOH}}{\text{Initial COOH}} \times 100 \quad (\mathbf{18})$$

$$\text{Degree of polymerization } (\overline{X}_n) = \frac{1}{1\text{-P}} \quad (\mathbf{19})$$

Solubility/precipitation measurements of PES

The solubility or precipitation properties of synthesized polyesters in the DMSO/H_2O binary system were studied as follows: 100 mg of polyesters (with different molecular weights) were dissolved in 10 mL of DMSO, which is a good solvent. Using an ISO Portable Turbidity Meter-HI98703 (Hanna Instruments) under continuous magnetic stirring at 25 °C, measurements were carried out on the precipitation of the resulting polyester solutions as a function of the dropwise addition of distilled H_2O (as a poor solvent).

The fractional precipitation technique was also utilized to calculate the constants of the Schulz equation (**Equation** (**20**)) typical of the solvent-polymer-precipitant systems A and B [228]. If we know the relevant coefficients (A and B), this approach is also acceptable for determining average molecular weight, according to the Schulz hypothesis. The linearized form of the Schulz equation (**Equation** (**20**)) was used to estimate the solvent-polymer-precipitant system's characteristic A and B constants. For this purpose, different fractions of PES with different molecular weights and known the corresponding volume fraction of water that was used to precipitate the PES from DMSO solution (good solvent).

$$\frac{1}{M} = \frac{100}{B}\Phi - \frac{A}{B} \quad (\mathbf{20})$$

By plotting the reciprocal of the molecular weight determined by ^{1}H-NMR (1/M) of a particular PES sample as a function of volume fraction (Φ) of H_2O, the slope of this line provides the value of B, and then A can be calculated from the value of B and the intercept value [228].

The turbidimetric titration, which was first developed by Elias and then improved by Cornet and van Ballegooijen [229], was used to evaluate the theta (Θ) compositions of mixed solvents for polyester. As a non-solvent, distilled H_2O was introduced dropwise to the PES-80 min solution in DMSO under continuous magnetic stirring until the start of the phase separation (precipitation) at room temperature. The turbidity was measured using an ISO Portable Turbidity Meter-HI98703 (Hanna instruments). The polyester (PES-80 min) solution was used in this technique at various concentrations (0.2–1% *w/v*). The Θ-composition was calculated from extrapolation to pure polyester (Φ_{PES} = 1) by plotting the logarithm of the volume fraction of H_2O (non-solvent) needed to initiate precipitation as a function of the logarithm of the corresponding volume fraction of polyester [229].

4.5.15. Characterization methods for NIMO-loaded PES samples

Study the precipitation properties of NIMO and PES in DMSO/ H_2O system

Since the nanoprecipitation technique was used to encapsulate NIMO into PES, first the solubilities of the NIMO drug and PES polyester were investigated in a DMSO/ H_2O (good solvent/poor solvent) system. An Ocean Optics USB2000 UV-VIS Spectrometer (Ocean Optics Ins., USA) with a 1 cm quartz cuvette at λ = 550 nm was used to monitor the change in absorbance caused by the formation of the precipitated drug or polymer particles. For this, 5 mL of 0.1% *w/v* PES-80 min and NIMO solutions were prepared in DMSO. This was followed by the dropwise addition of 15 mL of distilled H_2O under strong magnetic stirring to the prepared solution and recording the change in the absorbance.

The precipitation of PES-80 min and NIMO solutions was measured in a concentrated system to determine the optimal volume ratio at which both polyester and NIMO drug will be precipitated with each other to generate NIMO-loaded PES NPs. Before the measurement, 10 mL of 0.3% *w/v* NIMO and 6% *w/v* PES were prepared using DMSO as the solvent. The prepared NIMO or PES DMSO-based solution was dropwise added to 5 mL of distilled H_2O under strong magnetic stirring at 25 °C. The absorbance was continuously recorded as a function of the volume of solution added.

Stability of NIMO and PES-NIMO in the aqueous medium

Sedimentation measurement was used to assess the stability of NIMO and PES-NIMO in an aqueous medium, and the measurements are as follows: 10 mL of phosphate buffer saline solution (PBS) was used to prepare 0.05% *w/v* of NIMO-loaded PES with 5% *w/w* NIMO content referred to the polymer. The PES-NIMO dispersion was sonicated for 5 minutes and then quickly placed in a turbidimeter, and the sedimentation of the dispersion was monitored at 25 °C using an ISO-HI98703 portable turbidimeter (Hanna Instruments). Without stirring, the steady-state condition was used to quantify turbidity. The measurement was repeated with pure NIMO. Data were provided as mean ±SD, and each measurement was done in triplicate.

4.5.16. *In vitro* drug-releasing measurements

Mitomycin C (MMC) release from polymeric prodrug particles

A cellulose membrane with an average flat width of 10 mm (0.4 in.) from Sigma-Aldrich (Missouri, USA) was used for the in vitro MMC release tests. Spectrophotometric measurements of the MMC amounts released from the pure and conjugated forms were conducted by observing changes in the intensity of the MMC absorbance peak at $\lambda = 364$ nm. According to the calibration curve previously established within the range of 0–0.08 mg/mL MMC solution, the MMC concentration was directly proportional to the maximum absorption values observed at this wavelength [C_{MMC} (mg/mL) = ($A_{364\,nm}$)/20.418; $R^2 = 0.9998$]. In 20 mL of a PBS buffer (0.9 wt% NaCl content) solution with a pH of 7.4, solid powders of the drug in both its pure and conjugated forms (equal to 0.057 mg/mL MMC) were put in a cellulose membrane and sealed at 37 °C. The release of MMC from a physical mixture of pure MMC and PVA-SA particles (with the same ratio as the conjugated particles) was investigated to determine the impact of the conjugation of MMC to polymer in the releasing process. At predetermined intervals throughout the measurement, 3 mL of the aqueous solution from the release medium was taken to determine the MMC concentration. Each measurement was performed in triplicate, and the average MMC concentration and related standard deviations were calculated.

Tilorone release from the hydrogel network

Using a cellulose membrane with an average flat width of 25 mm (1.0 in.) from Sigma-Aldrich, the Tilorone dihydrochloride release tests were carried out in vitro. The hydrogel was made by combining 1 mL of PVA-CHO and CHIT-SH at the desired concentrations (2, 5, and 10% *w/v*) with the proper amount of Tilorone drug (2.3 mg), then allowing the mixture to sit for 5 minutes

to complete the gelation process. By examining the intensity of the characteristic Tilorone absorbance at λ = 270 nm, the quantity of Tilorone released from the pure drug and hydrogel forms at various concentrations (2, 5, and 10% *w/v*) was spectrophotometrically determined. Tilorone concentration was directly correlated with the maximum absorbance values seen at this wavelength [$C_{Tilorone}$ (mg/mL) = ($A_{270\ nm}$)/150; R^2 = 0.9997], according to the calibration curve that was previously determined to be within the range of 0–0.024 mg/mL of Tilorone solution. The same amount of Tilorone in solid powder and hydrogel form (2.3 mg; used in all tests) was put within a cellulose membrane, sealed, and submerged in 100 mL of a PBS buffer solution at 37°C (pH = 7.4; 0.9 wt% NaCl content). At set intervals during the release experiment, 3 mL of the aqueous buffer solution was collected from the dissolution media to compute the concentration of Tilorone. The same releasing measurement was repeated in the presence of 0.15% lysozyme (in PBS) solution. Each measurement was performed in triplicate, and the average values and standard deviations were computed.

Nimodipine release from PES polyester particles

Using a cellulose membrane (Munktell & Filtrak GmbH; grade = 390), the in vitro NIMO release measurements were carried out. Using spectrophotometry, the amount of NIMO released from PES samples of different molecular weights was quantified by following records of changes in the intensity of the NIMO characteristic peak (λ = 360 nm). The concentration of NIMO was determined using the pre-established calibration curve of NIMO, which has a range of 0–0.133 mg/mL and a formula of [C_{NIMO} (mg/mL) = (A_{360nm})/7.9127; R^2 = 0.93]. The membrane was filled with NIMO-loaded PES NPs powders (equal to 0.1 mg/mL of NIMO; the same quantity of NIMO was loaded in all measurements) and placed in 50 mL of phosphate buffer saline solution (PBS, 0.9 wt% NaCl content, pH = 7.4) at 37 °C (human body temperature). Since NIMO has very low solubility (0.653 μg/mL) in H_2O; thus, 0.5% sodium dodecyl sulfate (SDS) was added to the dissolution media to increase the solubility of the drug [230]. Throughout the experiment, 3 mL of the solution was taken from the dissolution/release media at regular times, and the concentration of NIMO was estimated. Each measurement was performed in triplicate, and the average values and standard deviations were computed.

5. Results and Discussion

During my doctoral work, I deal with synthetic or modified biocompatible polymers and polymer-based functionalized materials suitable for pharmaceutical applications. Since the selected drugs (MMC, Tilorone, and NIMO) have very different structures, material properties, and applications, it required a variant approach to customize the polymers to meet the desired properties and requirements. Thus, the choice of the polymer was determined by the purpose of the application and this work provides a good example of the versatile application possibilities of polymeric materials with variable sizes, shapes, and diverse functionality in drug delivery. **Figure 8** summarizes the schematic diagram of the modification of PVA with two types of terminate groups (COOH and CHO) and synthetic PES as well as the drug delivery system formed from them, indicating the possible areas of application. Initially, PVA was modified with succinic anhydride to produce PVA-SA (containing COOH and OH groups) that can be used to prepare polymeric prodrug for MMC as a potential therapy for treating throat cancer and to prevent scar tissue formation in the area of the head and neck surgery. Then, PVA was modified with 4-formyl benzoic acid to produce PVA-CHO (containing CHO groups) that can be crosslinked with thiolated chitosan (containing NH_2 and SH groups) to form injectable mucoadhesive hydrogel to incorporate Tilorone to provide a novel potential therapeutic approach for the local treatment of muscle atrophy (laryngotracheal atrophy). Eventually, the synthesis of PES polyester with different molecular weights and study in detail its solubility and precipitation properties to encapsulate the NIMO drug to enhance water solubility and drug bioavailability. I present the results according to **Figure 8** in the following chapters.

5.1. Development of mucoadhesive polymeric prodrug for MMC encapsulation

To decrease the severe adverse effect of MMC, polymeric prodrug nanoparticles with spontaneous, self-assembled particle formation ability and mucoadhesive characteristics were employed in this part. The particles were synthesized in a simple one-pot reaction by conjugating MMC and CYS with succinated PVA and then forming self-assembled particles using EDC (**Figure 10**). The physicochemical characteristics of polymeric prodrug for MMC, as well as its mucoadhesive properties, were investigated in order to prolong the drug's residence duration within the human body, hence increasing bioavailability and therapeutic efficiency. *In vitro* drug release measurements were performed under physiological conditions

to evaluate the effect of conjugation on prolonging drug release. *In vitro* tests for antibacterial and anticancer properties have also been performed.

5.1.1. Structural characterization of the synthesized samples

The initial PVA with OH groups was chemically modified as shown in **Figure 10** by appending succinic anhydride in a range of molar ratios (8 – 126 molar%) to the OH groups of PVA (15.8 mmol/g, as assessed by the acetic anhydride/pyridine titration [231,232]).

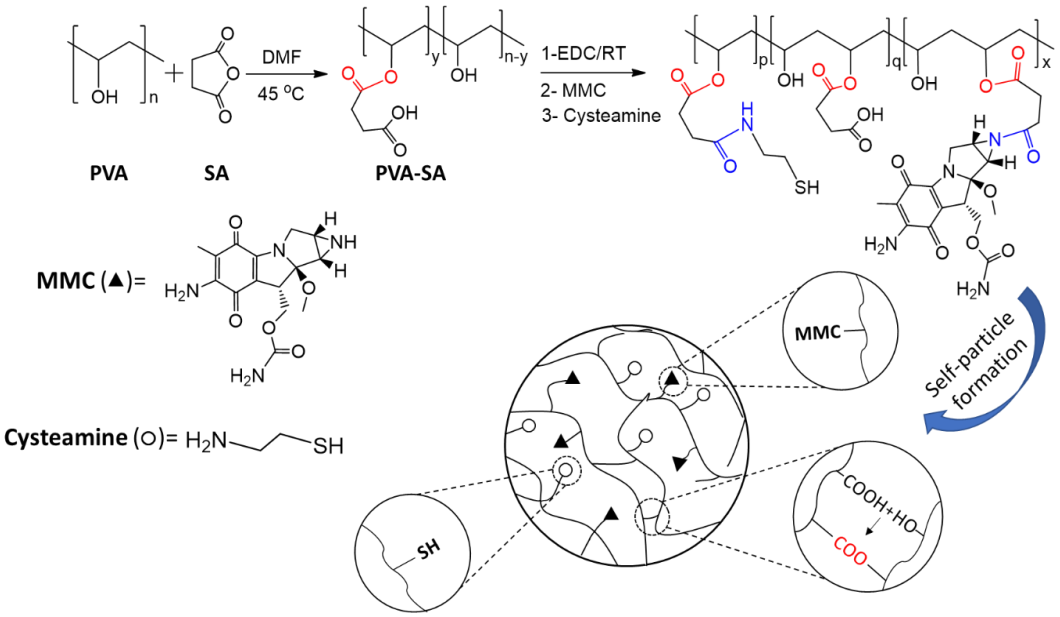

Figure 10. The succinylation reaction of PVA to produce PVA-SA and the conjugation of cysteamine and MMC (via amide bonds marked in blue) with PVA-SA, as well as the self-particle formation via ester bond crosslinking between the COOH group and OH group using EDC (marked in red) [232].

The initial molecular weight of PVA (M_w) was determined using a Debey plot and DLS measurements to be 46.83 kDa (**Figure 11A**). As the molar ratio of SA is increased, the percentage of substitution increases until it reaches a plateau value (saturation) of about 21.5% substitution when 90 molar% SA was applied (see **Figure 11B**). These results indicate that the use of DMF as a poor solvent for PVA and the moderate reaction conditions induced a succinylation process on the surface of PVA particles, resulting in a relatively low degree of substitution. Furthermore, according to Zhou et al. [233], applying severe circumstances will cause a crosslinking network between PVA and SA to form, which is inappropriate for our objective. However, partially succinated PVA with the simultaneous presence of COOH and OH groups is a promising candidate for the conjugation of many bioactive agents. Next, the CYS (0.05 to 0.34 mmol) and MMC (4 mg) were conjugated with the resulting PVA-SA via the formation of an amide bond by using EDC (coupling agent), wherein the binding percent of MMC was 80±3% according to the UV-VIS spectroscopy measurements. Additionally, through

ester linkages, the remaining COOH and OH groups enabled the self-particle formation to form MMC-loaded polymeric nanoparticles with mucoadhesive properties (see **Figure 10**) [234].

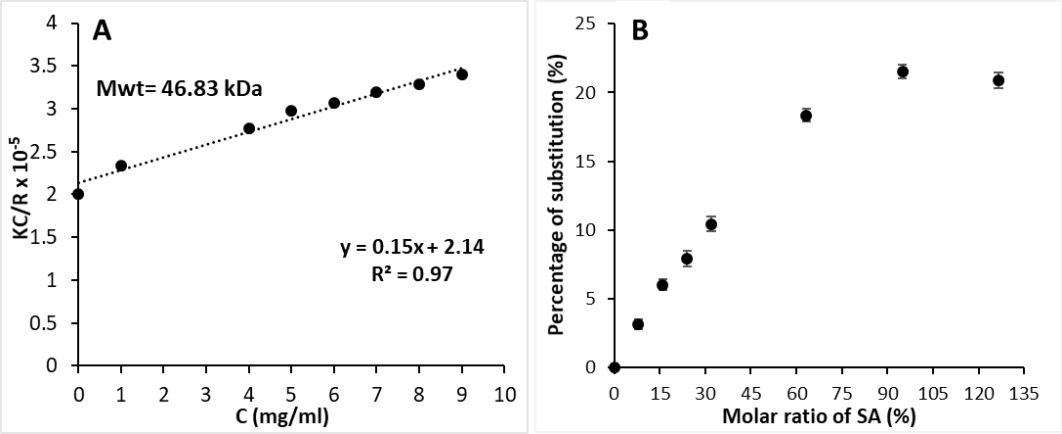

Figure 11. (**A**) Debye plot to calculate the initial PVA's molecular weight, (**B**) degree of substitution of the PVA-SA sample relative to the molar ratio (%) of SA and PVA's OH in the reaction [232].

FTIR measurements confirmed the successful reactions by investigating the chemical structure of the initial PVA and its modified derivatives, as well as the polymeric prodrug of MMC, as shown in **Figure 12**. PVA has main characteristic absorption peaks at 3280 cm^{-1} for the (O−H) stretching vibration, and 2960 and 2925 cm^{-1} associated with the asymmetric and symmetric stretching vibration of (C−H) of the alkyl group. The Peak at 1735 cm^{-1} related to the (C=O) stretch of the unhydrolyzed acetate group. The detected absorption peaks at 1425, 1380, 1325, 1245, 1100, and 840 cm^{-1} are assigned to (C−H) bending vibration of CH_2, (C−H) deformation vibration, (CH_2) wagging vibration, (C−O−C) stretching vibration, (C−O) stretching of acetyl groups, and (C−C) stretching vibration, respectively [231,235].

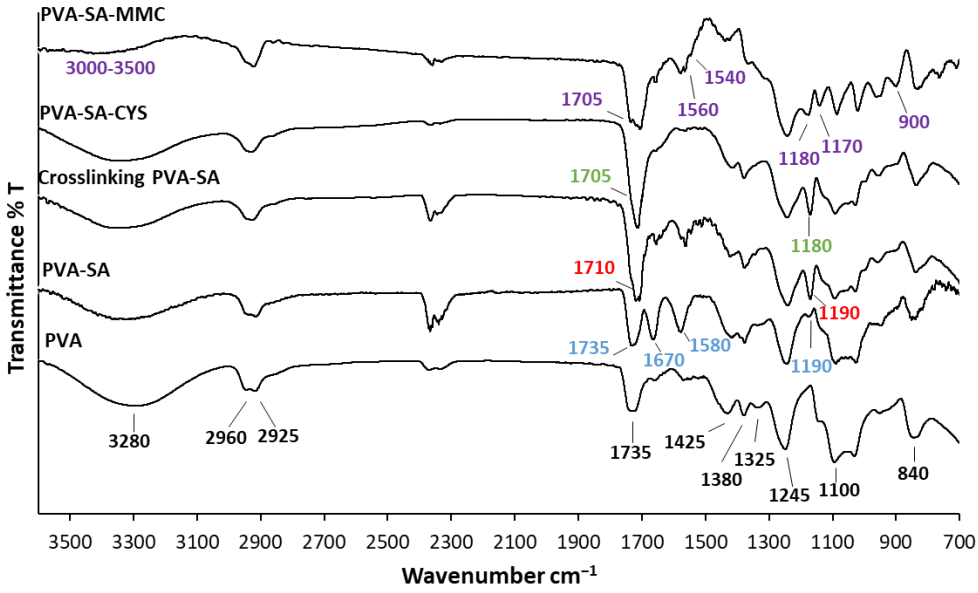

Figure 12. FTIR spectra of initial and modified PVA and polymeric prodrug of MMC [232].

Modification of PVA with succinyl groups was confirmed by diminishing the (OH) stretching vibration peak of PVA at 3280 cm^{-1}, and the appearance of three significant absorption bands 1670, 1580, and 1190 cm^{-1} were due to the carbonyl of carboxylate ($RCOO^-$) group, asymmetric stretch vibration of ($RCOO^-$) carboxylate group, and (C−O) stretch vibrations of the ester group, respectively [236–238].

A decrease in the band related to the carboxylate moiety of succinate and shifting of C=O stretching peak to 1710 cm^{-1} as well as the increase in the appearance of an absorption band at 1190 cm^{-1} for C−O stretching vibrations of the ester group [238], confirming the cross-linking by an ester bond, were used to confirm the spontaneous self-assemble particle formation by cross-linking reaction between the available (COOH) and (OH) groups of PVA-SA backbone chain [234].

The disappearance of the absorption band at 1670 and 1580 cm^{-1} associated with the carboxylate ($RCOO^-$) moiety, as well as the shift and increase in the intensity of the carbonyl (C=O) band at 1705 cm^{-1} due to the amide bond formation between the (COOH) group of PVA-SA and the (NH_2) group of cysteamine (CYS) [239], were evidence of the conjugation reaction of PVA-SA with CYS. In addition, the C−N stretching vibration that overlapped with the C−O ester that appeared at 1180 cm^{-1}, and the coupling of CYS with PVA-SA was also confirmed by EDX measurements (as we will see later).

The conjugation reaction between PVA-SA and MMC was also successful since the NH band of MMC at 3442 cm^{-1} disappeared, and the amide band (C=O) appeared at 1705 cm^{-1}. In the case of the conjugated products, there was also a shift in the area from 3000 to 3500 cm^{-1}, and decreasing the absorption band at 1670 cm^{-1} that related to carboxylate moieties. This demonstrated that a reaction took place between the (NH) group of MMC drug and the (COOH) group of PVA-SA. The appearance of additional peaks at 2850, 1560, 1540, 1383, 1170, and 900 cm^{-1} was characteristic of the MMC moiety [240].

DSC measurements were used to evaluate the thermal behavior of the PVA and its modified derivatives as shown in **Figure 13**. The initial PVA shows 3 main endothermic peaks at 80, 190, and 310 °C, corresponding to the polymer's water loss, melting, and thermal decomposition, respectively [241]. The melting point (see **Figure 13A**) and hydrophobicity (see **Figure 13B**) of conjugated particles are higher than the initial PVA because of the formation of a crosslinking network (between OH and COOH of the PVA-SA chain), which resulted in the enhancement of the thermal properties of prepared particles. DSC measurements

were also used to determine the water heat evaporation and desorption enthalpy value (see **Figure 13B**). When compared to the initial PVA, the conjugated particles exhibit a reduced desorption value of roughly 29 kJ/mol indicating the increasing hydrophobic nature of the polymer.

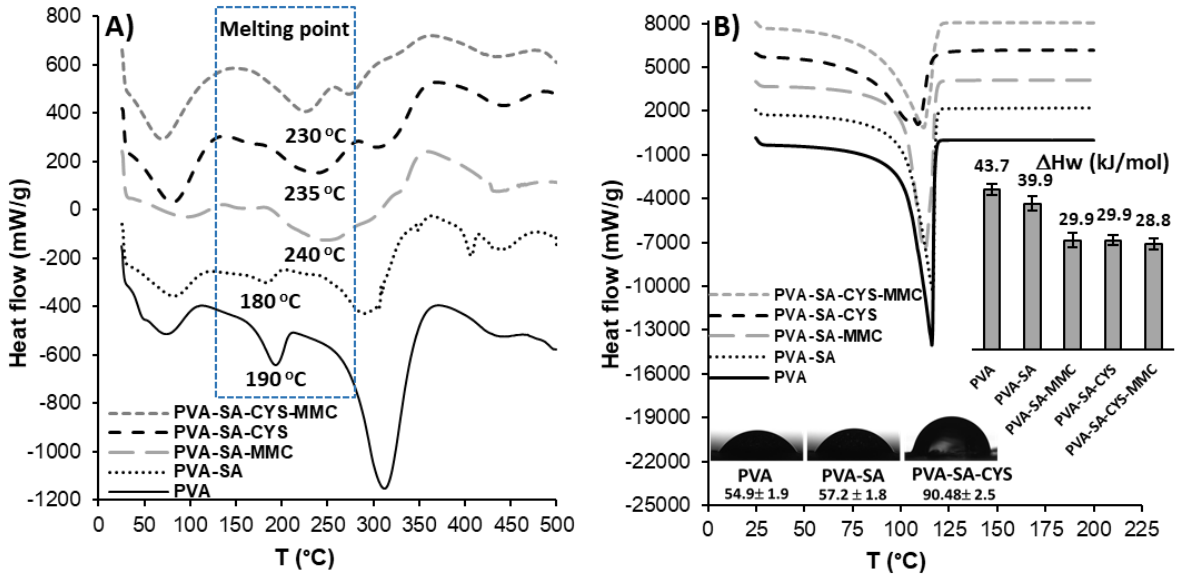

Figure 13. (**A**) DSC curves of PVA and its conjugated particles, (**B**) water evaporation curves of the PVA-based hydrogel samples, and water desorption enthalpy (ΔH_w) values (represented as grey columns). The inserted photos show the results of the contact angle measurement of films [232].

5.1.2. Self-assembled particle formation

As we know, dispersed polymeric particles may be produced from a dilute polymer solution while using high concentration one to produce the crosslinked 3D structure. To produce self-assembled particles, the viscosity change of PVA-SA solutions was investigated to determine the highest polymer concentration that could be used to produce separate particles rather than a 3D cross-linked gel structure. For this experiment, PVA-SA solutions with different (1, 2, 3, and 4% *w/v*) concentrations were prepared, and then the appropriate amount of EDC (1.5 equivalent to COOH contents) was added. The viscosity as a function of the polymer concentration is shown in **Figure 14A**. In the case of PVA-SA (1, 2, and 3% *w/v*) solutions, turbid and low-viscosity dispersions were generated. However, above this concentration, the viscosity significantly jumped to 16.3 mPa·s due to cross-linked hydrogel formation. According to our results, the critical polymer concentration of the PVA-SA in distilled H_2O is approximately 3%; Under this concentration, separate polymeric molecules are formed, but at higher concentration values, the macromolecule chains give a cross-linked hydrogel sample.

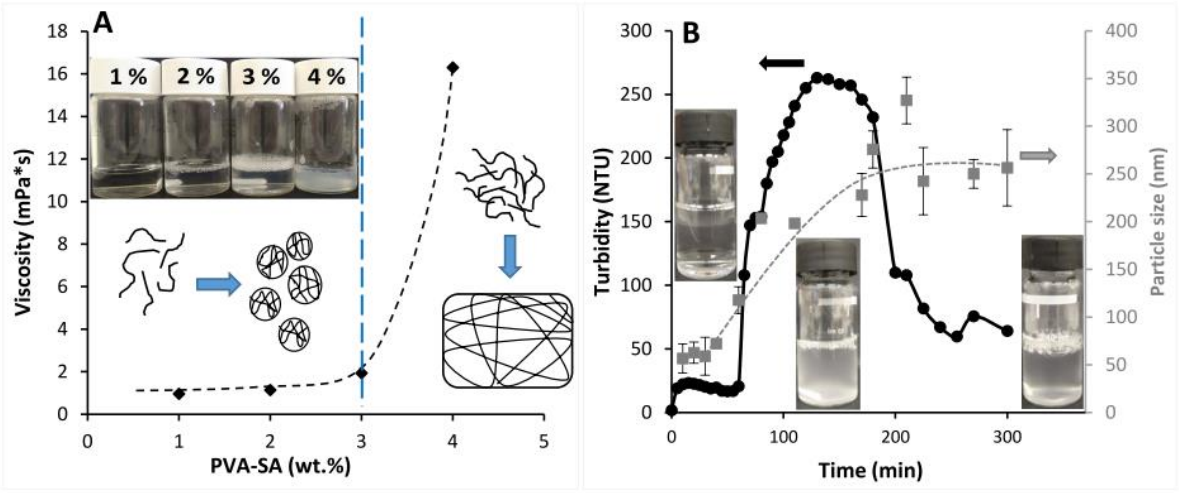

Figure 14. (**A**) Viscosity values as a function of the concentration of PVA-SA solutions, (**B**) the turbidity (presented in black) and particle size (presented in gray) data as a function of reaction time between PVA-SA (21% cross-link density) and EDC to form particles [232].

As a consequence of the dual existence of COOH and OH groups on the polymeric backbone allowing the creation of esters bonds using EDC between these functional groups, the turbidity measurements were used to support the development of self-particles. In order to investigate this phenomenon, an appropriate amount of EDC was added to 2 % *w/v* aqueous PVA-SA solution and then the turbidity was tracked over time, as shown in **Figure 14B**. After the addition of EDC, the turbidity increased abruptly (~20 NTU), due to the activation of the COOH groups of succinated PVA with EDC to produce o-acylisourea which is usually a long step and takes between 1 and 3 hrs [242]. After 60 minutes of measurement, the turbidity then increased significantly due to the self-particle formation caused by the cross-linking between the COOH groups and the OH groups of the PVA-SA backbone. Following 130 minutes, the turbidity reached a plateau value and remained stable until 180 minutes, when the coagulation of the particles caused it to decline. The results of the DLS measurement (see **Figure 14B**, gray), which was used to examine how the size of the produced particles changed over time. The maximum particle size was around 200 nm during the period of high turbidity (from 120 to 170 minutes), and the maximum particle size was 256 nm after 300 minutes. Particle size exhibited a tendency to grow over time.

TEM was also used to examine the shape and size of the synthesized conjugated particles. TEM picture of spherical polymeric prodrug particles (PVA-SA-CYS-MMC 21%) is shown in **Figure 15**, as well as a histogram of the corresponding particle size distribution (92 ± 30 nm, mean particle size). Likewise, with the corresponding particle size distribution histograms, **Figure 15** also displays the mean particle sizes for PVA-SA-CYS-MMC (10%) and PVA-SA-CYS-MMC (3%) at about 149 ± 66 nm and 260 ± 67 nm, respectively. It is evident that the

particle size of the synthesized polymeric prodrugs decreased with the increase of cross-linking density.

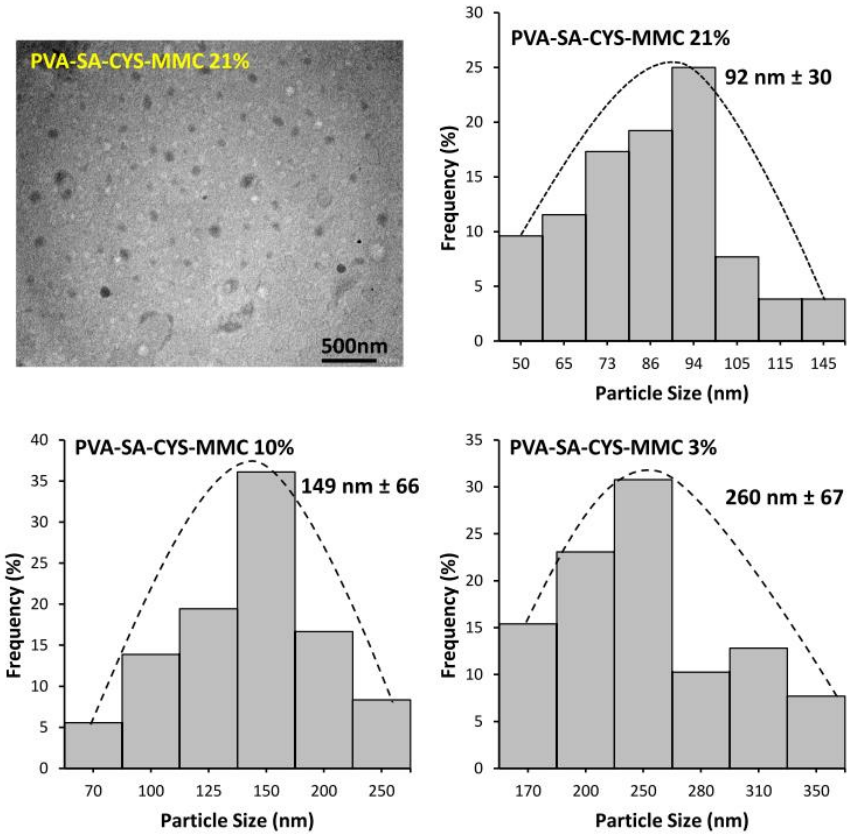

Figure 15. TEM picture of PVA-SA-CYS-MMC 21 mol.% particles with the size distribution histogram and corresponding size distribution histograms for PVA-SA-CYS-MMC 10 mol.% and PVA-SA-CYS-MMC 3 mol.% [232].

5.1.3. Mucoadhesive properties of polymeric prodrug particles

The terminal thiol groups guaranteed that the synthesized particles had the necessary mucoadhesive characteristics. According to the Volhard method, the thiol content values of the PVA-SA-CYS samples with cross-linking densities of 21, 10, and 3% were 0.8, 0.2, and 0.075 mmol/g, respectively.

The existence of the elements in their various conjugated forms was also determined by EDX measurements. PVA-SA-CYS and PVA-SA-CYS-MMC particles exhibit the sulfur (CYS) and nitrogen (MMC) elements, which supports the conjugation of CYS and MMC to PVA-SA via coupling reaction with EDC as shown in **Figure 16**.

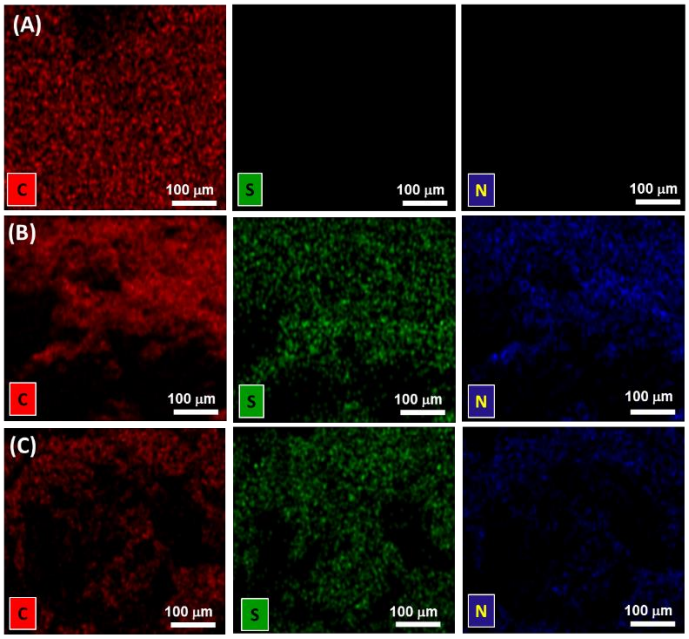

Figure 16. EDX of (**A**) PVA-SA cross-linking, (**B**) PVA-SA-CYS, and (**C**) PVA-SA-CYS-MMC particles, where C, S, and N are carbon, sulfur, and nitrogen elements, respectively [232].

Rheological measurements were used to confirm the mucoadhesive properties of polymeric prodrug particles by forming a viscous cross-linking hydrogel as the result of combining 1% *w/v* mucin (as mucus glycoproteins) with 1% *w/v* PVA-SA-CYS solution with 1% *w/v* mucin solution as shown in **Figure A1** and **Figure A2**, and the data were recorded in **Table 1**. The loss modulus (G″) indicates the viscous characteristic, whereas the storage modulus (G′) represents the elastic nature of the polymer. The so-called complex modulus (G*) is the 'sum' of the loss and storage moduli. **Table 1** shows that the PVA-SA-CYS-mucin hydrogel sample has high G′ and G″ values compared to PVA-SA-CYS and mucin solutions due to the formation of crosslinking hydrogel structure by disulfide and hydrogen linkages (**Figure A1**). The disulfide linkage was formed by the thiol/disulfide exchange mechanism. The mechanism of this gel formation is based on the use of PVA-SA-CYS (with SH-terminated group) as a crosslinker for long-chain mucin as shown in **Figure A1**, and our results are consistent with the literature [243]. Moreover, the inserted photos in **Figure A1** are also clearly shown the gel formation after mixing the PVA-SA-CYS polymer with mucin.

Table 1. Data of storage modulus (G′), loss modulus (G″), and complex modulus (G*) of PVA-SA-CYS (1%), mucin (1%), and a mixture of them [232].

Sample	**G′ (kPa)**	**G″ (kPa)**	**G* (kPa)**
1% PVA-CYS	24.7	7.55	32.25
1% Mucin	12.4	0.78	13.18
1% PVA-CYS-Mucin	158.3	23.2	181.5

Surface adsorption studies also confirmed that mucoadhesive polymeric prodrug particles formed disulfide bonds with the mucin-rich surface. This experiment involved submerging a pig intestinal membrane, which served as the model mucous surfaces, in an aqueous dispersion solution of 1% *w/v* PVA-SA-CYS (21% crosslinking density) under gentle stirring, and the turbidity reduction caused by the adsorption of particles were tracked over time. **Figure 17** shows the results of repeating the experiment using particles without CYS as a reference. The surface adsorption of PVA-SA-CYS 21% particles continued continuously till practically high adsorption was achieved, resulting in ~76% of maximum turbidity reduction in contrast to ~9% for thiol-free PVA-SA particles within 7 hrs. The mucoadhesive characteristics of PVA polymer were improved by the incorporation of CYS. Moreover, due to the presence of SH groups, our modified PVA-SA-CYS polymer (21% crosslinking density) exhibits self-healing ability in the bulk phase by forming inter and/or intra-chain disulfide bonds as shown in the inset photo in **Figure 17**. The polymeric prodrug particles showed strong mucoadhesive characteristics that are appropriate for prolonging the residence period of the polymeric prodrug of MMC inside the human body throughout the extended MMC release process and improving bioavailability [244].

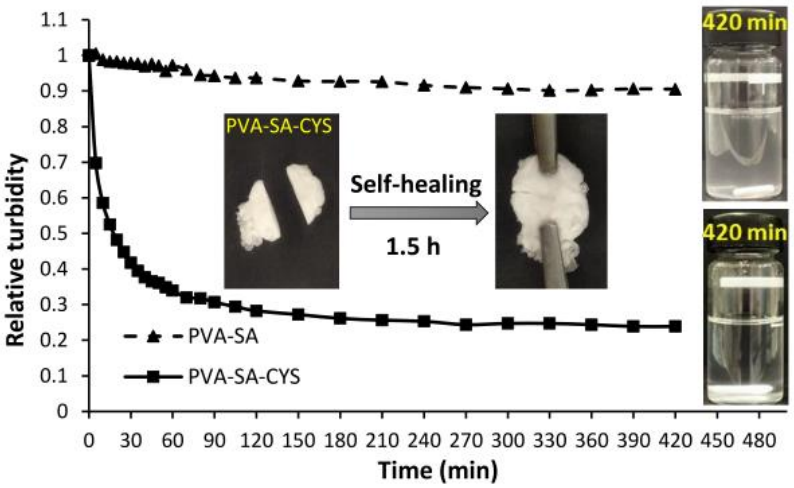

Figure 17. Surface adsorption measurements; change in relative turbidity as a function of time for immersing a 7 cm pig intestinal membrane in a 1% *w/v* aqueous dispersion of polymeric particles. The right inset photos indicate the aqueous dispersion of particles after the measurement is completed while the middle inset photos show the self-healing ability of PVA-SA-CYS in bulk phase by cutting to 2 parts and reattaching [232].

5.1.4. *In Vitro* MMC release measurements

MMC drug release was studied under physiological conditions (37 °C, 0.9 wt% NaCl, PBS buffer solution with pH 7.4). **Figure 18** depicts the MMC release profiles from various forms;

release from pure MMC form and the physical (MMC and PVA-SA without bonding) mixture form was excessively rapid, with maximum releasing quantities of ~92 and ~81%, respectively.

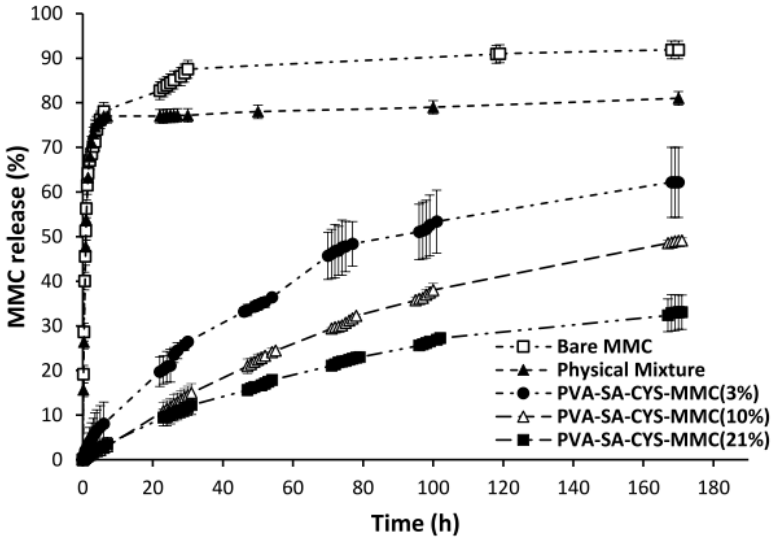

Figure 18. The *in vitro* MMC release curves from the pure and physical mixture forms, and polymeric prodrug particles with various cross-linking densities [232].

The release of MMC from pure and physical mixture forms mathematically fits Korsmeyer and Peppas model (**Equation 5**), as shown in **Table 2**. Fickian diffusion mechanism was suggested when $n \leq 0.43$, whereas the anomalous (non-Fickian) transport when $0.43 < n < 0.85$ [245,246]. For both the physical mixture of MMC and the bare MMC, $n < 0.2$, which denoted a Fickian diffusion release, or diffusion-controlled transport.

Table 2. Different kinetic models to interpret the MMC release experiment results [232].

Sample	Zero-order model		First-order model		Higuchi model		Hixson-Crowell model		Korsmeyer-Peppas model		
	r^2	k (h^{-1})	r^2	k (h^{-1})	r^2	k ($h^{-1/2}$)	r^2	k ($h^{-1/3}$)	n	r^2	k (h^{-n})
Bare MMC	0.277	0.249	0.546	0.011	0.491	4.327	0.125	0.006	0.161	0.722	49.59
Physical mixture	0.124	0.199	0.194	0.005	0.312	3.849	0.066	0.006	0.166	0.565	46.77
PVA-MMC (3%)	0.879	0.404	0.944	0.006	0.985	5.429	0.673	0.018	0.695	0.99	2.254
PVA-MMC (10%)	0.948	0.315	0.982	0.004	0.982	4.068	0.748	0.019	0.841	0.995	1.459
PVA-MMC (21%)	0.921	0.205	0.948	0.003	0.992	2.776	0.711	0.015	0.786	0.992	1.354

MMC release from the polymeric prodrug particles displayed significantly prolonged release patterns that were controlled by hydrolysis of the amide bond that connect the MMC with polymeric particles. In nature, the hydrolysis of amide bonds is a very slow process, and thus it took a while for them to achieve the plateau value. After 7 days, the cumulative MMC release values for PVA-SA-CYS-MMC with various crosslinking densities (3%, 10%, and 21%) were

around 62%, 49%, and 33%, respectively. **Table 2** shows that the Korsmeyer-Peppas model fits with the drug release data for all conjugated forms. The mechanism of drug release was based on both diffusion and erosion-controlled processes, according to an "n" value ranging from 0.43 to 0.85, which relates to a non-Fickian (anomalous) transport [247,248]. In other words, the conjugated form's hydrolysis process occurs first, followed by the diffusion of MMC. This leads to the conclusion that the use of our polymeric prodrug system can significantly slow down the rate of release of MMC. Additionally, the synthesis conditions can alter how much drug is released and how it is released.

5.1.5. Evaluation of *in vitro* antibacterial and anticancer activity of MMC samples

MMC has anticancer and antibacterial activity, and thus we examined the anticancer activity of MMC and its polymeric prodrug forms. During these tests, the release medium was removed after 1, 3, 5, and 7 days with increased MMC concentration (see **Table 3**), and the corresponding IC_{50} data were determined (**Table 3)**. The IC_{50} values ranged from 0.014 ± 0.001 to 0.054 ± 0.029 mg/mL, indicating a clear antitumor activity in all investigated MMC samples. For polymeric prodrug samples, the determined IC_{50} values were remarkably comparable to those of pure MMC, demonstrating that the anticancer activity was not affected by MMC conjugation and MMC release from particles. These findings demonstrated that the polymeric particles could effectively attach to mucous surfaces, and that the prolonged release of MMC allowed for the long-lasting anticancer impact. The developed PVA-SA biopolymer was nontoxic and biocompatible with MRC-5 (human embryonic lung fibroblasts) cells as shown in **Figure A3**.

Table 3. Measured IC_{50} values (in mg/mL) for samples examined on the Hep-2c cancer cell line, and MMC concentration values (measured by spectrophotometry) for solutions released from the encapsulated and pure MMC used during antitumor and antibacterial assays [232].

Sample	1st Day		3rd Day		5th Day		7th Day	
	Conc (mg/mL)	**IC_{50}** (mg/mL)	**Conc** (mg/mL)	**IC_{50}** (mg/mL)	**Conc** (mg/mL)	**IC_{50}** (mg/mL)	**Conc** (mg/mL)	**IC_{50}** (mg/mL)
Pure MMC	0.254	0.029 ± 0.001	0.270	0.041 ± 0.002	0.273	0.026 ± 0.006	0.275	0.05 ± 0.045
Control	0.000	0.000	0.000	0.000	0.000	0.000	0.000	0.000
PVA-MMC (3%)	0.063	0.014 ± 0.001	0.140	0.022 ± 0.007	0.173	0.043 ± 0.025	0.188	0.054 ± 0.029
PVA-MMC (21%)	0.029	0.037 ± 0.004	0.065	0.038 ± 0.01	0.089	0.039 ± 0.007	0.097	0.029 ± 0.004

Related to the antibacterial assay, **Figure 19** represents the inhibition zone diameters (IZD) for MMC release against Methicillin-resistant *Staphylococcus aureus* (MRSA) after 5 days. The acquired diameter values of the relevant specific inhibitory zone during the entire measurement

(1, 3, 5, and 7 days) of antibacterial actions are shown in **Figure A4**. Given that the diameter of the inhibition zone was indeed greater than 10 mm, thus pure and encapsulated MMC had an antibacterial activity that led to inhibiting the growth of MRSA bacteria at the observed concentrations. Furthermore, the antibacterial activity of MMC samples is dependent on the amount of MMC release, as the inhibition zone diameters (IZD ≈ 27, 19, and 12 mm) are reduced with increased cross-link [0 (pure MMC), 3, and 21%] densities (see **Figure 19**) due to the MMC release was controlled by cross-linking density.

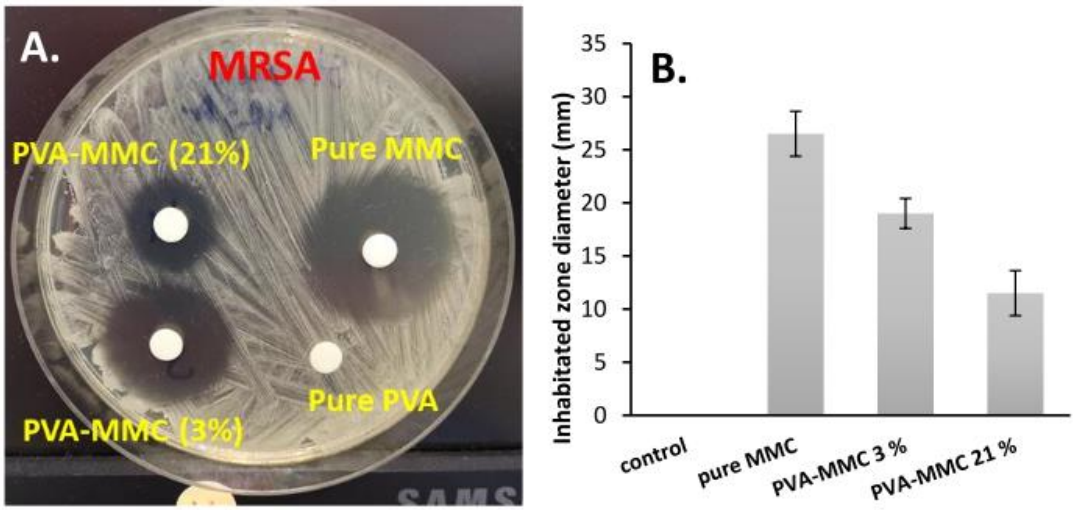

Figure 19. Photo of the antibacterial activity of pure and encapsulated forms of MMC on tested MRSA bacteria (**A**), the observed inhibition zone diameter values (**B**) after 5 days. Polymeric particles without MMC are the control [232].

In this part, we try to introduce novel mucoadhesive polymeric prodrug nanoparticles to reduce the severe side effect of MMC. As a summary, we can state that the developed PVA-SA prepolymer with varied (3–21%) COOH and (0.075–0.8 mmol/g) CYS content is suitable for the effective encapsulation (EE = 80 ± 3%) of MMC by self-assembled manner. The critical polymer concentration for this mechanism is about 3%. The particle size (92–260 nm) and drug release of MMC can be adjusted (from 33 to 62%) by the cross-link density (21–3%). The presence of the CYS moiety (0.6–6.2%) provides mucoadhesive properties for the nanoparticles as proved by rheological (G' = 158 kPa, G" = 23 kPa) and adsorption (~76%) measurements. Thus, the newly introduced particles exhibited a number of promising characteristics, including the capacity to self-assemble particles, strong mucoadhesive properties, self-healing properties, and a prolonged drug release process. We anticipate that the produced polymeric prodrug particles of MMC will eventually develop into an effective drug delivery system (DDS) and be helpful in the field of treating throat cancer.

5.2. Self-assembling injectable hydrogel for Tilorone

The purpose of this part was to develop an injectable mucoadhesive hydrogel suitable for the encapsulation, prolonged drug release and local injection of Tilorone, a well- water-soluble BMP inducer drug. The drug-loaded hydrogel could be advantageously used for effective local therapy for muscular atrophy. The self-assembling injectable hydrogel was physiochemically tested utilizing FTIR, NMR, viscosity, self-healing, mucoadhesive, and EDX assays. The drug release was adjusted by varying the hydrogel concentration/crosslinking density under physiological circumstances (37°C, pH 7.4). The cytotoxicity measurement was carried out to approve the biocompatibility of produced hydrogel.

5.2.1. Structural characterization of the modified polymers and hydrogel

Despite having good biocompatibility and biodegradability [108], CHIT has drawbacks such as poor solubility at a physiological (or neutral pH) and weak mucoadhesive characteristics that make it unsuitable for use in the creation of injectable hydrogels. As a result, we modified the CHIT with 3-mercaptopropionic acid (see **Figure 20**) to produce CHIT-SH with pendant thiol (SH) groups (thiol content = 201.85 ± 12 µmol/g) to enhance its water solubility and mucoadhesive properties [249]. In addition, the other component was the PVA which has good mechanical, biodegradability, and biocompatibility characteristics. We functionalized the OH groups of PVA by reacting with 4-formylbenzoic acid (see **Figure 20**) to produce PVA-CHO with free terminal CHO groups (with functionalization degree = 5.9 mol%) that can be used as a crosslinker for NH_2 groups of modified CHIT (CHIT-SH) to form dynamic (PVA-CHO/ CHIT-SH) hydrogel via Schiff base (imine bond) formation as shown in **Figure 20** [249].

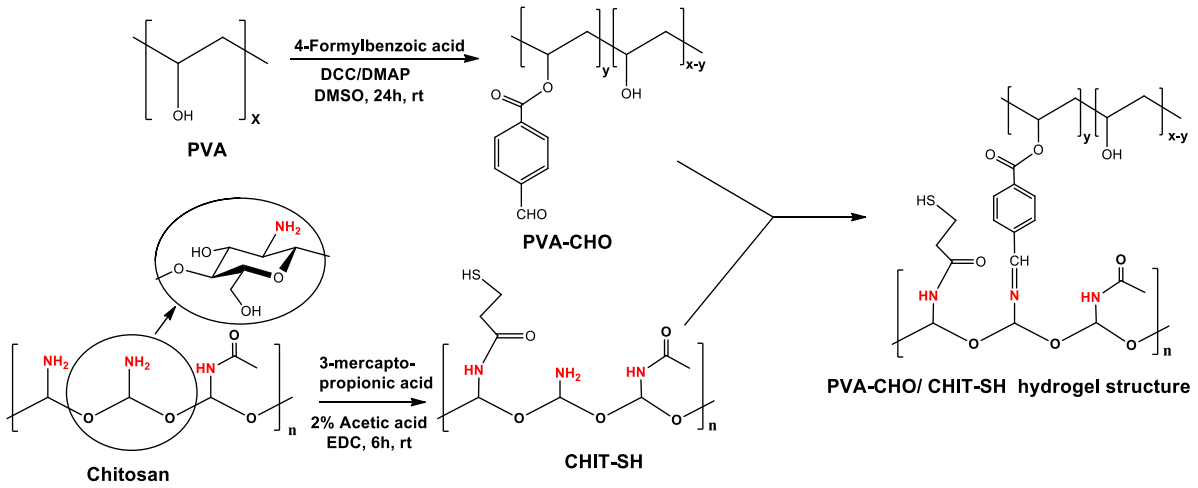

Figure 20. Scheme of modification of PVA with 4-formylbenzoic acid and CHIT with 3-mercaptopropionic acid as well as the hydrogel structure formation via imine bond between the modified macromolecules [249].

As we show later, our dynamical hydrogel is pH-dependent because a lower pH (≤4; acidic H^+ medium) causes imine bond cleavage while a higher pH (≥5; basic OH^- medium) promotes Schiff base (imine bond) formation [250].

The successful modification of the initial (PVA and CHIT) polymers and hydrogel formation was proven by the FTIR spectra, as demonstrated in **Figure 21**. The formation of PVA-CHO was confirmed by the appearance of absorption bands at 2860 and 1705 cm^{-1} related to the (C–H) stretching vibration of the CHO group and the (C=O) stretching vibration of the CHO group, respectively [251]. The intensity and wavenumber shifting of the unmodified OH of the PVA chain increased as a result of the development of an intramolecular hydrogen bond between the OH and CHO groups of PVA-CHO [251,252]. The aromatic ring's (C=C) stretching was responsible for the peaks between 1650 and 1505 cm^{-1}, whereas the peak at 1210 cm^{-1} was caused by the asymmetric stretching vibration band of the (C–O) ester. The detected absorption peaks at 760 and 820 cm^{-1} belong to the (=C–H) bending (out-of-plane) vibration on the aromatic ring [253].

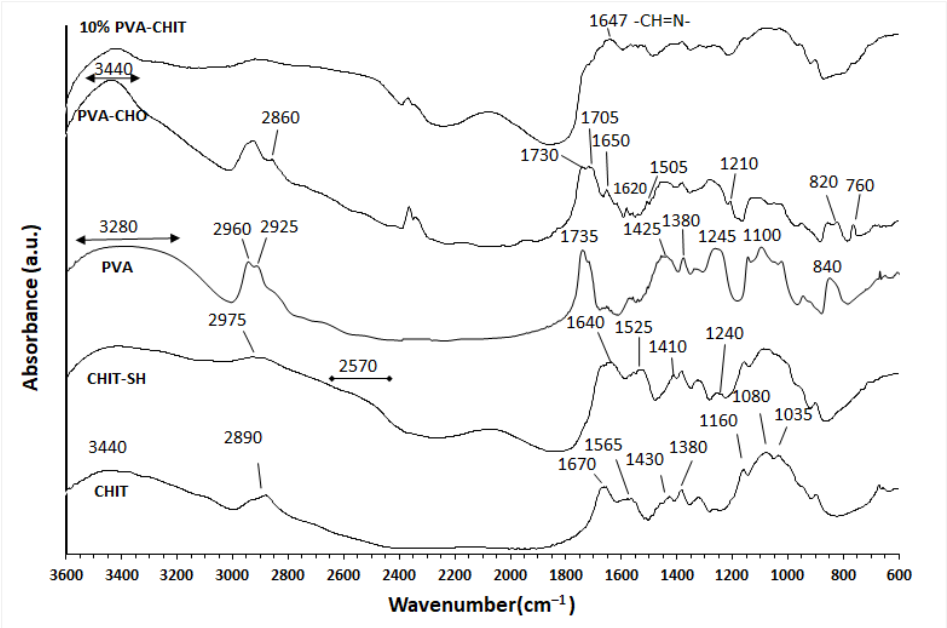

Figure 21. FTIR spectra of initial (CHIT and PVA) polymers, modified (CHIT-SH and PVA-CHO) polymers, and the PVA-CHO/CHIT-SH hydrogel [249].

The initial chitosan (CHIT) has main characteristic peaks at 3440 cm^{-1} (–OH and $–NH_2$ stretching vibrations), 2890 cm^{-1} (C–H stretching vibration), 1670 cm^{-1} (C=O stretching of the amide I band), 1565 cm^{-1} (N–H bending vibrations of the N-acetylated residues, amide II band), 1430 cm^{-1} (C–H bending), 1380 cm^{-1} (O–H bending), 1160 cm^{-1} (C–O–C bridge antisymmetric stretching), 1080 cm^{-1} and 1035 cm^{-1} (skeletal vibration involving C–O stretching) [254–256].

The modification of CHIT with 3-mercaptopropionic acid was confirmed by the appearance of the broad peak at 2570 cm^{-1} for the (S–H) group and the peak at 1240 cm^{-1} related to the (C–SH) stretching, and also dimension of the intensity peak at 3440 cm^{-1} related to the ($–NH_2$) and (–OH) groups [257,258]. Moreover, the conjugation of mercaptopropionic acid to the NH_2 of CHIT resulted in a 30 cm^{-1} shift of the amide I and amide II band peaks [257,258].

The development of a Schiff base (-CH=N-) bond by reacting of (CHO) groups of PVA-CHO and the (NH_2) groups of CHIT-SH for the production of the dynamic hydrogel was confirmed by the appearance of a new peak at 1647 cm^{-1} in the PVA-CHO/CHIT-SH hydrogel spectrum [259].

The ^{1}H-NMR spectra of the initial polymers and their modified derivatives were also obtained after the polymers were chemically characterized with FTIR (see **Figures A5–A8** in the Appendix). The PVA-CHO spectrum displayed the appearance of 2-2 aromatic protons signals (δ 8.04 and 8.13 ppm) and CHO signal at a higher ppm (δ 10.11 ppm; **Figure A6**), with the dimension of the hydroxyl peaks of PVA. The CHIT-SH spectrum likewise displayed the chitosan-specific peaks, along with two additional peaks at δ 2.70 ppm and δ 3.05 ppm that we speculated corresponded to the two CH_2 groups of 3-mercaptopropionate moiety (**Figure A8**). The degree of substitution (DS%) of thiolated chitosan (CHIT-SH) was 4.43%, while the degree of deacetylation (DD) of the initial chitosan was equivalent to 75.02% based on ^{1}H-NMR measurements. The typical yields for the PVA-CHO and CHIT-SH products, based on the collected polymers and the degree of modification (or substitution), were 91% and 84%, respectively.

To understand the mechanism of hydrogel formation and the bonds that could be responsible for the crosslinking network structure. It is worth noting that at physiological pH, an acetal bond cannot form between CHO and OH in our hydrogel system because this reaction required acidic pH which is often provided by acid catalysis [260]. However, as the reactive aldehyde moiety is frequently cytotoxic, the hydroxyl and aldehyde moieties of PVA-CHO might be masked as hemiacetal at a physiological pH, leading to the biocompatibility of PVA-CHO with a range of cellular strains [106,261]. The hemiacetal bond was shown as an equilibrium since the hemiacetal was unstable and eventually returned to the original aldehyde and alcohol. Another proposed bond between the CHO and SH groups was a thioacetal. The mechanism of the reaction was similar to that of acetal formation and required acid catalysis, such as that of Lewis acids (BF_3 or $ZnCl_2$) in an ether solvent; as a result, the formation of an acetal or thioacetal could not occur at a physiological pH in the absence of an acid catalyst [260].

The formation of disulfide bonds is essentially dependent on the local environment. Two important factors have a direct impact on the formation of a disulfide bond: (1) the redox environment (with lower reactivity under more reducing conditions and greater reactivity under more oxidizing conditions); and (2) the difference between the pK_a of the implicated thiol groups and the local environment's pH (a lower pH restricts reactivity and a higher pH encourages enhanced reactivity) [262]. In our hydrogel system, the disulfide bond was one conceivable bond that may form under physiological circumstances (pH ~7.4), but it was not the primary bond since our hydrogel formed in less time than 1 minute (see later) compared to the disulfide bond's slow rate of formation [263]. Additionally, the mucoadhesive results showed the presence of free thiol groups, which, as we will explain later, were in charge of our hydrogel's mucoadhesive property. **Figure A9** depicts some of the hydrogel system's potential bond forms based on the acetal and disulfide links, but none of them demonstrated gel formation, supporting our theory that the creation of the hydrogel is based on an imine bond as we will see in the next section.

5.2.2. Physicochemical characterization of PVA-CHO/CHIT-SH hydrogel

We hypothesized that the formation of a Schiff base (imine bond) when the PVA-CHO solution and CHIT-SH polymer were combined led to the formation of the self-assembled mucoadhesive hydrogel at a neutral pH. To prove this, the viscosities of the 2% *w/v* polymer solutions (CHIT-SH and PVA-CHO separately) and 2% *w/v* of their mixture are compared in **Figure 22A**. The viscosity of hydrogel (mixed polymer) increased noticeably and was more than 1,000 times greater than that of the initial (PVA-CHO and CHIT-SH) polymer solutions used. Moreover, the viscosity of the 2 and 3% *w/v* PVA-CHO/CHIT-SH hydrogels was investigated at various pH (~3–8) values using a different buffer solution as shown in **Figure 22B**. At pHs of 5.3 and 7.2, the viscosities of the two hydrogels were greater, reaching approximately 10,000 and >20,000 mPa·s for 2 and 3% *w/v* PVA-CHO/CHIT-SH, respectively. However, at an acidic pH, the viscosities were low because the imine bond broke down or disintegrated, as shown in **Figure 22B**. Also, **Figure 22B** displays the hydrogel formation mechanism as well as the inserted images of the gel (hydrogel) at a neutral pH and the sol (low viscosity solution) at an acidic pH. The pH dependence of the PVA-CHO/CHIT-SH hydrogel for the sol-gel transition in the presence of the drug Tilorone (1.15 mg/mL) is depicted in **Figure A10**. Due to its fast pH-dependent sol-gel transition and biocompatible nature (see later), PVA-CHO/CHIT-SH is a viable candidate that has been recommended for use in biomedical applications at a physiological pH, such as tissue engineering and drug delivery, as will be seen later.

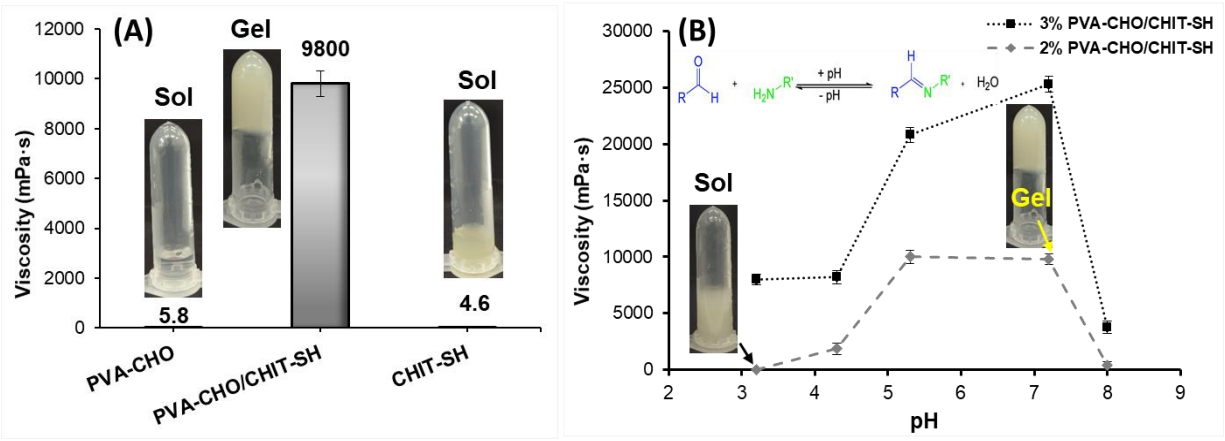

Figure 22. Viscosity measurements at 37°C for; (**A**) 2% *w/v* initial polymers used and 2% *w/v* hydrogel, (**B**) 2 and 3% *w/v* PVA-CHO/CHIT-SH hydrogels as a function of pH [249].

It is well-known that at a pH above 6 when CHIT lost its positive charge and started to form aggregates and precipitates, it showed low water solubility [264]. The solubility of the initial CHIT and CHIT-SH in various pH (6.1,7.4, and 8.1) buffer solutions are compared in **Figure A11**. Modification of CHIT with 3-mercaptopropionic acid (SD = 4.43%), makes it more soluble in neutral and basic media. The reason for this is that the hydrophilic functional groups of SH disrupted the intermolecular H-bond and crystalline structures of chitosan, which caused a significant increase in solubility in the case of CHIT-SH.

Next, the water contact angles of the dried polymer films made from the hydrogels at various (5 and 10% *w/v*) concentrations were measured and compared to the CHIT-SH and PVA-CHO films, which were all fabricated using the solvent-casting method. As shown in **Figure 23**, the original hydrophilic (55 ± 1°) PVA was modified with 4-formylbenzoic acid yielding a hydrophobic (91 ± 3°) PVA-CHO polymer, whereas the initial CHIT (73 ± 1°) was modified with 3-mercaptopropionic acid yielding a more hydrophilic (45 ± 2°) CHIT-SH polymer with better water solubility. In order to fabricate crosslinking films with moderate hydrophobic/hydrophilic properties (65 ± 3° and 75 ± 2° for 5% *w/v* and 10% *w/v* PVA-CHO/CHIT-SH hydrogels, respectively), the hydrophobic (91 ± 3°) PVA-CHO and the hydrophilic (45 ± 2°) CHIT-SH were mixed together as presented in **Figure 23**. Since the crosslinking network structure (imine bond) was increased by increasing the polymer concentration, this led to an increase in the hydrophobicity of the formed hydrogel, which may be a useful approach to control the drug release from the hydrogel matrix, as will be demonstrated in the *in vitro* drug release section.

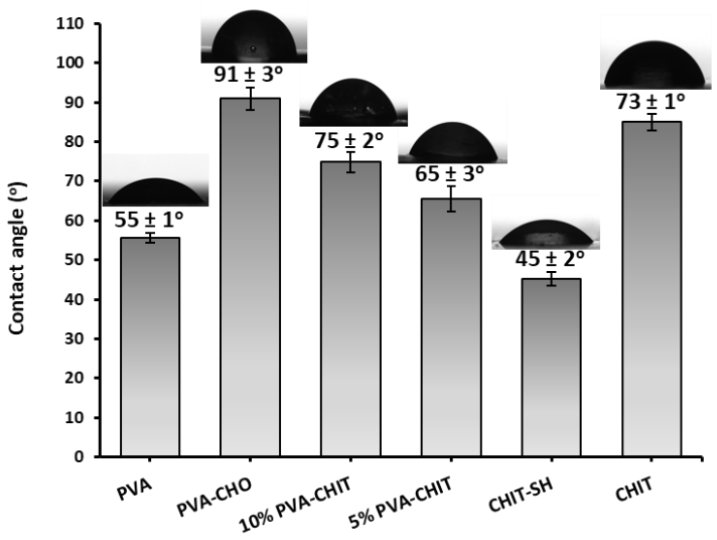

Figure 23. Water contact angle measurements (after 1 min) for dried films of initial and modified polymers and hydrogels [249].

The swelling of the lyophilized hydrogels with various concentrations (2, 5, and 10% *w/v*) was further examined after analyzing the wetting characteristics of the dry polymers under physiological circumstances (PBS, pH 7.4, 37°C). As shown in **Figure 24A**, reducing the swelling of the hydrogel in the PBS buffer solution was achieved by increasing the crosslink density by forming an imine bond between the PVA-CHO and CHIT-SH polymers. The equilibrium swelling ratio of the 10% *w/v* PVA-CHO/CHIT-SH was the lowest (1.7 g/g), while the equilibrium swelling ratio of the 2% *w/v* PVA-CHO/CHIT-SH was the greatest (2.9 g/g). The dry xerogel rapidly absorbed water due to its moderate hydrophilic/hydrophobic feature (see **Figure 23**), which then stayed constant. Using a 0.15% lysozyme/PBS buffer solution at 37°C, the enzymatic degradation of the PVA-CHO/CHIT-SH hydrogels with various concentrations was examined, as shown in **Figure 24B**. During the first 15 days of the experiment, the rate of degradation and hydrolysis was higher (51.5%) for 10% *w/v* PVA-CHO/CHIT-SH than for 2% *w/v* PVA-CHO/CHIT-SH (47.2%) due to the increased crosslinking structure and increased hydrolysis of the imine bond and enzymatic hydrolysis of glycosidic bonds of acetylated residues in chitosan by lysozymes. The final 5 days of the experiment, however, revealed a continuous increase in the rate of degradation with a very minor variation in the overall degradation percent (52−55%). The hydrogel included a 1:1 mass ratio of CHIT (which lysozymes could readily break down) and PVA, and after 20 days, the greatest degradation was only approximately 55%, which was still acceptable if we believed that just CHIT hydrolysis had taken place.

As will be seen later, the produced PVA-CHO/CHIT-SH hydrogels at various concentrations have the necessary physicochemical characteristics to support their usage for local drug delivery and tissue engineering applications.

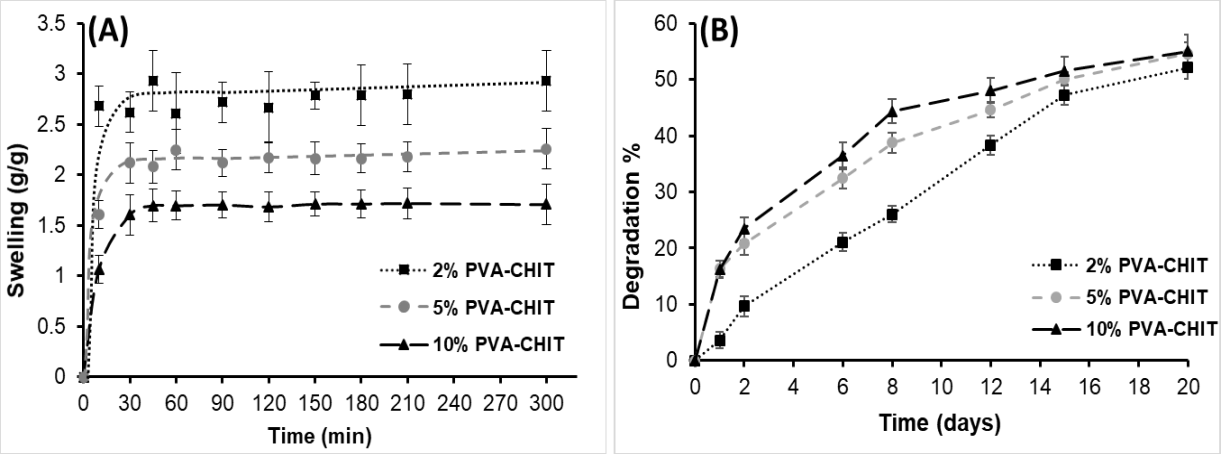

Figure 24. Swelling ratio (g/g) of PVA-CHO/CHIT-SH hydrogel with various (2, 5, and 10 *w/v*%) concentrations (**A**), Degradation of hydrogels in 0.15% lysozyme/PBS buffer solution at 37 °C at varied concentrations (2, 5, and 10 *w/v*%) (**B**) [249].

5.2.3. The mucoadhesive Characteristic of PVA-CHO/CHIT-SH Hydrogel

The thiolated polymer is among the most effective mucoadhesive polymers because it readily forms disulfide bonds (covalent bonds) with the mucous membrane via a thiol-disulfide exchange mechanism, in addition to hydrogen bonds and van der Waals forces resulting in increased *in vivo* residence time of the polymers and improved bioavailability [244]. The 3-mercaptopropionate moiety was employed to functionalize the NH_2 groups of CHIT to supply terminal thiol groups for our hydrogel. As a result, the hydrogel was able to create covalent disulfide bonds with the SH groups of the mucous membrane thanks to these free terminal thiol groups [244]. Ellman's reagent method was used to determine the thiol content of CHIT-SH. The result was 201.85 ± 12 µmol/g (4.43% modification degree), and the EDX measurement demonstrated the presence of a high sulfur content because of the thiol group of the 3-mercaptopropionate moiety of CHIT-SH, as shown in **Figure 25**. This was in contrast to pure CHIT, which lacked any indication that the sulfur element existed that would support the successful conjugation of 3-mercaptopropionic acid with CHIT.

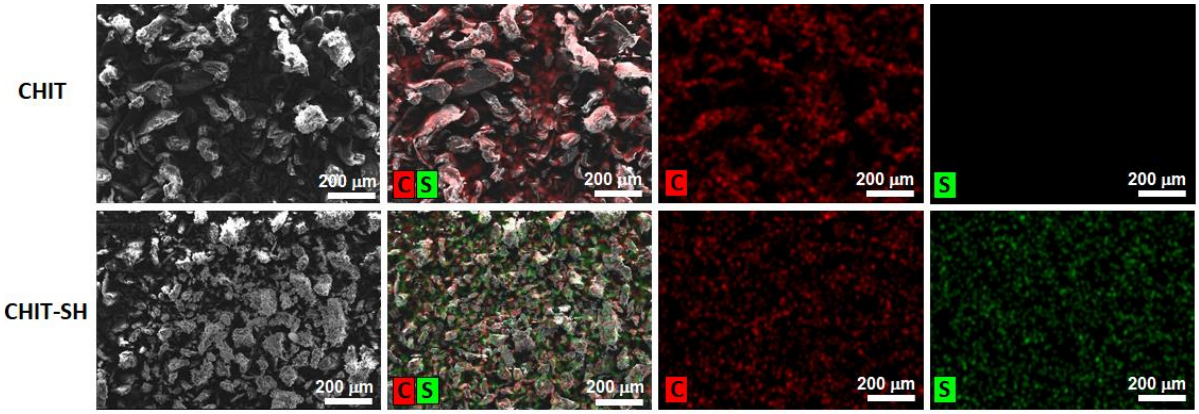

Figure 25. EDX analyses of CHIT and CHIT-SH (with 201.85 ± 12 µmol/g thiol content) powders, where S and C are sulfur and carbon, respectively [249].

Pure CHIT exhibited limited mucoadhesive strength and was poorly soluble in water at neutral and basic pHs, which were its two main drawbacks [265]. Consequently, the adhesion properties of the PVA-CHO/CHIT-SH hydrogel and the reference R-PVA-CHO/CHIT hydrogel (without SH groups) were evaluated using a mucous layer made from the intestinal membrane of a pig. It could be said that the thiol-containing polymer was more mucoadhesive (600 ± 155 mN/mm) than the reference (281 ± 45 mN/mm, without SH groups) since the work of adhesion it performed while in contact with the pig intestinal tissue was significantly ($p<0.05$) higher than that of the control (**Figure 26**). This phenomenon may be explained by the thiol-disulfide exchange mechanism, which results in the creation of disulfide bonds between the hydrogel and the mucosa. The findings showed that as compared to the PVA-CHO/CHIT combination, there was a strong attachment to the membrane which then led to a longer residence period on the mucosa [244].

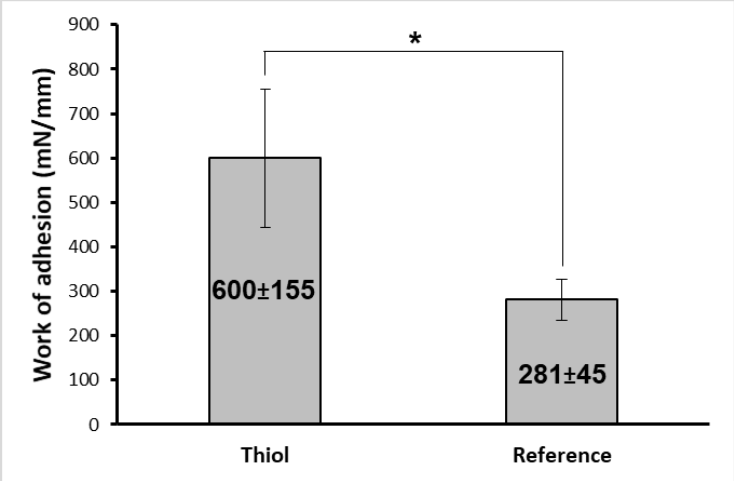

Figure 26. Work of adhesion (mN/mm) for 2% *w/v* PVA-CHO/CHIT-SH hydrogel (denoted as thiol) and 2% *w/v* reference hydrogel (denoted as reference), an asterisk (*) indicates a significant difference ($p < 0.05$) [249].

The formation of dynamic hydrogels based on chitosan has been reported in several studies using benzaldehyde derivatives [250,266,267]. However, in our study, we introduced a novel approach for the injectable hydrogel by increasing its mucoadhesive characteristics as shown in **Figure 26** and increasing the water solubility of CHIT as shown in **Figure A11**, which enhanced the drawbacks of the chitosan and raised the interest in using.

5.2.4. Self-healing and self-assembled hydrogel formation

In situ forming hydrogels are preferred over premade hydrogels for biomedical applications because they can gel upon injection under physiological conditions without the requirement for surgical procedures. Additionally, due to the fluid nature of the precursor polymer solution, which ensures proper shape adaptation, the hydrogel may include bio-components and drug particles by simply mixing them with the solution [268]. Through a Schiff-base reaction involving the aldehyde groups of PVA-CHO and the amino groups of CHIT-SH, the injectable hydrogel was crosslinked and self-assemble formed. The applicability of injecting the 7% *w/v* PVA-CHO/CHIT-SH hydrogel into the PBS solution at 37°C is shown in **Figure 27A**. The hydrogel was formed by pushing both polymers at the same rate, followed by a mixing process in the needle that gathered the exits of both syringes. We used methylene blue to stain the hydrogel (with pale white color) to demonstrate the formation of the hydrogel and to validate its encapsulating property, as shown in **Figure 27A**. The gelation periods, which varied from 45 to 7 s depending on the concentration of the polymers employed (2, 5, and 10% *w/v*, respectively), were measured using a vial inversion test (see **Figure 27B**).

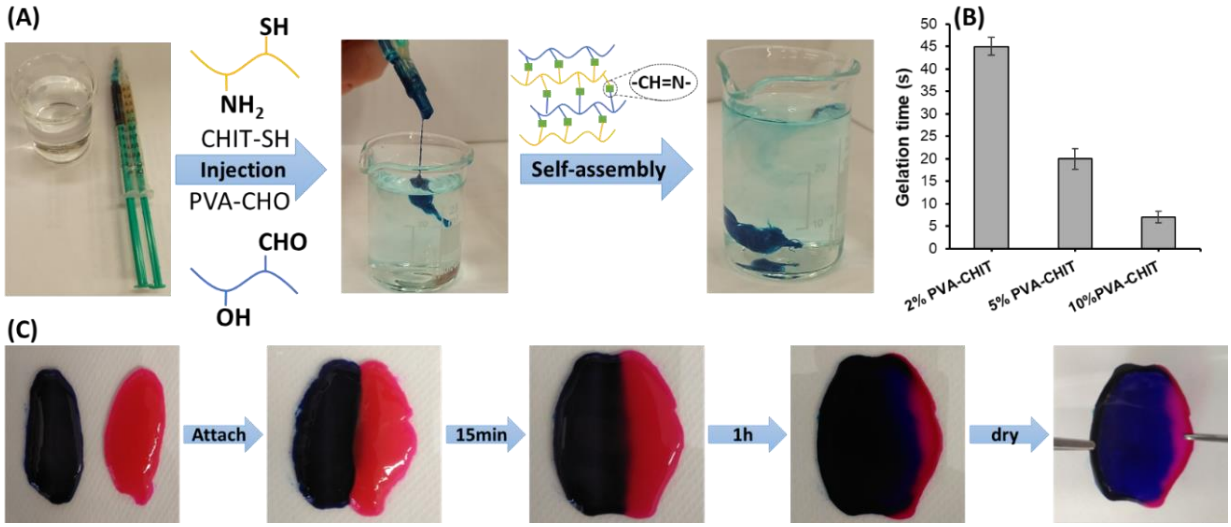

Figure 27. (**A**) The injectability of 7% *w/v* self-assembled PVA-CHO/CHIT-SH polymer solution in PBS, (**B**) the gel formation time of the hydrogel as a function of polymer concentration, as well as (**C**) the self-healing capability of the 2% *w/v* hydrogel [249].

Moreover, the PVA-CHO/CHIT-SH hydrogel showed self-healing qualities as well as in situ gel formation, which were related to the dynamics of Schiff base formation. Due to the use of methylene blue dye and rhodamine B dyes, **Figure 27C** represents the self-healing ability of 2% *w/v* PVA-CHO/CHIT-SH hydrogel with two distinct colours. The hydrogels were attached and allowed to heal for one hour. The two half-hydrogels were fully bonded as one whole after the healing period, and the resulting hydrogel was dried in the oven at 60°C overnight. The PVA-CHO/CHIT-SH dried layer demonstrated resilience against the detachment force as shown in **Figure 27C**.

The PVA-CHO/CHIT-SH hydrogel's elastic response and capacity for self-healing were evaluated by rheological recovery tests utilizing the continuous step strain technique by administering a severe deforming shear and then allowing the hydrogel to recover. The gel-sol transition shear strain for our gel system was identified by oscillatory rheology measurements, and it was 500% at a fixed angular frequency of 10 rad/s at 37°C. As a consequence of applying a large oscillatory amplitude (strain = 500%) and recovering at a low strain (strain = 1%), **Figure 28** represents the variations in the strain-dependent modulus across the three hydrogels and the changes in the sol-gel transition.

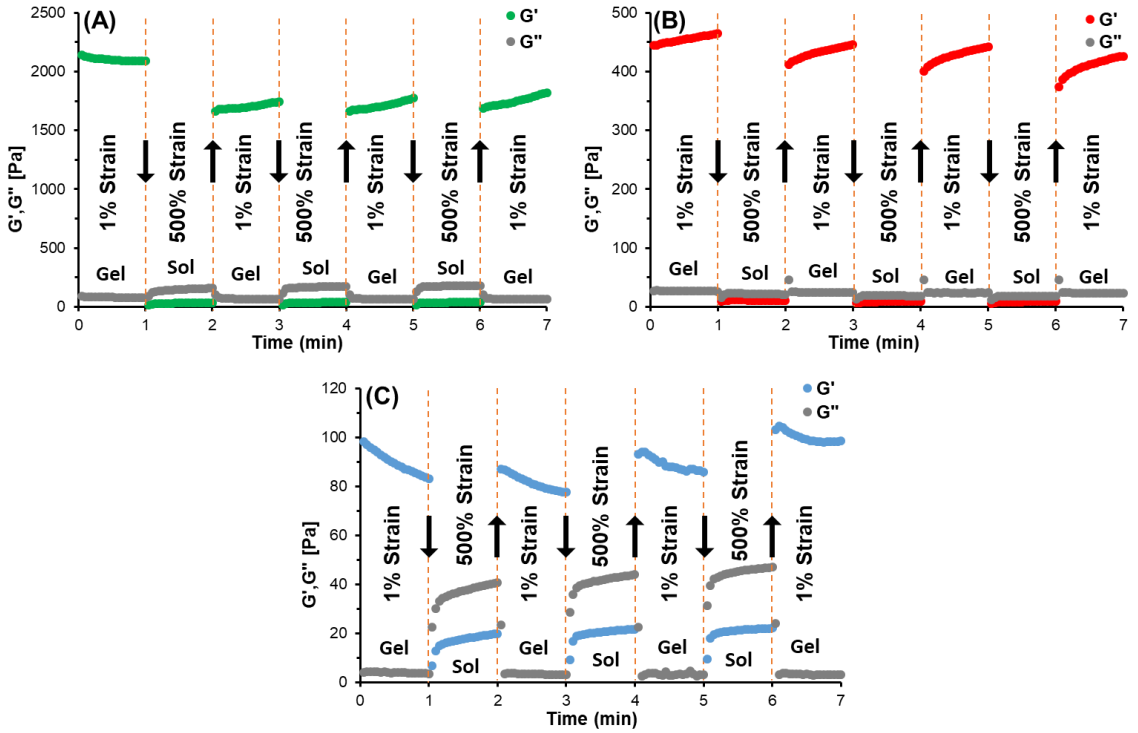

Figure 28. The recovery and self-healing of the hydrogels by using a continuous step (1% strain → 500% strain → 1% strain) strain method; (**A**) for 10% *w/v* PVA-CHO/CHIT-SH, (**B**) for 5% *w/v* PVA-CHO/CHIT-SH, and (**C**) for 2% *w/v* PVA-CHO/CHIT-SH. The storage modulus (G′) change is depicted by the arrow [249].

As shown in **Figure 28A**, the G′ value for 10% *w/v* PVA-CHO/CHIT-SH hydrogel abruptly dropped from 2090 Pa to 30 Pa when the strain was raised from 1 to 500%, but it quickly rebounded to 1700 Pa when the strain was reduced to 1% repeating this cycle twice gives the same results. Furthermore, both the 5% *w/v* PVA-CHO/CHIT-SH hydrogel (see **Figure 28B**) and 2% *w/v* PVA-CHO/CHIT-SH hydrogel (see **Figure 28C**) showed the same self-healing characteristics as the 10% *w/v* PVA-CHO/CHIT-SH hydrogel. The G′ shows a direct relationship with the increasing concentration of hydrogel as a result of the increased crosslinking density of the hydrogel structure caused by the increasing concentration of the polymers. Consequently, our dynamic hydrogels (Schiff base) have a very rapid and effective self-healing ability, as evidenced by the ability to replicate the breaking and healing properties of the hydrogel as well as the rapid recovery of the inner network of the hydrogel.

Self-healing refers to the quality of some materials that allows them to recover naturally after being damaged [269]. Our PVA-CHO/CHIT-SH hydrogel displayed self-healing characteristics as demonstrated in **Figure 28** because of the dynamic equilibrium between the Schiff-base linkage and the aldehyde and amine reactants. Hydrogels with self-healing properties are great candidates for use in drug/cell delivery applications and 3D printing because they may be injected through thin needles and retained at target places to preserve the drug/cell and enable an extended-release process.

Tissue engineering was also an application for injectable hydrogel [270]. The injectable hydrogels have a low mechanical disadvantage compared to solid-state polymeric scaffolds, however, the advantages of hydrogels, especially for in situ gel formation, are unrivaled, suggesting that injectable hydrogels can function not only as scaffolds for supporting purposes but also as functional implants for the regulation of tissue generation [270]. Poldervaart et al. created a hydrogel scaffold for bone tissue engineering based on calcium-crosslinked alginate [271]. Using the same strategy, PVA-CHO/CHIT-SH can be utilized to increase the muscle mass of the atrophied vocal fold by inducing muscular hypertrophy by adding the BMP inducer Tilorone. BMP signaling was stimulated by Tilorone, and BMP-7 expression increased [193]. 2% *w/v* PVA-CHO (in ethanol-water) and 2% *w/v* CHIT-SH (in distilled H_2O) were mixed with a dual syringe to investigate the 3D printing application of self-assembled hydrogel. **Figure A12** represents how the 2% *w/v* PVA-CHO/CHIT-SH hydrogel may be used as bio-ink to write the acronym for the University of Szeged (SZTE) as an example of the scaffold for tissue engineering application.

5.2.5. *In Vitro* Tilorone release measurements

Due to the objectives of delayed release and biodistribution control, topical drug delivery via injectable hydrogels is preferred over systemic administration [272,273]. Both water-soluble and insoluble drugs with high loading capacity can be encapsulated in injectable hydrogels [52]. Additionally, the injectable hydrogel may also contain the bioactive component, which includes genes, peptides/proteins, and living cells [52,274,275]. **Figure 29** shows the Tilorone (anti-muscle atrophy) release from various (2, 5, and 10% *w/v*) concentrations of PVA-CHO/CHIT-SH hydrogels under different conditions. In the absence of lysozyme enzyme (**Figure 29A**), pure Tilorone was released too fast, with 98% (0.023 mg/mL) cumulative drug release, whereas Tilorone release from hydrogel was slow. The percentage of cumulative drug release was around 81% (0.0187 mg/mL) and 50% (0.0114 mg/mL) from the 2 and 10% *w/v* PVA-CHO/CHIT-SH hydrogel, respectively, under physiological conditions (37°C, PBS, pH 7.4) for 7 hrs. As shown in **Figure 29B**, which shows the decline in the maximum released concentration of the Tilorone (water-soluble) drug with the increase of the hydrogel concentration as a result of higher crosslinking densities, this can delay the diffusion of the drug from the hydrogel matrix.

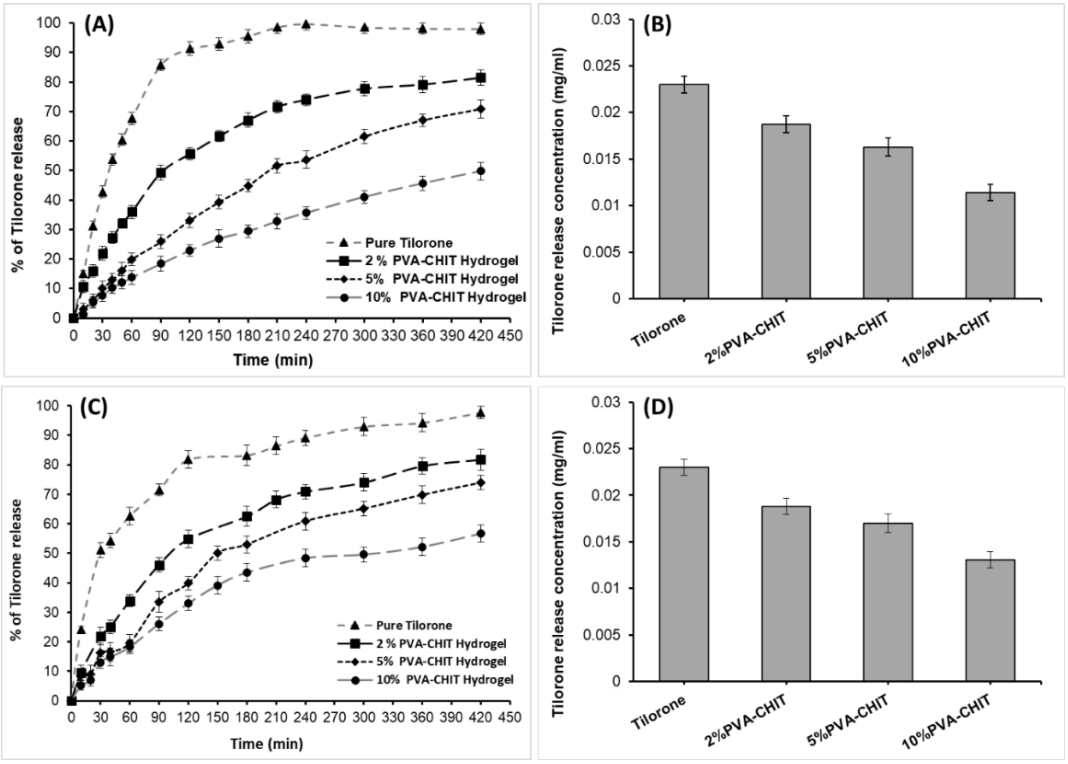

Figure 29. (**A**) The *in vitro* Tilorone release curve from various concentrations (2, 5, and 10% *w/v*) of PVA-CHO/CHIT-SH hydrogels in absence of lysozymes, (**B**) the corresponding maximum concentration (mg/mL) of Tilorone release in absence of lysozymes, (**C**) The *in vitro* Tilorone release curve in the presence of lysozymes, and (**D**) the corresponding maximum concentration (mg/mL) of Tilorone release in the presence of lysozymes [249].

As shown in **Figure 29C**, the release of Tilorone in a PBS solution containing 0.15% lysozymes was also studied. Based on the crosslinking density, the release of the drug from the hydrogel structure increased by 1–6% compared to using pure PBS buffer solution. After 7 hrs, the cumulative drug release percentage was around 82% (0.0188 mg/mL) and 56.6% (0.013 mg/mL) from the 2 and 10% *w/v* PVA-CHO/CHIT-SH hydrogel, respectively. This was caused by the enzymatic degradation of the hydrogel structure, which also increased the release of the drug. The various kinetic models depicted in **Table 4** were used to understand the drug release kinetics in the absence of lysozyme. In contrast to the release from the hydrogel form of various concentrations, which fits with the Higuchi release model and suggested that the drug was released by diffusion from the hydrogel network, the release of pure Tilorone was explained by a first-order model which indicated that the release kinetics depended on the concentration of the drug in the dosage form [157]. Furthermore, it is evident that upon increasing the concentration of the hydrogel, the K_H (Higuchi's release constant) decreased as a result of the increase in crosslinking density, which hindered drug diffusion from the hydrogel network.

Table 4. Different kinetic models to interpret the Tilorone release experiments results in the absence of lysozymes [249].

	Zero-Order Model		First-Order Model		Higuchi Model		Hixson–Crowell Model		Korsmeyer–Peppas Model		
Sample	**r^2**	**k (h^{-1})**	**r^2**	**k (h^{-1})**	**r^2**	**k ($h^{-1/2}$)**	**r^2**	**k ($h^{-1/3}$)**	**n**	**r^2**	**k (h^{-n})**
Pure Tilorone	0.6602	12.49	0.8142	0.65	0.7841	35.375	0.5194	0.218	0.546	0.5745	41.029
2% PVA-CHIT	0.8273	11.27	0.9403	0.25	0.962	34.553	0.5293	0.373	0.649	0.3946	25.834
5% PVA-CHIT	0.9513	10.59	0.9946	0.18	0.9956	32.519	0.6979	0.428	0.906	0.6579	13.810
10% PVA-CHIT	0.9643	6.911	0.9901	0.096	0.9997	21.662	0.8091	0.307	0.909	0.702	9.687

Additionally, using the same kinetic models, the kinetics of Tilorone release in the presence of lysozymes was examined as shown in **Table 5**. The drug release results from the pure Tilorone and the hydrogel forms mathematically fit with the first-order and the Higuchi release models, respectively. Due to the degradation of hydrogel (~2–5%) throughout the release studies as shown in **Figure 24B**, the drug release rate from the hydrogels was somewhat (1–2 $h^{-1/2}$) higher than in the experiments without the enzymes as shown in **Table 4** and **Table 5**. Eventually, our hydrogel system can control drug release based on crosslinking density and/ or concentration of hydrogel.

Table 5. Different kinetic models to interpret the Tilorone release experiments results in the presence of lysozymes [249].

	Zero-Order Model		First-Order Model		Higuchi Model		Hixson–Crowell Model		Korsmeyer–Peppas Model		
Sample	**r^2**	**k (h^{-1})**	**r^2**	**k (h^{-1})**	**r^2**	**k ($h^{-1/2}$)**	**r^2**	**k ($h^{-1/3}$)**	**n**	**r^2**	**k (h^{-n})**
Pure Tilorone	0.744	8.388	0.972	0.442	0.886	28.69	0.637	0.174	0.333	0.915	57.042
2% PVA-CHIT	0.855	11.03	0.966	0.243	0.982	35.05	0.548	0.387	0.702	0.399	22.563
5% PVA-CHIT	0.911	10.55	0.977	0.191	0.979	33.39	0.629	0.397	0.727	0.487	18.150
10% PVA-CHIT	0.886	7.544	0.934	0.116	0.972	24.43	0.778	0.279	0.739	0.535	14.467

Finally, human embryonic lung fibroblasts (MRC-5) cells were used to examine the biocompatibility and cytotoxicity of our hydrogel. As demonstrated in **Figure 30**, our hydrogels at various doses were safe and biocompatible with utilized cells. The increased growth of the cells on the hydrogel's solid surface was also evident in the fact that the number of cells (cell proliferation) rose higher in the hydrogel samples (OD = 0.289 ± 0.036 for 5% *w/v* PVA-CHO/CHIT-SH hydrogel and OD = 0.273 ± 0.031 for 10% *w/v* PVA-CHO/CHIT-SH hydrogel) compared to the control (OD = 0.14 ± 0.028) (see **Figure 30B**). Other biocompatible hydrogels have seen similar results as well, as reported [276,277].

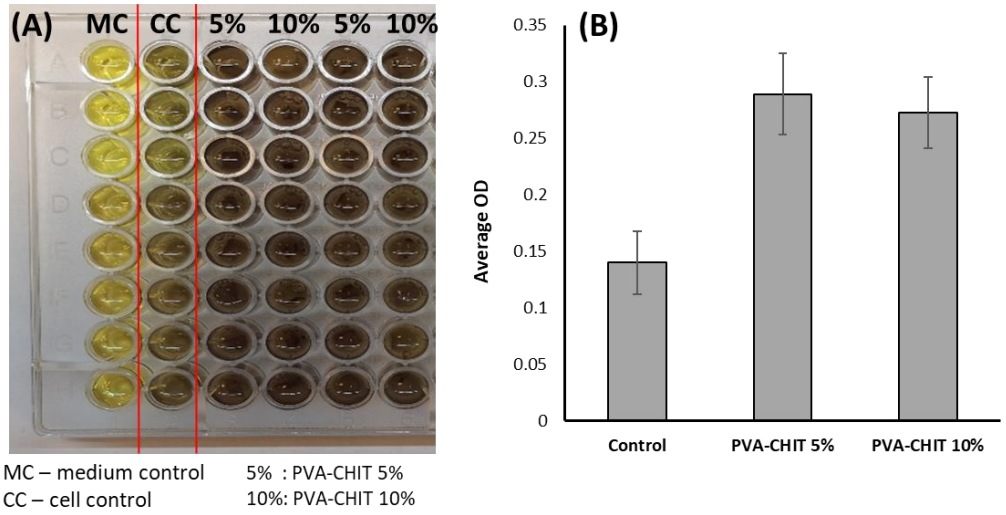

Figure 30. Biocompatibility evaluation of the PVA-CHO/CHIT-SH hydrogel; (**A**) photo of MRC-5 cell viability for two hydrogels and comparison to cell control (CC), (**B**) the average optical density (OD) for two hydrogels and comparison to cell control [249].

As we have seen in sections **5.1.4** and **5.2.5**, the first strategy—which involves the covalent bond of the drug with the polymer chain—is advised for prolonging the drug release process over days, while the hydrogel approach is advised for a single day of release.

In this part, we try to introduce a novel potential therapeutic approach for the local treatment of muscle atrophy (laryngotracheal atrophy) by developing a dynamic injectable mucoadhesive PVA-CHO/CHIT-SH hydrogel incorporating Tilorone, a BMP inducer. The viscosity of the 2% *w/v* hydrogel is more than a thousand times (9800 mPa·s) compared to the viscosities (5.8 and 4.6 mPa·s) of the polymer solutions used. It has higher adherence (600 ± 155 mN/mm) to the pig intestinal membrane compared to reference hydrogel (281 ± 45 mN/mm, without SH groups). The hydrogel could control the drug release (81–50%, 82–56.6% in the absence and presence of 0.15% lysozyme) based on the crosslinking density/concentration (2–10%) of the hydrogel. In summary, we can state that the developed PVA-CHO/CHIT-SH hydrogel is a suitable candidate for the controlled release of Tilorone drug due to its various advantages including injectability (easy delivery by syringe), prolonged drug release, self-healing, rapid in situ gelation, minimal surgical wounds, biocompatibility, and strong mucoadhesive properties.

5.3. Biocompatible poly(ethylene succinate) polyester for Nimodipine

The objective of this part was to develop a viable drug delivery system (DDS) for increasing the bioavailability and reducing the undesirable side effects of Nimodipine (NIMO) as a calcium channel blocker drug. Therefore, PES polymers with different molecular weights were prepared as suitable for the encapsulation of NIMO and the physical and chemical characteristics of the polymer were investigated. Thus, the bioavailability of the poorly water-soluble NIMO drug is increased by encapsulating it in biodegradable and biocompatible PES, which reduces the crystallinity of the drug and increases the stability of the encapsulated form in an aqueous medium. Moreover, NIMO drug release can also be controlled by altering the molecular weights of the synthesized PES polymers.

5.3.1. Structural and physicochemical characterizations of PES polyesters

In an effort to produce a suitable biocompatible and biodegradable polyester that might be used in biomedical applications like drug delivery applications, PES polyester was synthesized using a direct condensation polymerization method with polymerization time-dependent molecular weight. Without the use of catalysts, polycondensation between dicarboxylic acid (succinic acid) and diol (ethylene glycol) in an equimolar ratio at 185 °C (see **Figure 31**) was carried out in order to synthesize PES polyester [278]. The polycondensation of the initial monomers and the synthesis of the polyester macromolecules was indicated by the production of a yellow waxy (photo inset in **Figure 31**) from the clear reactants [278].

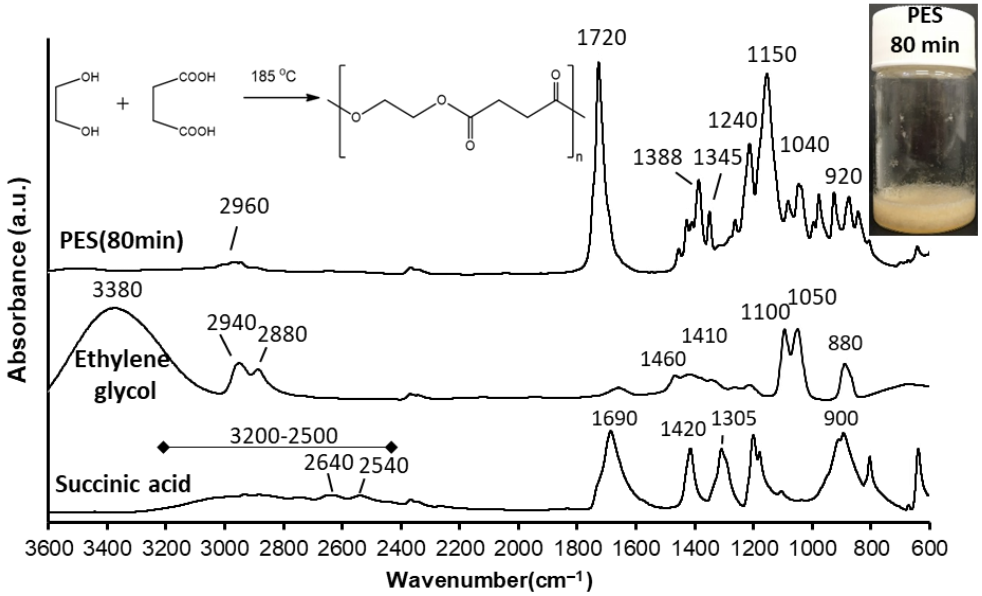

Figure 31. FTIR spectra of initial monomers and the synthesized PES polyester sample (polycondensation time = 80 min). The enclosed scheme illustrates how succinic acid and ethylene glycol condense to form PES (inserted up-right photo) [278].

To adjust the molecular weight of the synthesized PES polyester, the polymerization time was systematically increased during the step-growth polycondensation reaction [279,280]. FTIR and NMR measurements were used to confirm the successful polycondensation reaction and synthesis of PES polyester. **Figure 31** shows the FTIR spectra of initial monomers (ethylene glycol and succinic acid) and synthesized PES. Succinic acid has the main characteristic peaks at 3200–2500 cm^{-1} (O–H broad stretching vibration), 2640 and 2540 cm^{-1} (C–H stretching), 1690 cm^{-1} (C=O stretching vibration), 1420 cm^{-1} (C–O–H in-plane bending), 1305 cm^{-1} (C–O stretching vibration), and 900 cm^{-1} (–OH out of plane bending) [281]. Moreover, the ethylene glycol has the main characteristic peaks at 3380 cm^{-1} (OH stretching vibration), 2940 and 2880 cm^{-1} (C–H asymmetric and symmetric stretching), 1460 cm^{-1} (CH_2 bending), and 1410 cm^{-1} (C-O-H bending), 1100 and 1050 cm^{-1} (C–O stretching), and 880 cm^{-1} (CH_2 rocking) [282]. The success of the polymerization reaction was demonstrated by the FTIR spectrum of PES, which exhibits the appearance of a new absorption peak at 1720 cm^{-1} due to the (C=O stretch vibration) of the ester bond, as well as the disappearance of absorption peaks of the (OH stretching vibration) of ethylene glycol and the (C=O stretching vibration) of succinic acid. The absorption peaks at 1150–1240 cm^{-1} due to the (–C–O–C–) ester bond stretching vibration, while the peak at 1040 cm^{-1} relates to (–O–C–C–) stretching vibrations and 920 cm^{-1} (–C–OH) bending for the (COOH) groups of PES polyester. Also, the peaks at 1388 cm^{-1} and 1340 cm^{-1} correspond to the CH_2 deformational vibrations for the PES main chain [283].

DSC and TGA measurements were used to examine the thermal characteristics of the produced PES samples and initial monomers. **Figure 32A** displays the DSC curves of the initial monomers utilized, succinic acid and ethylene glycol monomers have decompositions temperatures of 255 and 205 °C, respectively, whereas succinic acid has a melting point of 184 °C. **Figure 32B** depicts the DSC (grey) and TGA (black) curves of PES (80 min) with the absence of corresponding peaks of monomers in the prepared PES samples, indicating that the purification process was successful. In order to achieve melted succinic acid and prevent the decomposition of monomers and the polyesters produced, the optimal polymerization temperature must be between 184 and 195 °C based on the decomposition temperature and melting point of the monomers employed. According to **Figure 32B**, the peaks of PES-80 min at about 55.3 and 80°C are related to crystallization temperature (T_c) and melting point (T_m) [284], respectively, the decomposition of polyester began after 210 °C in both curves, indicating that the first decomposition step with a weight loss of about 25% was between 215 and 315 °C, and from 315 to 500 °C was the second decomposition step with a weight loss of about 65%, and the total weight loss was about 90%. According to these findings, it is advised to utilize a polymerization temperature of less than 200 °C while synthesizing polyester to prevent polyester from degrading and losing molecular weight due to thermal degradation.

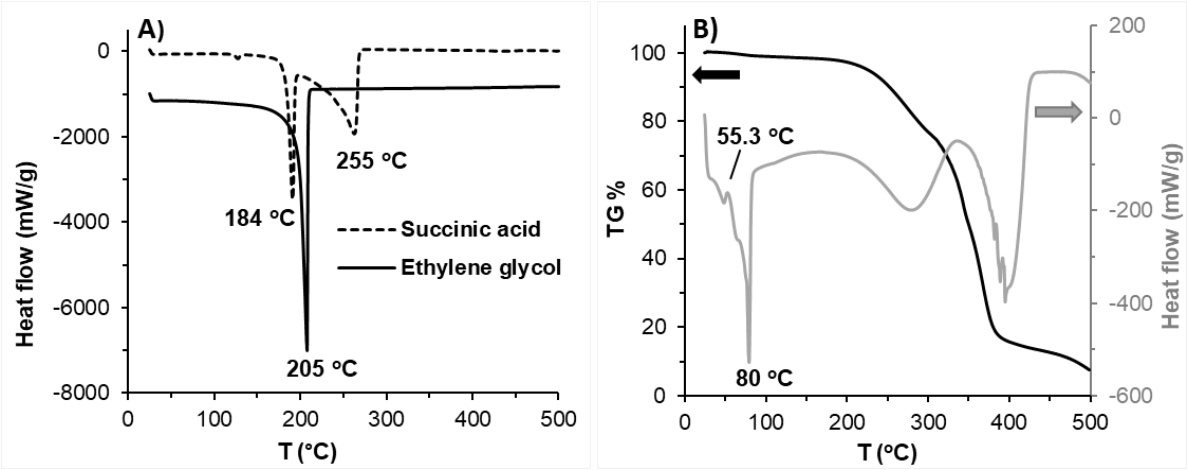

Figure 32. (**A**) DSC curves of the succinic acid and ethylene glycol (initial monomers), (**B**) TGA and DSC curves of PES (polycondensation time = 80 min) polyester [278].

The polymerization yield of the produced PES was determined at the optimal polycondensation temperature (~185 °C), and **Figure 33** illustrates this as a function of polymerization time. This was done by using a simple acid-base titration to detect the quantity of reacted succinic acid with ethylene glycol. Due to the step-growth process, the percentage of polymerization rapidly rose with increasing reaction time as a dime, trimer, oligomer, and finally, long-chain polymers

were formed. The maximum polymerization percentage was reached at approximately 92% after an 80–100 min reaction time, indicating a gradual reduction of the available COOH groups over time until reaching a plateau value.

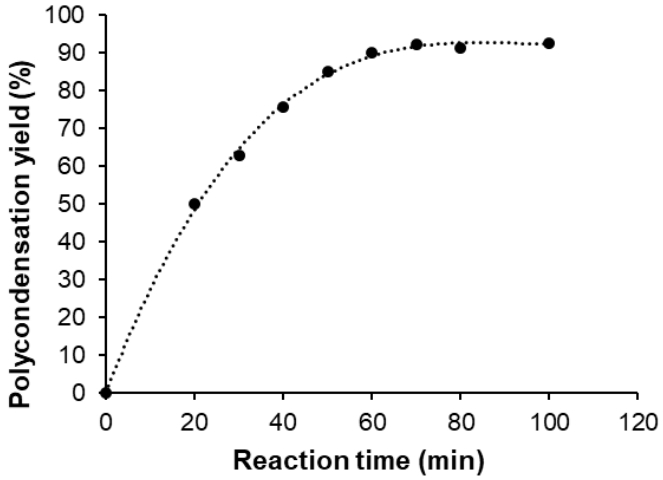

Figure 33. Polycondensation yield (%) of PES formation as a function of polycondensation time [278].

The degree of polymerization ($\overline{X}_n$) as a function of the conversion percent of monomers (P%) was shown in **Figure 34**. According to the curve, we can conclude that the current mechanism of polymerization for ethylene glycol and succinic acid is the step-growth mechanism in which $\overline{X}_n$ increases gradually with the increase of the conversion percent until it reaches ~75%, then the $\overline{X}_n$ dramatic increase until reaching to12.67 at a maximum conversion percent of 92%.

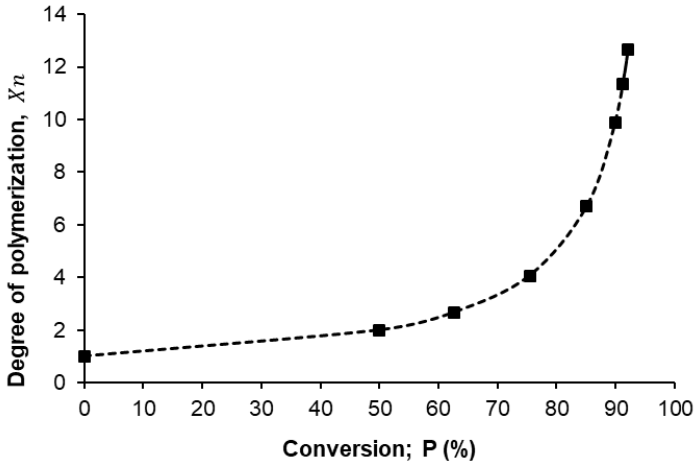

Figure 34. Degree of polymerization ($\overline{X}_n$) as a function of monomer conversion (P %) [278].

Following that, we investigated how the molecule mass varies with the increasing time of polycondensation. By using ^{1}H-NMR spectroscopy, the chemical structure and molecular weight of synthesized PES were determined. It is anticipated that the resultant PES will

statistically terminate at one end with a carboxylic group (end group I) and the other end with a hydroxyl group (end group II) since the polymer was produced by the reaction of an equimolar number of monomers (ethylene glycol and succinic acid). The integration of the characteristic proton peaks was used to compute the number of repeating units (n) and, consequently, the number-average molecular weight (M_n) of the PESs [223]. The partial ^{1}H-NMR spectrum of PES-80 min is depicted in **Figure 35** along with peak assignments, the chemical structure, and the estimated molecular masses of the repeating unit and end groups. The methylene protons ***c*** and ***d*** in the repeating units of PES were attributed to the singlet peaks that appeared at 4.21 (δH^c) and 2.57 (δH^d) ppm [285]. While the methylene protons of end group (I) yield overlapping signals (δH^a and δH^b) with those of the used solvent (DMSO-d_6) at 2.46–2.53 ppm, the triplets of CH_2 protons of end group (II) could be seen at 4.02 (δH^e) and 3.55 (δH^f) ppm, respectively, with low intensity. The equation shown below (**Equation (21)**) can be used to calculate the M_n of PESs:

$$M_n = 144 \times \frac{I(c)}{2 \times I(f)} + 101 + 61 \qquad (21)$$

where $I(f)$ and $I(c)$ are the peak areas of the corresponding methylene protons, while the values 101, 61, and 144 are the molecular weights of the end groups I and II and the repeating unit of PES, respectively (see **Figure 35**).

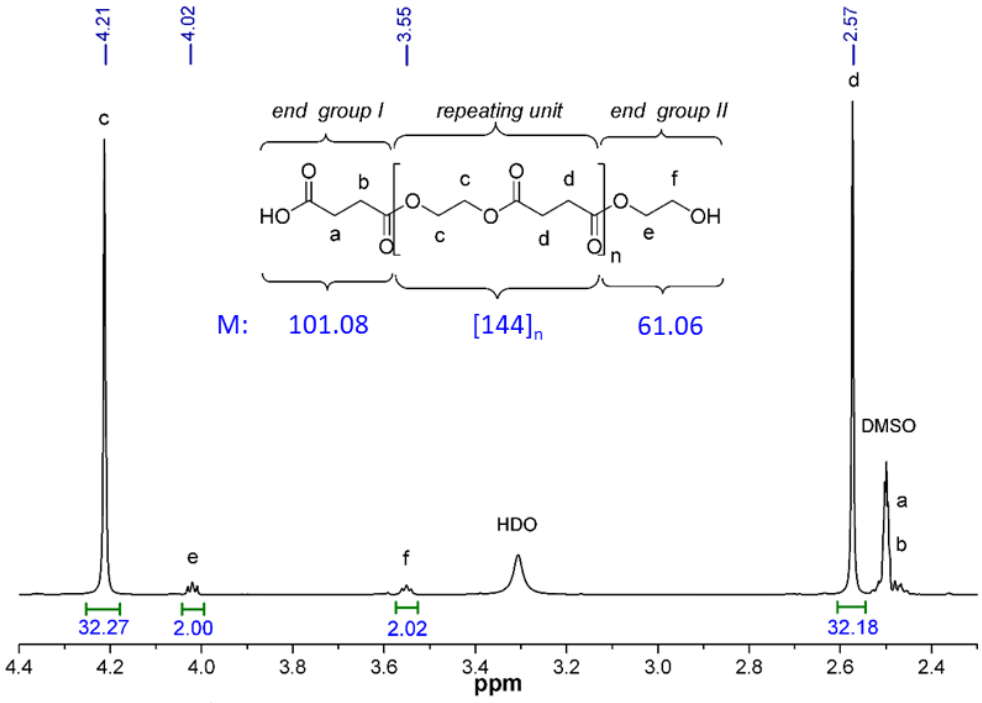

Figure 35. The extended ^{1}H-NMR partial spectrum of PES-80 min including peak assignments and calculated molecular masses of the structural units [278].

The calculation also accounts for the fact that there are twice as many "***c***" protons in the repeating unit as there are "***f*** " protons in end group II. This also implies that there are n = 8 repeating units in a PES-80 min (**Table 6**). The results presented in **Table 6** show that relatively low molecular weight polyesters (between M_n = 846 to 1312 g/mol) were produced without the need for a catalyst, however, the M_n values increased continuously up to 80 minutes of polymerization times. However, the measured M_n showed a slight decrease (1110 g/mol) with the extension of the reaction time, indicating that the ideal time for polycondensation is about 80 minutes and that after this reaction time, even at the optimal (T = 185 °C) temperature, thermal degradation is observed. The number (M_n) and weight average molecular weights (M_w) of the polyesters were also measured by GPC in addition to the above-mentioned M_n values obtained by NMR. **Table 6** provides a summary of the findings, and **Figure A13** displays a typical GPC molecular weight distribution curve for polyester derived with an 80 minutes polycondensation period. As can be shown, the results found from ^{1}H-NMR end-group analysis (846–1312 g/mol) are lower than the M_n values found by GPC (2592–3394 g/mol). The literature has mentioned this difference in M_n levels for the identical polymers obtained by NMR and GPC studies several times [286,287]. Despite being the most common method for determining the molecular weight distribution of polymers, GPC still has limitations due to the data's high reliance on the calibrant (in this case, polystyrene). The hydrodynamic radii of the standard and the measured polymer may need to be assumed to be the same at an equivalent molecular weight in order for this comparison to make sense. Additionally, it could be required to assume that the polymers have comparable elution volume/chain length properties while the GPC calibration curve is in its linear selective permeation domain. In contrast, NMR is a precise technology that provides accurate data on the molecular weight and structure of polymers. As a result, the M_n from NMR, and M_w from GPC were utilized for further evaluations.

Table 6. The number of repeating units (n), polydispersity index, M_n, and M_w values for the synthesized PES samples [278].

Polymer	*I* (*c*) *	*I* (*f*)*	Number of Repeating Units (n)	M_n * (g · mol^{-1})	M_n ** (g · mol^{-1})	M_w ** (g · mol^{-1})	M_w/M_n **
PES-40 min	20.03	2.11	5	846	2592	4287	1.653
PES-60 min	24.27	2.05	6	1014	2819	4462	1.584
PES-70 min	28.21	2.09	7	1134	3158	4675	1.480
PES-80 min	32.27	2.02	8	1312	3394	5046	1.513
PES-100 min	28.18	2.14	7	1110	2964	4466	1.507

* Determined by the integrated intensity of the corresponding peaks in the respective ^{1}H-NMR spectrum;
** Determined by GPC measurements.

Moreover, the polydispersity index values (PDI, ratio of M_w to M_n) revealed that comparatively monodisperse polymers were formed as shown in **Table 6**, and the M_w values increased (from 4287 to 5046 g/mol) with the increasing polycondensation duration (from 40 to 80 min).

It is necessary to synthesize polymeric material with intermediate hydrophilicity because the polymer needs to be compatible with both the aqueous medium and the hydrophobic drug to construct an appropriate drug delivery system (DDS) for a poorly water-soluble drug like NIMO. A too-high molecular mass is not favorable in this regard because it is well-known that the solubility of polymers diminishes with increasing molecular weight. Importantly, the hydrophilicity of the polyester was also dependent on the polycondensation time and/or the molecular weight of PES. To increase the bioavailability and biodegradable characteristics of PES after it has achieved its main drug delivery function, moderate hydrophilicity of PES is a crucial aspect in improving the stability of NIMO-loaded NPs in the aqueous medium. The biocompatibility of polymers also depends on their hydrophobicity such as their biodegradability. Increased hydrophilicity of the polymer may greatly accelerate biodegradation as water more readily attacks the chains of hydrophilic polymers during hydrolysis [288]. Previous studies have reported that hydrophobic polymers are less biocompatible than hydrophilic ones since cell attachment and grow more quickly and efficiently on hydrophilic surfaces [289–291].

Water contact angle (Θ) measurements were carried out to assess the surface hydrophilicity of the produced PES samples, and the related results are shown in **Figure 36**. Continuous polycondensation of monomers produced polyester macromolecules with progressively more hydrophobic characteristics during the production of PES. As a result, increasing the polymerization time also raised the contact angle measurement since it increased the hydrophobicity and molecular weight as well, as shown in **Figure 36**. The highest M_w PES-80 min (M_w = 5.05 kDa) had the highest Θ value at about 41.3 ± 0.83°, while the lowest M_w PES-40 min (M_w = 4.3 kDa) had the lowest Θ value at around 26.8 ± 0.51°. According to the findings, we can say that the prepared PES have moderately hydrophilic surfaces that are suitable for the encapsulation of drugs that are poorly water-soluble and will improve their stability in an aqueous system, as we will see in the stability (**5.3.2**) section. The surface hydrophilicity of the PES samples also decreased with the increase in polymerization time and molecular weight due to decreasing hydrophilic groups and increasing polyester chain length.

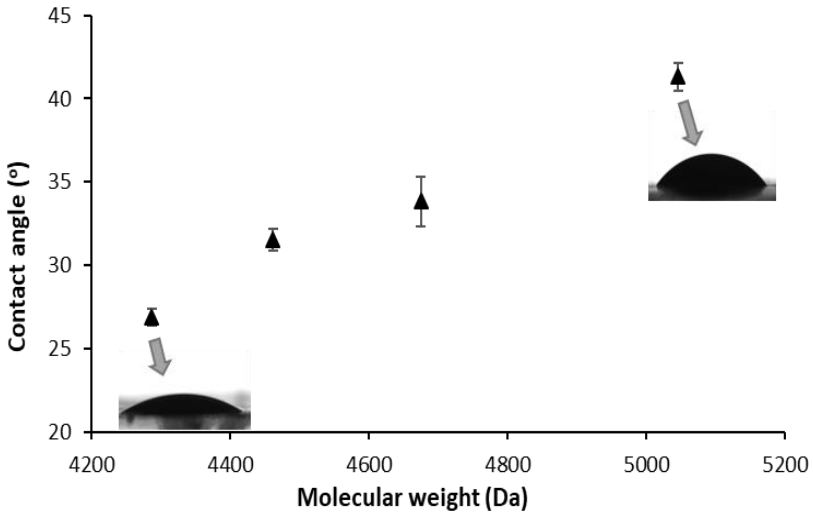

Figure 36. Water contact angle measurements for PES films as a function of increasing molecular weights (M_w) [292].

Next, DSC measurements were used to examine the thermal properties of the obtained PES samples. The thermal behaviors of several PES samples are depicted in **Figure 37A**. There is a clear trend for the melting point to increase with increasing polymerization time and/or molecular weight since the melting point (T_m) of PES-40 min (M_w = 4.3 kDa) was only 60 °C while the T_m of PES-80 min (M_w = 5.05 kDa) was 80 °C (see the inserted table in **Figure 37A**). Poly(alkylene succinate)s have very low glass transition temperatures (T_g) due to the significant degree of elasticity of the aliphatic polyester chain, with the reported value for PES being about 12 °C [293].

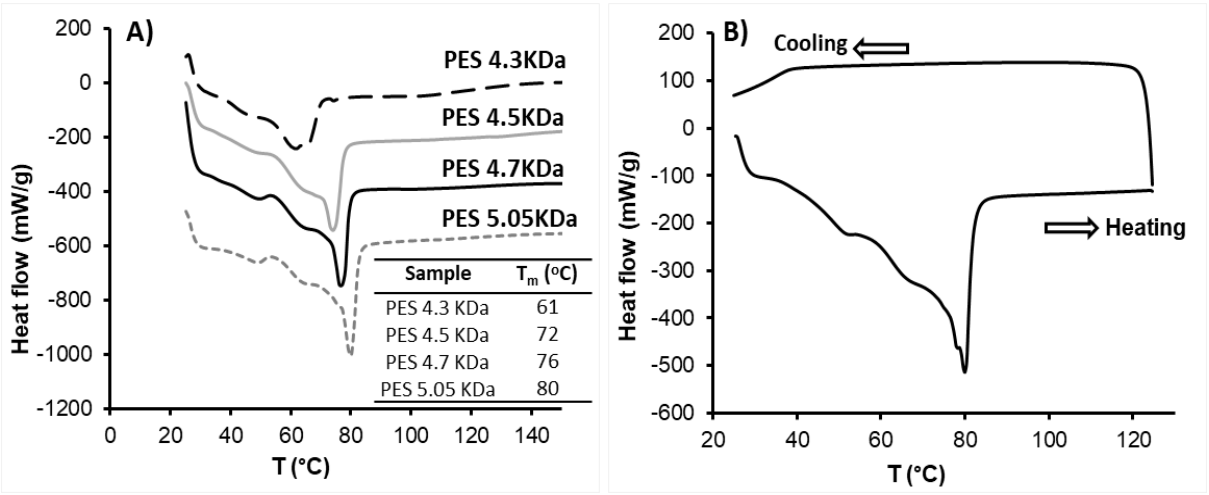

Figure 37. (**A**) DSC curves of polyester samples (PES) with different molecular weights, (**B**) the heating and cooling DSC curves for the PES 80 min (5.05 kDa) sample. The enclosed table displays the melting temperatures (T_m) of PES as M_w increases [292].

The produced PES shows significantly lower crystallinity as shown in **Figure 37B** because of its amorphous structure, and as previously observed by Zhou et al. [284], the crystallization peak could not be identified in the PES's DSC cooling curve. For our purposes, lower crystallinity is appropriate because the crystal structure of the sample also affects solubility (and biodegradability). Therefore, the incorporation of NIMO into an amorphous form of PES will help provide a suitable carrier with increased solubility, which means increased stability in an aqueous medium and improved bioavailability.

Moreover, we were interested in how the mechanical characteristics of PES vary with temperature since the thermal analysis of the PES sample clearly demonstrates temperature-dependent phase transition with rising temperature. Rheological measurements were used to examine how temperature affected the viscosity of PES samples, as shown in **Figure A14**. The viscosity of the PES-80 min (M_w = 5.05 kDa) and PES-40 min (M_w = 4.3 kDa) samples was observed as a function of cooling till it reached 30 ^oC after the samples had been heated to 150 ^oC. As shown in **Figure A14**, the viscosity of the PES samples was comparatively higher at a temperature lower than that of the human body (37 ^oC), but considerably lower above this temperature. The temperature at which the PES liquefies/solidifies was found to be 38.4 °C by finding the intercept of the two lines with different slopes, which shows that this temperature is quite similar to that of the human body. The release will be regulated by converting solid PES to a liquid-like or partially molten state with drug molecule diffusion and PES molecular weight variation, as we shall see later in the *in vitro* drug release section (**5.3.3**). This makes PES a good choice as a drug delivery system for the human body.

Traditional (nano)precipitation was frequently used to encapsulate drug molecules with various solubility qualities in a polymeric matrix, which required an understanding of the polymer (and drug) solution behavior parameters. As a result, the solubility and precipitation characteristics of the synthesized PES were thoroughly investigated utilizing water as a precipitant and biocompatible DMSO as a solvent. First, turbidimetric titration was used to determine the Θ-composition of these biocompatible solvents for the PES. Distilled H_2O was added to several concentrations (0.2, 0.4, 0.6, 0.8, and 1% *w/v*) of PES-80 min (M_w = 5.05 kDa) in DMSO, and polymer precipitation was observed using a turbidimeter to determine the volume fraction of the water at which the polyester began to precipitate. The intercept in **Figure 38** between the logarithm of the volume fraction of H_2O **(**Log Φ_{water}) and the logarithm of the corresponding volume fraction of polyester (Log Φ_{PES}) was −0.5099, indicating that the theta solvent for PES

in the H_2O/DMSO mixture is approximately 0.309 of the volume fraction of H_2O, which was in perfect agreement with the data shown in **Figure 39**.

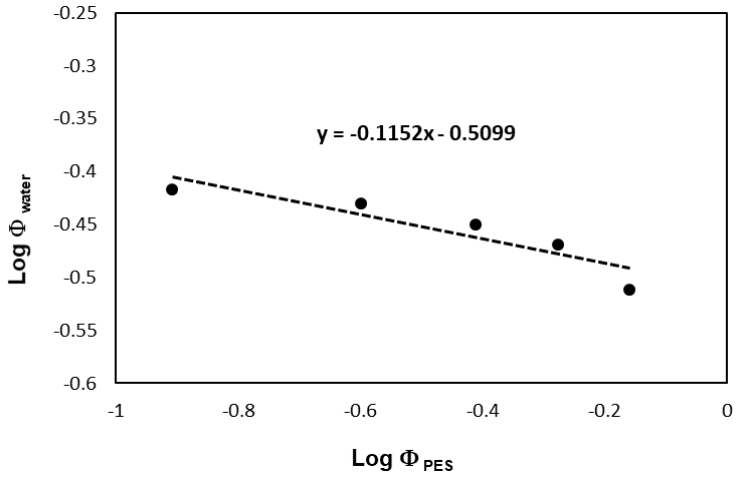

Figure 38. Turbidimetric titration of PES-80 min solution in DMSO with H_2O; Log Φ_{water} required for initiation precipitation as a function of Log Φ_{PES} [278].

Having determined the Θ-composition of the PES polyester solution in an H_2O/DMSO system, we are seeking to understand how the molecular weight of the polymer affects the precipitation characteristics of the polymer. The solubility of PES polyester samples with increasing molecular mass was also investigated using the precipitation method, as presented in **Figure 39**, because it is widely known from previous studies that the solubility characteristics of polymers are dependent on their molecular weight [294,295].

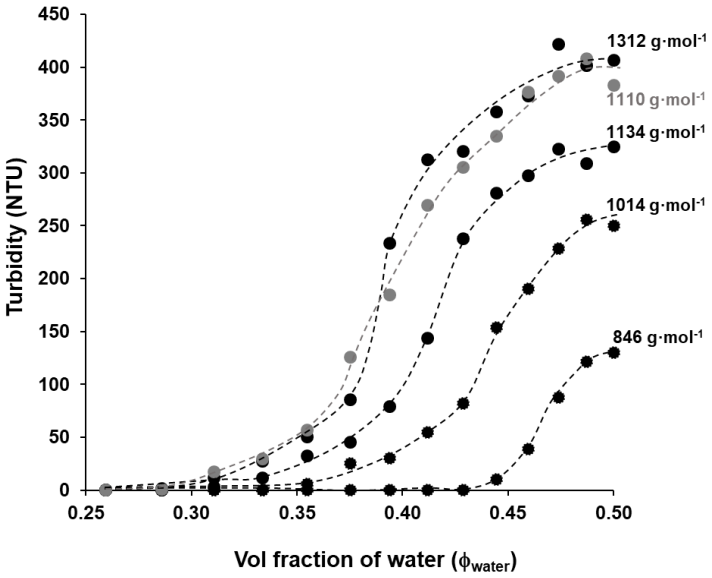

Figure 39. The precipitation curves of the synthetic PES polyester as increased molecular weight in relation to the amount of H_2O fraction in the H_2O/DMSO mixture (by drop-wise adding distilled H_2O to precipitate 10 mL 1% *w/v* PES solution in DMSO) [278].

Figure 39 shows that the lowest H_2O need (Φ_{water} = 0.286) is for the PES polyester with the highest molecular weight (M_n = 1312 g/mol), but for the lowest molecular weight PES (M_n = 846 g/mol), the precipitate forms when the amount of added H_2O surpasses around 0.44 (v/v). In other words, the molecular weight of PES and the volume fraction of H_2O (Φ_{water}) are inversely correlated. These observations are completely consistent with the hypothesis put out here, according to which the solubility of the PES can vary depending on its molecular mass, as seen in both **Table 6** and **Figure 39**. After adding 10 mL of distilled H_2O to 1% *w/v* PES solution in DMSO, the maximum turbidity values clearly changed due to variations in the molecular weight. For example, PES 80 min (M_n = 1312 g/mol) and PES 40 min (M_n = 846 g/mol) had turbidity values of 400 NTU and 130 NTU, respectively. The turbidity of the polymer solution rises as the highest molecular weight macromolecules precipitate. This phenomenon is suitable for tracking polymer precipitation and calculating the molecular weight. Thus, it can be concluded that under the aforementioned reaction conditions (T = 185 °C, polycondensation time = 40 – 80 min, catalyst-free equimolar reaction), the molecular weights of polyester varied between M_n = 846 and 1312 g/mol, but even on this relatively narrow range of molecular weights, the solubility/precipitation properties of polyester were significantly changed in the DMSO/H_2O mixture between Φ_{water} = 0.28 and 0.44. In other words, when the time of polycondensation increased, the observed M_n values increased as well, which is evident in the polymer's solubility. Low molecular weight oligomers are produced under catalyst-free conditions (M_n values not surpassing 1312 Da by ^{1}H-NMR), possibly as a result of the reversibility of the esterification reaction (hydrolysis may also occur, particularly when terminal groups are not protected by an appropriate active form of catalyst) and the degradation of the polymer over a longer period of synthesis time (e.g. PES-100 min).

The Schulz equation (**Equation** (**20**)) may be used to calculate the relevant A and B coefficients if we know the values of M_n (**Table 6**) and Φ_{water} (**Figure 39**). The Schulz-theory states that provided we know the relevant coefficients; this approach may also be used to determine the molecular weight [228]. The linearized Schulz equation (**Equation** (**20**)) was utilized to determine these distinctive A and B coefficients of the solvent-polymer-precipitant system. The plot of 1/M as a function of the volume fraction of H_2O (Φ_{water}) for the various PES samples (40, 60, 70, and 80 min) is shown in **Figure 40**. The constant values of A and B were determined from the plot, where B was calculated from the slope value and A was calculated from known B and intercept values according to **Equation 20**, and the corresponding data were reported in

Table 7. These values make it possible to calculate the PES molecular mass using the straightforward precipitation method.

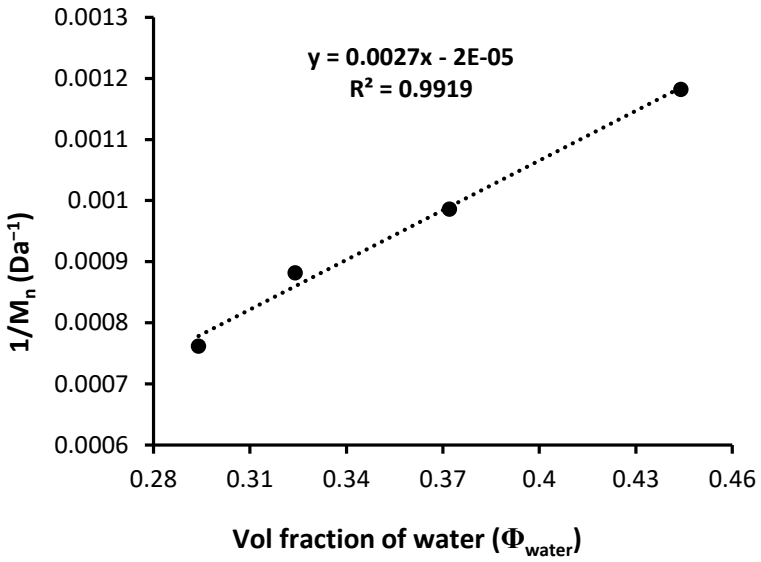

Figure 40. The $1/M_n$ (from ^{1}H-NMR) values as a function of Φ_{water} for various PES samples (40, 60, 70, and 80 min) in an H_2O/DMSO system [278].

Table 7. The molecular mass and volume fraction values are used to calculate the A and B constants in the Schulz equation [278].

Polymerization Time (min)	M_n (Da)	$1/M_n$ (Da^{-1})	Φ_{water}	Data from Figure 40	Constants
40	846	0.00118	0.444		
60	1014	0.00099	0.372	slope: 0.002709	**B = 36913**
70	1134	0.00088	0.324	intercept: $-1.814E^{-05}$	**A = 0.67**
80	1312	0.00076	0.294		

Viscometric measurements of PES with various molecular weights were performed to relatively estimate the intrinsic viscosity to determine the KMH modulus (K_η) and exponential (α) according to the Kuhn-Mark-Houwink equation (**Equation (10)**). **Figure 41A** depicts the effect of PES molecular weight on viscosity values, as well as the trend of rising viscosity with increasing concentration of PES in DMSO. The rheological behavior of polymer solutions may be explained using the theory of solubility and miscibility parameters. In order to identify the theta solvent conditions (KMH exponent value = 0.5), it may be useful to compare the hydrogen bonding components (δ_h) of the solubility parameter for the solvent and the polymer. The K_η constant's value in such solvents depends on the polarity (δ_p) and dispersion (δ_d) components of their solubility parameters. DMSO probably acts as a theta or near-theta solvent for PES

because the δ_h components of the solubility parameters for the PES polymer and DMSO are both equal to around 10 $MPa^{0.5}$ [296].

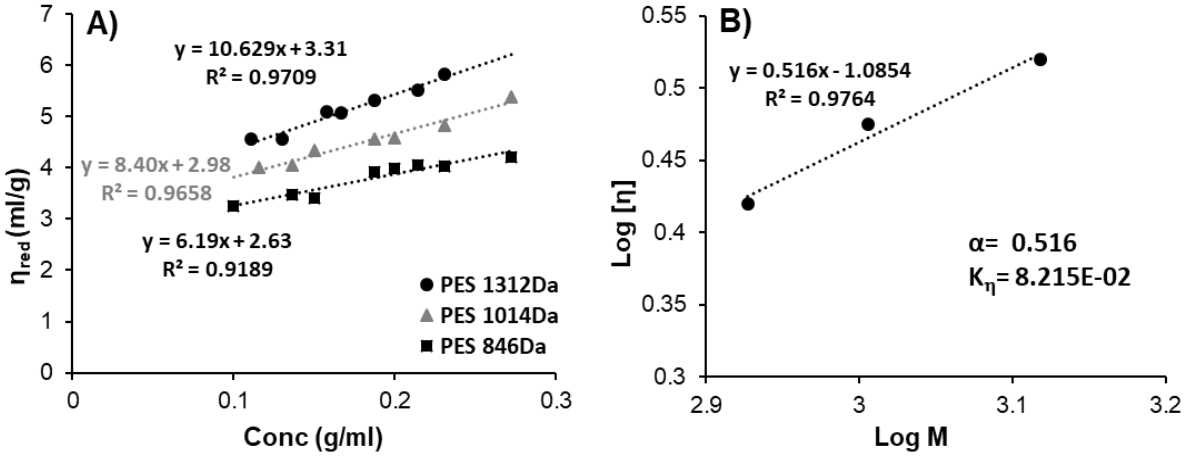

Figure 41. (**A**) The reduced viscosity as a function of the concentration of PES at various molecular weights to estimate the corresponding intrinsic viscosities [η], (**B**) The log of intrinsic viscosity as a function of the log of molecular weight to determine the KMHS coefficient (K_η) and exponent α [278].

On the other hand, the comparatively low molecular weight (M_n = 850 – 1300 Da) of poly(ethylene succinate) oligomers may be directly related to the low viscosity of PES solution in DMSO. The examination of solubility and miscibility characteristics may thus only provide support for the experimental approach. According to the Kuhn-Mark-Houwink equation and the dependency of the constant on solubility factors, the viscosity of the polymer solution may be calculated. The experimentally determined values of K_η and α constants for PES in DMSO (see **Figure 41B**), were found to be equivalent to 8.22×10^{-2} cm^3/g and 0.52, respectively. The conformation of the macromolecules in the solvent was defined by a value of α that was about 0.52 in the range of 0.5 to 0.8 which means we have a flexible chain [224]. The aforementioned results show that DMSO is a near theta solvent for PES polymer, making the DMSO/H_2O binary combination excellent for the precipitation of the polymer necessary for drug encapsulation.

Moreover, several studies have confirmed the biodegradability of PES polyester. The enzymatic hydrolysis of PES showed that it has a higher rate of degradation than poly(butylene succinate) PBSu, and that rate was also influenced by the molecular weight and crystallinity, according to the study reported by Bikiaris et al. [136]. In their investigation of PES degradation using the lipase enzyme, Seretoudi et al. found that the crystalline structure had an impact on the biodegradation rate [297]. Using cutinase, Bai et al. studied the enzymatic degradation of PES and discovered that the weight loss of PES was ~60% during 4 hrs of degradation, and it achieved ~95% after 12 hrs of enzymatic hydrolysis [124]. In water from lakes and rivers, PES

films were hydrolyzed at a comparatively high rate as well. According to Kasuya et al., the biodegradability was approximately 100% and the films entirely decomposed during 28 days in freshwater [298]. Additionally, Pseudomonas sp. AKS2's esterase was able to hydrolyze the ester linkages in PES at a rate of 1.65 mg per day, resulting in succinic acid and ethylene glycol which were then incorporated into metabolism through the tricarboxylic acid (TCA) cycle [299,300].

5.3.2. Characterization of NIMO-loaded PES NPs

In the previous section (**5.3.1**), we studied in detail the chemical compositions, thermal properties, and solubility/ precipitation characteristics of the synthesized PES and it was found that DMSO and H_2O are good and bad solvents for this polyester, respectively. In order to develop a successful technique for producing NIMO-loaded PES NPs, the solubility of PES and NIMO in a DMSO/H_2O combination was investigated. Initially, distilled H_2O was added dropwise as a poor solvent to both 0.1% *w/v* NIMO and PES solutions (in DMSO), and then the change in the absorbance was recorded as shown in **Figure 42A**. In contrast to the NIMO solution, which required a significant amount of water (Φ_{water} = 0.52) to start precipitating, the PES solution demonstrated rapid precipitation by adding distilled H_2O at about Φ_{water} = 0.20. The PES sample also reached the plateau value of its precipitation at the same H_2O fraction value that needs to initiate the precipitation of NIMO. According to the findings, it is not advised to encapsulate the NIMO into PES based on this precipitation method, which involves adding distilled H_2O to the DMSO-based solution. This is because the NIMO will begin to precipitate after the PES has completely precipitated and will also produce large particles, as seen in the inserted photos in **Figure 42A**.

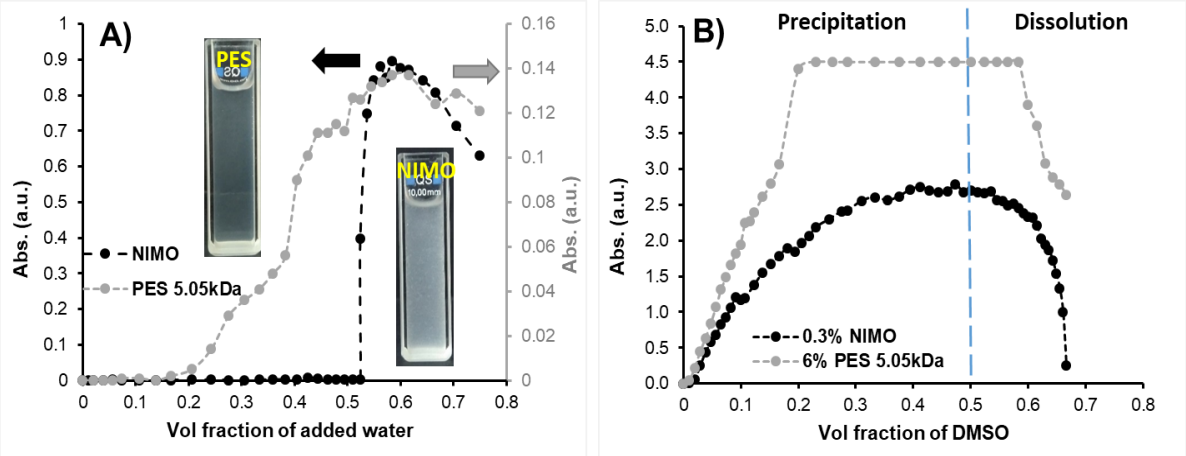

Figure 42. (**A**) NIMO (black) and PES (grey) precipitation curves after adding distilled H_2O (as poor solvent) to 0.1% *w/v* DMSO-based solutions, (**B**) the precipitation curves of 0.3% *w/v* of NIMO and 6% *w/v* of PES 80 min after adding them to distilled H_2O [292].

Based on our previous results, the precipitation process was reversed where the drug and polymer DMSO-based solutions were introduced to distilled H_2O. Under vigorous magnetic stirring, 6 *w/v* % PES 80 min (M_w = 5.05 kDa) DMSO solution was dropwise added to 5 mL of distilled H_2O. The nanoparticle formation was observed by measuring the absorbance. The relevant outcomes were displayed in **Figure 42B** after the same procedures were carried out again with 0.3% *w/v* NIMO solution. When PES and NIMO solutions were added to distilled H_2O, they quickly precipitated and reached a plateau value when a volume fraction of ~0.5 was reached. After that, the turbidity started to decrease as a result of the dilution process brought on by raising the volume fraction of DMSO, which caused the prepared particles to re-dissolve. Because at this ratio sufficiently small particles are generated (as we will see later) without resolving, the addition of DMSO-based solution to distilled H_2O should be halted at Φ_{DMSO} = 0.5 (dash-line in **Figure 42B**) during this procedure. According to our findings, we were able to develop an effective method for creating NPs that are loaded with NIMO.

Encapsulation of NIMO into PES polyesters was confirmed by FTIR, TEM, and XRD measurements. The FTIR spectra of NIMO, PES-80 min (M_w = 5.05 kDa), and NIMO-loaded PES are shown in **Figure 43**. NIMO drug has the main characteristic absorption peak at 3298, 1695, 1645, 1620, 1523, 1378, and 1135 cm^{-1}. These absorption peaks were attributed to the (N–H) stretching vibration, (C=O) stretching vibration, (NH) bending of aliphatic secondary amine, (C=C) aromatic ring, (–NO_2) stretching vibration, (–C–CH_3) stretching vibration, and (C–O) stretching vibration of ester, respectively [301]. As shown in the FTIR spectrum of NIMO-loaded PES NPs, two distinctive NIMO peaks at 1695 and 1523 cm^{-1} attributable to the (C=O) and (NO_2) groups were also detected without any shifts, which indicates trapping of NIMO in the polyester matrix and no chemical reaction between the NIMO drug and polyester exists. Based on UV-Vis spectroscopy measurements, the encapsulation efficiency (EE%) ranged between 90 and 95 % by using this simple precipitation method since the EE% of PES-NIMO (M_w = 4.3 KDa), PES-NIMO (M_w = 4.5 KDa), and PES-NIMO (M_w = 5.05 KDa) were 94.47%, 94.78%, and 89.99 %, respectively.

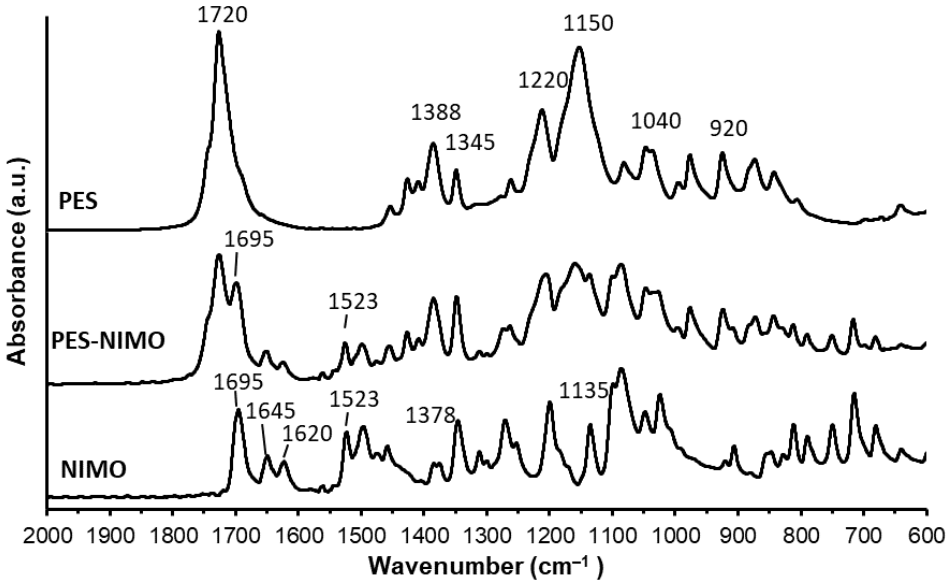

Figure 43. FTIR spectra of PES-80 min (M_w = 5.05 KDa), NIMO-loaded PES (5%w/w NIMO content), and NIMO drug [292].

The morphological characteristics and particle size of bare NIMO microparticles and NIMO-loaded PES NPs were examined by TEM after precipitation. The optimal DMSO/H_2O ratio was used to collect these samples (Φ_{DMSO} = 0.5). In **Figure 44A**, the precipitation of bare NIMO is depicted as producing needle-like crystals with a size of a few microns, whereas in **Figure 44B**, the precipitation of NIMO with PES produces spherical nanoparticles of NIMO-loaded PES with an average particle size of around 270 ± 103 nm. Since the precipitation was conducted without the use of a surfactant or stabilizing agent, the size distribution of the particles collected was, as can be seen, rather broad. The precipitation was performed without the need for a surfactant and stabilizing agent due to the presence of terminal functional (COOH and OH) groups of linear PES chains with low M_w and moderate hydrophilicity, as these groups provide the stability during the precipitation of the particles. It should be emphasized, however, that the particles were generated using a simple batch precipitation technique, resulting in a broad particle size range that may be limited by a continuous flow approach, as stated many times in the previous studies [302–306]. The XRD measurements were used to study the changes in crystallinity. The XRD patterns for the PES, NIMO, and NIMO-loaded PES NPs are shown in **Figure 44C**. The encapsulated NIMO form (NIMO-loaded PES NPs) has a very low intensity in comparison to the uncoated form (bare NIMO), which is associated with decreasing crystallinity of the drug. In general, a highly crystalline drug has a lower solubility than an amorphous drug with a high surface area, because the solubility of the drug depends on the formation of hydrogen bonds between the drug (the solute) and the solvent. Therefore, it is

better to reduce crystallization to enhance solubility, which leads to a higher dissolution rate and improves the bioavailability of the drug [230,307].

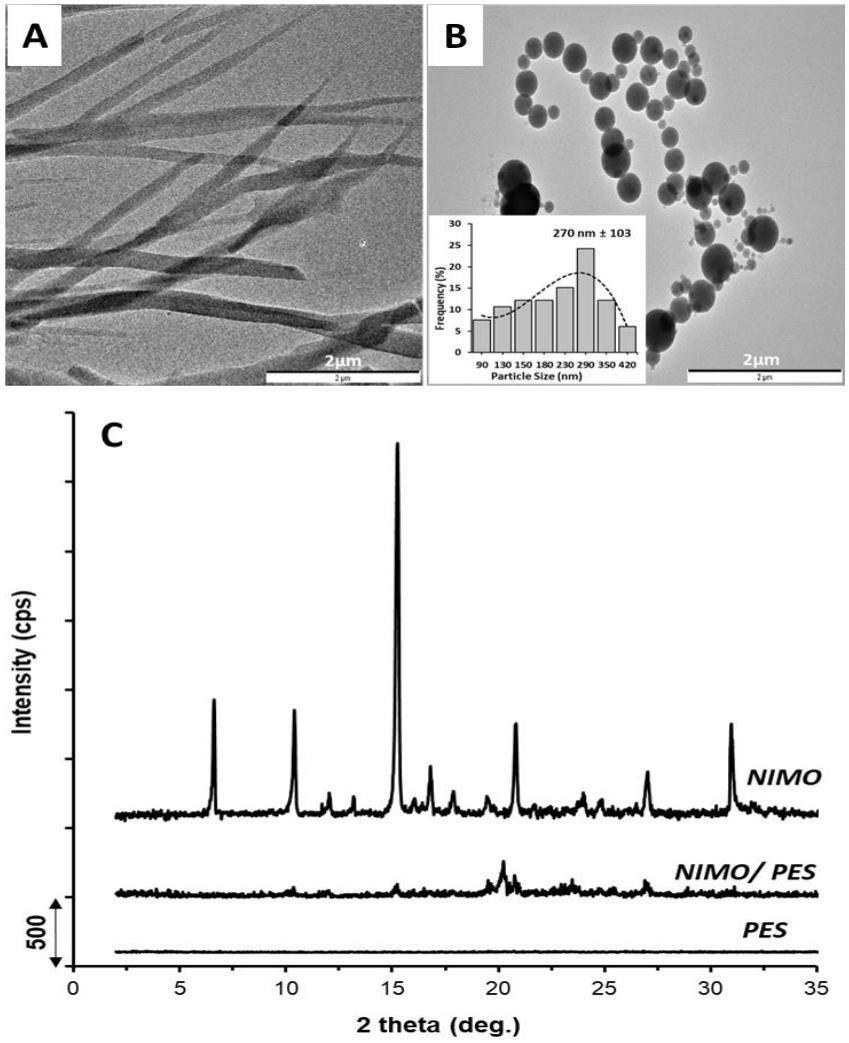

Figure 44. (**A**) TEM image of NIMO microcrystals precipitated by distilled H_2O from DMSO solution without PES polyester shell, (**B**) TEM image of the NIMO-loaded PES particles and the inserted image shows the size distribution histogram, and (**C**) XRD patterns of PES (M_w = 5.05 KDa), NIMO, and NIMO-loaded PES particles (5% *w/w* NIMO content) [292].

The above-mentioned lower particle size and crystallinity of the NIMO drug are favourable in terms of drug release; moreover, the inclusion of PES has improved the NIMO's water dispersibility due to the particles exhibiting a negative surface charge based on the zeta-potential analyses (see **Figure 45**). As previously indicated, the produced PES with low molecular weight (M_w =4287 to 5046 g/mol) has terminal COOH groups which can be the reason for this negative charge. Naturally, the measured zeta-potential (ζ) values were dependent on the ionic strength of the medium; consequently, the zeta potential (ζ) of both PES (M_w = 5.05 kDa) and NIMO-loaded PES show lower values in the PBS buffer solution (–29.12

± 0.74 and –30.2 ± 2.5 mV, respectively) compared to water (–45.48 ± 2.8 and –46.98 ± 1 mV, respectively) because of the presence of ions in PBS buffer solution, the ionic strength increases, causing a decrease in zeta potential (ζ) values. According to zeta potential (ζ) measurements, the particles are moderately stable in PBS buffer solution and have good stability in water [308]. Thus, the NIMO-loaded PES particles exhibit increased stability in an aqueous media, which was further supported by turbidity tests.

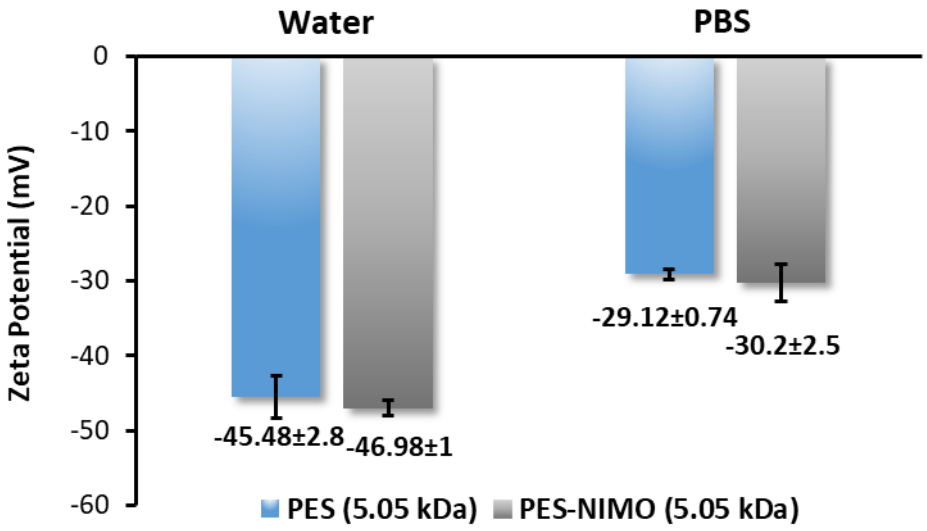

Figure 45. The zeta potential measurements of PES and NIMO-loaded PES particles in distilled H_2O and PBS buffer solution [292].

To understand the impact of encapsulating NIMO in the PES shell, the stability of pure NIMO and NIMO-loaded PES with 5% *w/w* nominal NIMO content in an aqueous PBS buffer solution was examined. The relative turbidity is shown as a function of time in **Figure 46**. As can be observed, the incorporation of PES notably boosted the NIMO's dispersibility in an aqueous solution. The relative turbidity of NIMO-loaded PES particles (d_{DLS} = 292 ± 37 nm) was steady and dropped by around 19% within 5 hrs of the measurement, whereas the relative turbidity of uncoated NIMO dropped by 85%. Due to its small particle size (see **Figure 44B**) and moderate hydrophilicity (see **Figure 36**), the PES polyester exhibits excellent dispersion in the aqueous medium. In other words, it would be appropriate to utilize a PES polyester shell to improve the water solubility/ dispersibility of the NIMO (poorly soluble in H_2O) drug.

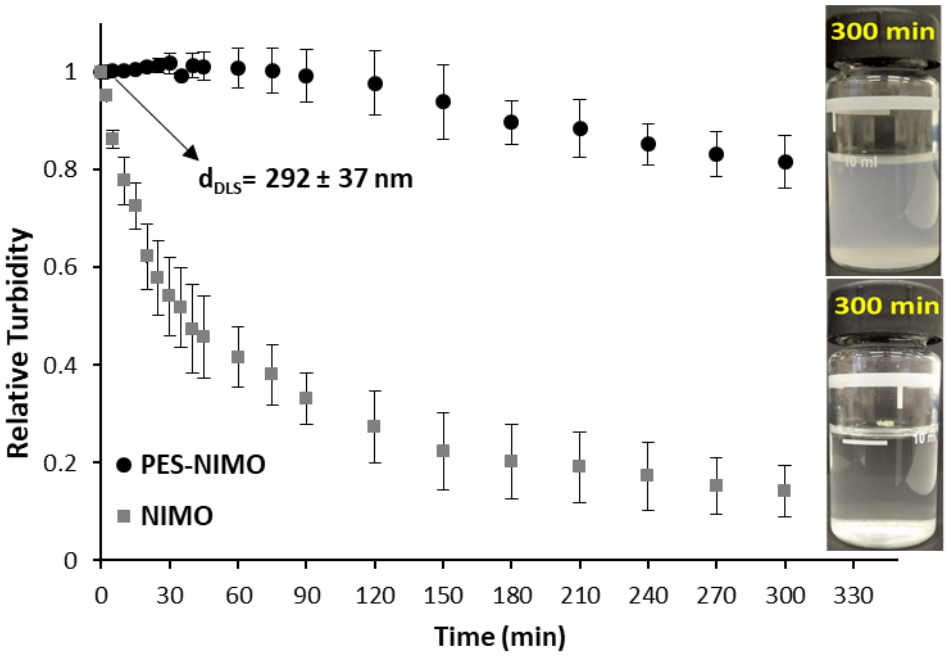

Figure 46. The turbidity of (0.05% *w/v*) NIMO and NIMO-loaded PES particles (5% *w/w* NIMO content) in an aqueous PBS medium, as a function of time [292].

Moreover, NIMO has poor water solubility, therefore when it is diluted with glucose or saline solutions during a prospective intravenous (IV) drug administration, crystallization might happen, endangering the health of the patient [205]. Based on the turbidity and zeta-potential measurements, we could prove our idea of providing a suitable drug delivery system for NIMO to improve the drawbacks of NIMO and demonstrate the effect of changes in particle size, water solubility, and water stability for our approach.

5.3.3. *In Vitro* NIMO release measurements

Given the purpose of this work, PES demonstrates the relevant factors that make it a potential candidate for use in NIMO delivery. Here, the controlled release of NIMO is impacted by variations in the molecular weight of PES polyester. The NIMO release patterns from the pure NIMO form and the encapsulated PES forms with various molecular weights are shown in **Figure 47**. Both the NIMO-loaded PES-40 min (M_w = 4.3 kDa) and NIMO-loaded PES-60 min (M_w = 4.5 kDa) samples demonstrate reasonably significant percentages of NIMO release compared to pure NIMO after 8 hrs of the drug release measurements, with maximum releasing values of 63.1% and 51.8%, respectively. The reason for that is the amorphous NIMO drug was more soluble and diffused than the crystalline form due to the low particle size and low crystallinity that was encapsulated in the low molecular weight PES (PES 4.3 kDa and PES 4.5 kDa) samples. That is why the pure NIMO drug with high crystallinity showed a maximum

release percentage of only 41.5%. PES-80 min (M_w = 5.05 kDa) has the highest molecular weight and the longest carbon chain structure, which causes a delayed NIMO release process with a maximum drug release percentage of 30.6%.

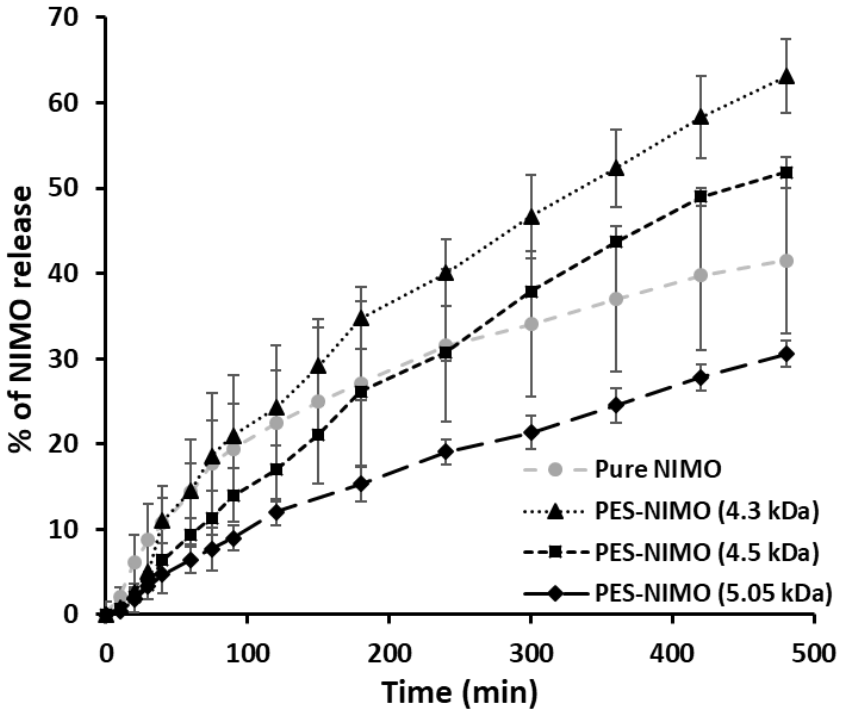

Figure 47. The *in vitro* NIMO release profiles from the pure NIMO and various encapsulated PES forms with various molecular weights [292].

Table 8. Various kinetic models to interpret the NIMO release data [292].

Sample	Zero-order model		First-order model		Higuchi model		Hixson-Crowell model		Korsmeyer-Peppas model		
	r^2	$k(h^{-1})$	r^2	$k\ (h^{-1})$	r^2	$k\ (h^{-1/2})$	r^2	$k\ (h^{-1/3})$	n	r^2	$k\ (h^{-n})$
Pure NIMO	0.897	4.924	0.938	0.065	0.989	15.858	0.582	0.2697	0.684	0.941	12.30
PES-NIMO (4.3 kDa)	0.963	7.957	0.995	0.1232	0.983	24.658	0.702	0.3672	1.016	0.939	10.33
PES-NIMO (4.5 kDa)	0.985	6.795	0.998	0.094	0.968	20.67	0.762	0.3619	1.073	0.969	7.259
PES-NIMO (5.05 kDa)	0.978	3.798	0.989	0.045	0.981	11.682	0.728	0.2854	0.775	0.994	6.333

As shown in **Table 8**, various models (including the zero-order, first-order, Higuchi, Hixson-Crowell, and Korsmeyer-Peppas models) were used to analyze the NIMO released data [157–159]. The first-order model was fitted with the NIMO releasing data for PES-NIMO (40 min, M_w = 4.3 kDa), and PES-NIMO (60 min, M_w = 4.5 kDa). This model shows how the concentration of the drug affects how quickly the drug is released from pharmaceutical formulations, hence the higher the concentration, the quicker the process [157,159]. Because of

the effect of molecular weight for PES, the releasing rate constant for NIMO-loaded PES-40 min (M_w = 4.3 kDa) (K_1 = 0.1232 h^{-1}) was higher than NIMO-loaded PES-60 min (M_w = 4.5 kDa) (K_1 = 0.094 h^{-1}). While the Higuchi model, which characterizes the release of weakly water-soluble drugs as a diffusion process based on Fick's law [157,159], was fitted with the releasing data of bare NIMO drug. Additionally, the Korsmeyer-Peppas model was fitted with the NIMO releasing data for NIMO-loaded PES-80 min (M_w = 5.05 kDa). Also, the drug release mechanism is reliant on both erosion-controlled and diffusion-controlled mechanisms because the "n" value (diffusional exponent) was between 0.43 and 0.85 mean anomalous (non-Fickian) diffusion, which led to a decrease in the amount of releasing NIMO drug and a prolongation of the releasing process. These findings show conclusively that while the relatively high molecular mass of PES polyester is good for prolonging the release, the lower molecular weight PES samples were capable of enhancing the drug release of the NIMO.

In this part, we try to introduce a novel controlled drug delivery system for NIMO to overcome poor water solubility and enhance drug bioavailability as well as introduce safe and efficient NIMO formulations by encapsulating NIMO inside poly(ethylene succinate) (PES) shells with various molecular weights. As a summary, we can state that the synthesized PES (M_w, 4.3–5.05 kDa) is suitable for the effective encapsulation (EE = 90–95%) of NIMO by the nanoprecipitation method. The particle size (270 ± 103 nm) and drug release of NIMO can be adjusted (from 63.1% to 30.6%) by increasing molecular weight (4.3–5.05 kDa). The encapsulated NIMO form with high zeta potential (ζ = –30.2 ± 2.5 mV in PBS and –46.98 ± 1 mV in H_2O) shows good water stability in an aqueous media (19% decrease in relative turbidity) based on turbidity measurements. Moreover, the PES can enhance or prolong the NIMO release based on the molecular weight. Thus, the newly introduced NIMO formulation exhibited many promising characteristics, including good water stability, enhance NIMO solubility, enhance NIMO bioavailability, ease of preparation, and a enhance/ prolonged drug-releasing process. We anticipate that our NIMO formulation can be used in the future as a potential controlled drug delivery system.

6. Summary

Polymer-based controlled drug delivery systems are preferred over traditional drug delivery methods due to numerous advantages, including improved bioavailability, increased stability, and reduced toxicity, drug protection from *in vitro* and *in vivo* degradation, prolonged drug release process, and the ability to deliver drugs more precisely by targeting specific areas of the body, increasing the pharmaceutical efficiency. During my dissertation study, novel polymer-based controlled drug delivery systems were developed for three distinct drugs (Mitomycin C, Tilorone Dihydrochloride, and Nimodipine). These systems were developed by modifying and synthesizing biocompatible polymers to provide new approaches to therapy and solve problems associated with the use of conventional drug delivery methods. The summary of these works is as follows:

In the first part of my dissertation study, to reduce the severe side effect of MMC, I prepared novel, MMC-loaded mucoadhesive polymeric prodrug NPs with spontaneous, self-assembled particle formation ability and mucoadhesive properties. In a straightforward and reproducible one-pot reaction, (4 mg) MMC and (0.05 to 0.34 mmol) CYS were conjugated with 1 wt% succinated PVA (containing pendant COOH [0.5–3.4 mmol/g] and OH [15.3–12.4 mmol/g] functional groups) using EDC to produce self-assembly polymeric prodrug MMC particles. Due to the crosslinking and conjugation reactions, the formed particles showed high hydrophobicity ($\Theta = 90 \pm 2\ ^{o}$) and high thermal stability (T_m = 230–240 ^{o}C) as well as low water desorption enthalpy (ΔH_w) values (~29 kJ/mol). The optimal reaction time should not exceed 3 hrs, as well as the optimal concentration for particle formation should be less than 3% *w/v* according to turbidimetric and rheology measurements. A simple acid-base reaction was used to determine the variable (3–21%) substitution degree of PVA-SA, while turbidimetric measurements demonstrated the self-assembled particles (~250 NTU, ~200 nm by DLS) formation. The TEM measurements showed the formation of spherical nanoparticles with mean particle sizes varying from 92 to 260 nm, depending on the cross-linking (3–21%) densities, where a higher cross-linking density results in smaller particles. The mucoadhesive properties were investigated using rheology and turbidity measurements. When mixing conjugated particles with porcine mucin (as a mucosa model), they showed high storage ($G' = 158.3$ kPa) modulus and loss ($G'' = 23.2$ kPa) modulus compared to the initial polymer solutions due to crosslinking hydrogel formation by disulfide linkage between SH of conjugated particles and cysteine-rich sub-domains of the (mucin) glycoproteins by thiol/disulfide exchange mechanism. The conjugated particles had a strong adhesion (~76%) to the pig intestinal test

membrane compared to non-thiolated particles (~9%). Under physiological circumstances (pH = 7.4, 37 ^{o}C), the *in vitro* drug release assays were carried out for 7 days, demonstrating that variable crosslinking density can be used to adjust the drug release process. For polymeric prodrug of MMC particles, PVA-SA-CYS-MMC (3% crosslinking density) was the fastest (k_{KP} = 2.25 h^{-n}), with a cumulative drug release of 62% contrasted to 33% (k_{KP} = 1.35 h^{-n}) for PVA-SA-CYS-MMC (21% crosslinking density), as well as all MMC released data from the polymeric prodrugs fit with the Korsmeyer–Peppas model (where $0.43 < n < 0.85$), which assumed that the drug release mechanism was regulated by both erosion and diffusion. This denotes that the conjugated form will first undergo a hydrolysis process, then the MMC drug will diffuse. By using our polymeric prodrug MMC, it is possible to significantly slow down the MMC release rate, and the synthesis conditions also allow us to control the amount and kinetics of drug release. The antibacterial activity (inhibition zone diameter) was influenced by the amount or concentration of MMC that was released, with diameters decreasing (26.5, 19, and 11.5 mm) as cross-link density increased (0 /pure MMC/, 3, and 21%). The anticancer activities of the polymeric prodrugs were extremely comparable (IC_{50} = 0.0345 ± 0.011 mg/mL) to those of pure MMC (IC_{50} = 0.0356 ± 0.0096 mg/mL), indicating that the conjugation of MMC had no impact on the pharmacological effect of MMC. Thus, the developed particles (thiol content = 0.075–0.8 mmol/g; 0.6–6.2 wt%) are suitable for localization, extending the residence time of the polymeric prodrug of MMC inside the human body during the prolonged process of MMC release, and improving bioavailability. We anticipate that polymeric prodrug molecules produced from MMC will one day become a potent topical drug delivery system appropriate for throat cancer treatment and can be applied to prevent scar tissue formation in the area of head and neck surgery.

In the second part of my dissertation study, I introduced the synthesis of a dual-component injectable PVA-CHO/CHIT-SH hydrogel for the encapsulation and prolonged release of Tilorone (a BMP inducer, anti-muscular atrophy drug) as a novel potential therapeutic approach for the local treatment of muscle atrophy. The developing Schiff-base linkages between the CHO groups of 4-formyl benzoate PVA (PVA-CHO, 5.9 mol% functionalization degree) and the NH_2 groups of 3-mercaptopropionate chitosan (CHIT-SH, 4.43% substitution degree) induced fast (7–45 s, based on the concentration of polymer solutions) *in situ* solidifications of the PVA-CHO/CHIT-SH hydrogel. FTIR spectrum of hydrogel revealed the appearance of a new absorption peak at 1647 cm^{-1} demonstrating the Schiff base (–CH=N–) formation and verifying the bonding between CHO and NH_2 groups of modified polymers. Consequently, the

viscosity of the 2% *w/v* polymer mixture solution (containing both PVA-CHO and CHIT-SH) significantly increased (9800 mPa·s) compared to the viscosities of pure polymer solutions (5.8 and 4.6 mPa·s, respectively) with the same concentration. Moreover, increasing the hydrogel concentration decreased the swelling ratio (1.7 g/g and 2.9 g/g for 10% *w/v* and 2% *w/v* PVA-CHO/CHIT-SH, respectively). The *in vitro* biodegradation of our hydrogel systems was between 52–55% during 20 days in the presence of lysozyme under physiological conditions. To improve the mucoadhesive characteristics of hydrogel, mercaptopropionic acid was also conjugated to initial chitosan (thiol content = 201.85 ± 12 μmol/g). As a result, the developed hydrogel shows significantly strong adhesion (600 ± 155 mN/mm) to the pig intestinal membrane in comparison to the reference hydrogel without SH groups (281 ± 45 mN/mm). The *in vitro* Tilorone release measurements were carried out in physiological circumstances (pH = 7.4, 37 ^{o}C) with the absence and presence of lysozyme. Tilorone was released from the hydrogel dependent on the crosslinking density and/ or concentration of hydrogel. The fastest Tilorone release was from 2% *w/v* PVA-CHO/CHIT-SH hydrogel (~81%, $k_H = 34.55 h^{-1/2}$) compared to the slowest one from 10% *w/v* PVA-CHO/CHIT-SH hydrogel (~50%, $k_H = 21.66\ h^{-1/2}$). The presence of 0.15% lysozyme somewhat increases the drug release rate (1–2 $h^{-1/2}$) due to the enzymatic degradation (~2–5%) of the hydrogel during the releasing experiments. The biocompatibility of our injectable self assemble hydrogel was also presented using MRC-5 cells. Hopefully, we anticipate that the developed injectable hydrogel with encapsulated Tilorone dihydrochloride will be useful in the local treatment of muscle atrophy, such as laryngotracheal atrophy.

In the third part of my dissertation study, I developed a novel poly(ethylene succinate) based controlled drug delivery system for Ca^{+2} channel blocker NIMO drug to improve drug bioavailability, overcome low water solubility, and introduce safe and effective NIMO formulations. Biodegradable and biocompatible PES polyester is a promising candidate for a variety of biomedical applications, however, the lack of knowledge of its solubility and precipitation properties restricts its applicability. To comprehensively explore these effects, PES was synthesized by direct condensation polymerization using ethylene glycol and succinic acid monomers in a 1:1 monomer ratio at ideal polymerization temperature (T = 185 °C) without a catalyst to produce relatively low molecular weight PES polyester, wherein the molecular weight was controlled by variation of reaction time (40–80 min). The molecular weight (M_n and M_w) and polydispersity (M_w/M_n) index of synthesized PES polyester were estimated by GPC measurements that showed the formation of relatively monodisperse

polyesters ($M_w/M_n \approx 1.5$) with M_w ranged from 4.3 to 5.05 kDa. Additionally, M_n was estimated using ^{1}H-NMR measurements that revealed the M_n values ranged from 850 to 1300 Da depending on the reaction time (from 40 to 80 min). We have demonstrated an inverse relationship between solubility and molecular weight of PES in the H_2O/DMSO system and based on these precipitations and capillary viscometry data, significant parameters from the Schulz equation, including the coefficients A (0.67) and B (3.69×10^4), as well as the α (0.52) and K_η (8.22×10^{-2} cm^3/g) constants from the Kuhn–Mark–Houwink equation were calculated. These parameters can be used to determine the molecular weight of PES by simply fractional precipitation and capillary viscometry. Increasing molecular weight (M_w = 4.3–5.05 kDa) of synthesized polyester led to an increase in the thermal stability (T_m = 61–80 °C) and the hydrophobicity (Θ = 27– 41°) of our PES samples. The encapsulation of the NIMO drug into PES polyester with increasing M_w through nanoprecipitation resulted in spherical 270 ± 103 nm NIMO-loaded PES NPs compared to the needle-like crystals with a size of a few microns for bare NIMO. Furthermore, XRD studies revealed that the encapsulated form had decreased drug crystallinity, which improved not only the water solubility of NIMO but also its water stability in an aqueous media. These improvements were supported by zeta potential (ζ) measurements (–30.2 ± 2.5 mV in PBS and –46.98 ± 1 mV in water) and turbidity measurements (~19% decrease in relative turbidity) enabling the use of the particles intravenously without the need for organic solvents. The *in vitro* NIMO release results demonstrated that varying the molecular weights of PES might also accelerate or even prolong the release of the encapsulated NIMO. The drug was fast released (k_1 = 0.1232 h^{-1} and k_1 = 0.094 h^{-1}) from the lower M_w PES (4.3 kDa and 4.5 kDa; cumulative drug release of 63.1% and 51.8%, respectively) in comparison to pure crystalline NIMO (cumulative drug release of 41.5%, k_1 = 0.065 h^{-1}) because of the low particle size and crystallinity of encapsulated NIMO. However, increasing the molecular weight of PES (5.05 kDa) resulted in a reduction in the amount of drug released (30.6%, k_1 = 0.045 h^{-1}), which extends the therapeutic action and improves the bioavailability of the NIMO drug. Hopefully, our NIMO formulation can be used in the future as a potential controlled drug delivery system.

7. References

[1] Arshad, M.; Zubair, M.; Rahman, S.S.; Ullah, A. Chapter 14-Polymers for advanced applications. In *Polymer Science and Nanotechnology*; Narain, R., Ed.; Elsevier: Amsterdam, The Netherlands, **2020**; pp. 325–340.

[2] Baranwal, J.; Barse, B.; Fais, A.; Delogu, G.L.; Kumar, A. Biopolymer: A Sustainable Material for Food and Medical Applications. *Polymers* **2022**, *14*, 983.

[3] Velazco-Medel, M.A.; Camacho-Cruz, L.A.; Bucio, E. Modification of relevant polymeric materials for medical applications and devices. *Med. Devices Sens.* **2020**, *3*, 1–17.

[4] Gebelein, C.G.; Cheng, T.C.; Yang, V.C. *Cosmetic and Pharmaceutical Applications of Polymers*. Springer, Boston, MA., **1991**; pp.1–414.

[5] Liu, F.; Wang, X. Synthetic Polymers for Organ 3D Printing. *Polymers* **2020**, *12*, 1765.

[6] Boni, R.; Ali, A.; Shavandi, A.; Clarkson, A.N. Current and novel polymeric biomaterials for neural tissue engineering. *J. Biomed. Sci.* **2018**, *25*, 90.

[7] Habibzadeh, F.; Sadraei, S.M.; Mansoori, R.; Chauhan, N.P.S.; Sargazi, G. Nanomaterials supported by polymers for tissue engineering applications: A review. *Heliyon* **2022**, 8, e12193

[8] Loh, X.J. *Polymers for Personal Care Products and Cosmetics*. The Royal Society of Chemistry: Croydon, United Kingdom, **2016**; pp.1–248.

[9] Tajeddin, B.; Arabkhedri, M. Polymers and food packaging. In *Polymer Science and Innovative Applications*; AlMaadeed, M.A.A.; Ponnamma, D.; Carignano, M.A., Eds.; Elsevier: Oxford, United Kingdom, **2020**; pp. 525–543.

[10] Begum, S.A.; Rane, A.V.; Kanny, K. Applications of compatibilized polymer blends in automobile industry. In *Compatibilization of Polymer Blends: Micro and Nano Scale Phase Morphologies, Interphase Characterization and Properties*; Ajitha, A.R.; Thomas, S., Eds.; Elsevier: Oxford, United Kingdom, **2020**; pp. 563–593.

[11] Shen, J.; Liang, J.; Lin, X.; Lin, H.; Yu, J.; Yang, Z. Recent progress in polymer-based building materials. *Int. J. Polym. Sci.* **2020**, *2020*, 8838160.

[12] Chan, J.X.; Hassan, A.; Wong, J.F.; Majeed, K. Plastics in outdoor applications. In: *Encyclopedia of materials: plastics and polymers;* Hashmi M.S.J., Ed.; Elsevier: Oxford, United Kingdom, **2022**; pp 237–248.

[13] Goyal, M.; Agarwal, S.N.; Bhatnagar, N. A review on self-healing polymers for applications in spacecraft and construction of roads. *J. Appl. Polym. Sci.* **2022**, *139*, e52816.

[14] Rathod, V.T.; Kumar, J.S.; Jain, A. Polymer and ceramic nanocomposites for aerospace applications. *Appl. Nanosci.* **2017**, *7*, 519–548.

[15] Zeng, Y.; Gordiichuk, P.; Ichihara, T.; Zhang, G.; Sandoz-Rosado, E.; Wetzel, E.D.; Tresback, J.; Yang, J.; Kozawa, D.; Yang, Z.; Kuehne, M.; Quien, M.; Yuan, Z.; Gong, X.; He, G.; Lundberg, D.J.; Liu, P.; Liu, A.T.; Yang, J.F.; Kulik, H.J.; Strano, M.S. Irreversible synthesis of an ultrastrong two-dimensional polymeric material. *Nature* **2022**, *602*, 91–95.

[16] Thakur, M.; Sharma, A.; Chandel, M.; Pathania, D. Chapter 9-Modern applications and current status of green nanotechnology in environmental industry. In *Green Functionalized Nanomaterials for Environmental Applications*; Shanker, U., Hussain, C.M., Rani, M., Eds.; Elsevier: Amsterdam, The Netherlands, **2022**; pp. 259–281.

[17] Shrivastava, A. Introduction to plastics engineering; In *Plastics Design Library, Introduction to Plastics Engineering*; Shrivastava, A., Eds.; William Andrew Publishing; New York, USA, **2018**; pp. 1–16.

[18] Numata, K. How to define and study structural proteins as biopolymer materials. *Polym. J.* **2020**, *52*, 1043–1056.

[19] Aravamudhan, A.; Ramos, D.M.; Nada, A.A.; Kumbar, S.G. Natural polymers. In *Natural and synthetic biomedical polymers*; Kumbar, S.G., Laurencin, C.T., Deng, M., Eds.; Elsevier: UK, **2014**; pp. 67–89.

[20] Minchin, S.; Lodge, J. Understanding biochemistry: structure and function of nucleic acids. *Essays Biochem.* **2019**, *63*, 433–456.

[21] Litwack, G. Chapter 9 - Lipids, *Human Biochemistry*; Litwack, G. Ed.; Academic Press, **2018**; pp. 199–255.

[22] Alizadeh-Osgouei, M.; Li, Y.; Wen, C. A comprehensive review of biodegradable synthetic polymer-ceramic composites and their manufacture for biomedical applications. *Bioact. Mater.* **2019**, *4*, 22–36.
[23] Mariani, E.; Lisignoli, G.; Borzì, R.M.; Pulsatelli, L. Biomaterials: Foreign bodies or tuners for the immune response? *Int. J. Mol. Sci.* **2019**, *20*, 636.
[24] Vieyra, H.; Molina-Romero, J.M.; Calderón-Nájera, J.d.D.; Santana-Díaz, A. Engineering, Recyclable, and Biodegradable Plastics in the Automotive Industry: A Review. *Polymers* **2022**, *14*, 3412.
[25] Gunatillake, P.A.; Adhikari, R. Chapter 2—Nondegradable synthetic polymers for medical devices and implants. In *Woodhead Publishing Series in Biomaterials*; Poole-Warren, L., Martens, P., Green, R., Eds.; Woodhead Publishing: Cambridge, UK, **2016**; pp. 33–62.
[26] Germershaus, O.; Lühmann, T.; Ritzer, J.; Meinel, L. Application of natural and semi-synthetic polymers for the delivery of sensitive drugs. *Int. Mater. Rev.***2015**, *60*, 101–130.
[27] Patil, A.; Sandewicz, R.W. Cosmetic science and polymer chemistry: Perfect together. In *Polymers for Personal Care and Cosmetics*; Patil, A.; Ferritto, M.S., Eds.; American Chemical Society: Washington, DC, USA, **2013**; 1148, pp. 13–37.
[28] LaVan, D. A.; McGuire, T.; Langer, R. Small-scale systems for in vivo drug delivery. *Nat. Biotechnol*. **2003**, *21*, 1184–1191.
[29] Allen, T. M.; Cullis, P. R. Drug delivery systems: Entering the mainstream. *Science* **2004**, *303*, 1818–1822.
[30] Langer, R. New Methods of Drug Delivery. *Science* **1990**, *249*, 1527–1533.
[31] Kraljevic, S.; Pavelic, K. Navigare necessere est—Improved navigation would help to solve two crucial problems in modern drug therapy: Toxicity and precise delivery. *Embo.Rep*. **2005**, *6*, 695–700.
[32] Liechty WB, Kryscio DR, Slaughter BV, Peppas NA. Polymers for drug delivery systems. *Annu. Rev. Chem. Biomol. Eng.* **2010**, *1*, 149-173.
[33] Nyamweya, N.N. Applications of polymer blends in drug delivery. *Futur. J. Pharm. Sci.* **2021**, *7*, 18.
[34] Yang, W.W.; Pierstorff, E. Reservoir-based polymer drug delivery systems. *J. Lab. Autom.* **2012**, *17*, 50–58.
[35] Freiberg, S.; Zhu, X. Polymer Microspheres for Controlled Drug Release. *Int. J. Pharm*. **2004**, *282*, 1–18.
[36] Kuramoto, K.; Shoji, T.; Nakagawac, Y. Usefulness of the final filter of the IV infusion set in intravenous administration of drugs—contamination of injection preparations by insoluble microparticles and its causes. *Yakugaku Zasshi* **2006**, *126*, 289–295.
[37] Hornig, S.; Heinze, T.; Becer, C. R.; Schubert, U.S. Synthetic polymeric nanoparticles by nanoprecipitation. *J. Mater. Chem.* **2009**, *19*, 3838–3840.
[38] Vasir, J. K.; Tambwekar, K.; Garg, S. Bioadhesive microspheres as a controlled drug delivery system. *Int. J. Pharm*. **2003**, *255*, 13–32.
[39] Bodmeier, R.; Chen, H.G. Preparation of biodegradable poly(+/−)lactide microparticles using a spray-drying technique. *J. Pharm. Pharmacol.* **1988**, *40*, 754–757.
[40] Sperry, P.J.; Cua, D.J.; Wetzel, S.A.; Adler-Moore, J.P. Antimicrobial activity of amBisome and non-liposomal amphotericin B following uptake of *candida glabrata* by murine epidermal langerhans cells. *Med. Mycol*. **1998**, *36*, 135–141.
[41] Bory, C.; Boulieu, R.; Souillet, G.; Chantin, C.; Guibaud, P.; Hershfield, M.S. Effect of polyethylene glycol-modified adenosine deaminase (PEG-ADA) therapy in two ADA-deficient children: measurement of erythrocyte deoxyadenosine triphosphate as a useful tool. In: *Purine and Pyrimidine Metabolism in Man VII. Advances in Experimental Medicine and Biology*; Harkness, R.A.; Elion, G.B.; Zöllner, N., Eds.; Springer, Boston, UK, **1991**; 309A, pp. 173–176.
[42] Muggia, F.; Hamilton, A. Phase III data on caelyx (R) in ovarian cancer. *Eur. J. Cancer* **2001**, *37*, S15–S18.
[43] Glantz, M.J.; LaFollette, S.; Jaeckle, K.A.; Shapiro, W.; Swinnen, L.; Rozental, J.R.; Phuphanich, S.; Rogers, L.R.; Gutheil, J.C.; Batchelor, T.; Lyter, D.; Chamberlain, M.; Maria, B.L.; Schiffer, C.; Bashir, R.; Thomas, D.; Cowens, W.; Howell, S.B. Randomized trial of a slow-release versus a standard formulation of cytarabine for the intrathecal treatment of lymphomatous meningitis. *J. Clin. Oncol.* **1999**, *17*, 3110–3116.

[44] Olsen, E.; Duvic, M.; Frankel, A.; Kim, Y.; Martin, A.; Vonderheid, E.; Jegasothy, B.; Wood, G.; Gordon, M.; Heald, P.; Oseroff, A.; Pinter-Brown, L.; Bowen, G.; Kuzel, T.; Fivenson, D.; Foss, F.; Glode, M.; Molina, A.; Knobler, E.; Stewart, S.; Cooper, K.; Stevens, S.; Craig, F.; Reuben, J.; Bacha, P.; Nichols, J. Pivotal phase III trial of two dose levels of denileukin diftitox for the treatment of cutaneous T-cell lymphoma. *J. Clin. Oncol.* **2001**, *19*, 376–388.

[45] Glue, P.; Rouzier-Panis, R.; Raffanel, C.; Sabo, R.; Gupta, S. K.; Salfi, M.; Jacobs, S.; Clement, R.P. A dose-ranging study of pegylated interferon alfa-2b and ribavirin in chronic hepatitis C. *Hepatology* **2000**, *32*, 647–653.

[46] Nabhan, C.; Tallman, M.S. Early phase I/II trials with gemtuzumab ozogamicin (mylotarg (R)) in acute myeloid leukemia. *Clin. Lymphoma* **2002**, *2*, S19–S23.

[47] Siena, S.; Piccart, M. J.; Holmes, F. A.; Glaspy, J.; Hackett, J.; Renwick, J.J. A combined analysis of two pivotal randomized trials of a single dose of pegfilgrastim per chemotherapy cycle and daily filgrastim in patients with stage II-IV breast cancer. *Oncol. Rep.* **2003**, *10*, 715–724.

[48] Gombotz, W.R.; Pettit, D.K. Biodegradable polymers for protein and peptide drug-delivery. *Bioconjugate Chem.* **1995**, *6*, 332–351.

[49] Hoare, T.R.; Kohane, D.S. Hydrogels in drug delivery: progress and challenges. *Polymer* **2008**, *49*, 1993–2007.

[50] Hoffman, A.S. Hydrogels for biomedical applications. *Adv. Drug Deliv. Rev.* **2002**, *54*, 3–12.

[51] Liu, Y.; Geng, Y.; Yue, B.; Lo, P.-C.; Huang, J.; Jin, H. Injectable hydrogel as a unique platform for antitumor therapy targeting immunosuppressive tumor microenvironment. *Front. Immunol.* **2022**, *12*, 832942.

[52] Lee, J.H. Injectable hydrogels delivering therapeutic agents for disease treatment and tissue engineering. *Biomater. Res.* **2018**, *22*, 27.

[53] Chao, Y.; Chen, Q.; Liu, Z. Smart injectable hydrogels for cancer immunotherapy. *Adv. Funct. Mater.* **2020**, *30*, 1902785.

[54] Yu, S.; He, C.; Chen, X. Injectable hydrogels as unique platforms for local chemotherapeutics-based combination antitumor therapy. *Macromol. Biosci.* **2018**, *18*, e1800240.

[55] Yamamoto, M.; Takahashi, Y.; Tabata, Y. Controlled release by biodegradable hydrogels enhances the ectopic bone formation of bone morphogenetic protein. *Biomaterials* **2003**, *24*, 4375–4383.

[56] Casadei, M.A.; Cerreto, F.; Cesa, S.; Giannuzzo, M.; Feeney, M.; Marianecci, C.; Paolicelli, P. Solid lipid nanoparticles incorporated in dextran hydrogels: a new drug delivery system for oral formulations. *Int. J. Pharm.* **2006**, *325*, 140–146.

[57] Nakagawa, T.; Sakamoto, T.; Hiraumi, H.; Kikkawa, Y. S.; Yamamoto, N.; Hamaguchi, K.; Ono, K.; Yamamoto, M.; Tabata, Y.; Teramukai, S.; Tanaka, S.; Tada, H.; Onodera, R.; Yonezawa, A.; Inui, K.; Ito, J. Topical insulin-like growth factor 1 treatment using gelatin hydrogels for glucocorticoid-resistant sudden sensorineural hearing loss: a prospective clinical trial. *BMC Med.* **2010**, *8*, 76.

[58] Wang, X.B.; Dellamary, L.; Fernandez, R.; Ye, Q.A.; LeBel, C.; Piu, F. Principles of inner ear sustained release following intratympanic administration. *Laryngoscope* **2011**, *121*, 385–391.

[59] Piu, F.; Wang, X.B.; Fernandez, R.; Dellamary, L.; Harrop, A.; Ye, Q.A.; Sweet, J.; Tapp, R.; Dolan, D.F.; Altschuler, R.A.; Lichter, J.; Lebel, C. OTO-104: A sustained-release dexamethasone hydrogel for the treatment of otic disorders. *Otol. Neurotol.* **2011**, *32*, 171–179.

[60] Wang, X.B.; Dellamary, L.; Fernandez, R.; Harrop, A.; Keithley, E.M.; Harris, J.P.; Ye, Q.; Lichter, J.; LeBel, C.; Piu, F. Dose-dependent sustained release of dexamethasone in inner ear cochlear fluids using a novel local delivery approach. *Audiol. Neurotol.* **2009**, *14*, 393–401.

[61] Vigata, M.; Meinert, C.; Hutmacher, D.W.; Bock, N. Hydrogels as drug delivery systems: a review of current characterization and evaluation techniques. *Pharmaceutics* **2020**, *12*, 1188.

[62] Jacob, S.; Nair, A.B.; Shah, J.; Sreeharsha, N.; Gupta, S.; Shinu, P. Emerging role of hydrogels in drug delivery systems, tissue engineering and wound management. *Pharmaceutics* **2021**, *13*, 357.

[63] Lei, L.; Bai, Y.; Qin, X.; Liu, J.; Huang, W.; Lv, Q. Current understanding of hydrogel for drug release and tissue engineering. *Gels* **2022**, *8*, 301.

[64] Ringsdorf, H. Structure and properties of pharmacologically active polymers. *J. Polym. Sci. Polym. Symp.* **1975**, *51*, 135–153.

[65] Greco, F.; Vicent, M.J. Combination therapy: opportunities and challenges for polymer-drug conjugates as anticancer nanomedicines. *Adv. Drug Deliv. Rev.* **2009**, *61*, 1203–1213.
[66] Gillies, E.; Goodwin, A.; Frechet, J. Acetals as pH-sensitive linkages for drug delivery. *Bioconjugate Chem.* **2004**, *15*, 1254–1263.
[67] Torchilin, V. Recent advances with liposomes as pharmaceutical carriers. *Nat. Rev. Drug Discov.* **2005**, *4*, 145–160.
[68] Matsumura, Y.; Maeda, H. A new concept for macromolecular therapeutics in cancer chemotherapy: mechanism of tumoritropic accumulation of proteins and the antitumor agent smancs. *Cancer Res.* **1986**, *46*, 6387–6392.
[69] Maeda, H. The enhanced permeability and retention (EPR) effect in tumor vasculature: the key role of tumor-selective macromolecular drug targeting. *Advances in Enzyme Regulation* **2001**, *41*, 189–207
[70] Zelikin, A.; Ehrhardt, C.; Healy, A. Materials and methods for delivery of biological drugs. *Nature Chem.* **2016**, *8*, 997–1007.
[71] Feng, Q.; Tong, R. Anticancer nanoparticulate polymer-drug conjugate. *Bioeng. Transl. Med.* **2016**, *1*, 277–296.
[72] Delplace, V.; Couvreur, P.; Nicolas, J. Recent trends in the design of anticancer polymer prodrug nanocarriers. *Polym. Chem.* **2014**, *5*, 1529−1544.
[73] Chang, M.; Zhang, F.; Wei, T.; Zuo, T.; Guan, Y.; Lin, G.; Shao, W. Smart linkers in polymer–drug conjugates for tumor-targeted delivery. *J. Drug Target.* **2016**, *24*, 475–491.
[74] Larson, N.; Ghandehari, H. Polymeric conjugates for drug delivery. *Chem. Mater.* **2012**, *24*, 840–853.
[75] Feng, Q.; Tong, R. Anticancer nanoparticulate polymer-drug conjugate. *Bioeng. Transl. Med.* **2016**, *1*, 277–296.
[76] Xu, H.; Ma, H.; Yang, P.; Zhang, X.; Wu, X.; Yin, W.; Wang, H.; Xu, D. Targeted polymer-drug conjugates: current progress and future perspective. *Colloids Surf. B Biointerfaces* **2015**, 136, 729–734.
[77] Manandhar, S.; Sjöholm, E.; Bobacka, J.; Rosenholm, J.M.; Bansal, K.K. Polymer-drug conjugates as nanotheranostic agents. *J. Nanotheranostics* **2021**, *2*, 63–81.
[78] Parveen, S.; Arjmand, F.; Tabassum, S. Clinical developments of antitumor polymer therapeutics. *RSC Adv.* **2019**, *9*, 24699–24721.
[79] Mohanty, A.K.; Dilnawaz, F.; Prasad Mohanta, G.; Kumar Sahoo, S. Polymer–drug conjugates for targeted drug delivery. In *Targeted Drug Delivery: Concepts and Design*; Devarajan, P.V.; Jain, S., Eds.; Springer, Heidelberg, Germany, **2015**; pp. 389–407.
[80] Pang, X.; Du, H.-L.; Zhang, H.-Q.; Zhai, Y.-J.; Zhai, G.-X. Polymer–drug conjugates: present state of play and future perspectives. *Drug Discov. Today* **2013**, *18*, 1316–1322.
[81] Alven, S.; Nqoro, X.; Buyana, B.; Aderibigbe, B.A. Polymer-drug conjugate, a potential therapeutic to combat breast and lung cancer. *Pharmaceutics* **2020**, *12*, 406.
[82] Marasini, N.; Haque, S.; Kaminskas, L.M. Polymer-drug conjugates as inhalable drug delivery systems: A review. *Curr. Opin. Colloid Interface Sci.* **2017**, *31*, 18–29.
[83] Ekladious, I.; Colson, Y.L.; Grinstaff, M.W. Polymer–drug conjugate therapeutics: advances, insights and prospects. *Nat. Rev. Drug Discov.* **2019**, *18*, 273–294.
[84] Xu, J.; Lin, S.; Hu, H.; Xing, Q.; Geng, J. Tumor-targeting polymer–drug conjugate for liver cancer treatment in vitro. *Polymers* **2022**, *14*, 4515.
[85] Malugin, A., Kopečková, P. and Kopeček, J. Liberation of doxorubicin from HPMA copolymer conjugate is essential for the induction of cell cycle arrest and nuclear fragmentation in ovarian carcinoma cells. *J. Control. Release* **2007**, *124*, 6–10.
[86] Larson, N.; Ray, A.; Malugin, A.; Pike, D.; Ghandehari, H. HPMA copolymer-aminohexylgeldanamycin conjugates targeting cell surface expressed GRP78 in prostate cancer. *Pharmaceutical Research* **2010**, *27*, 2683–2693.
[87] Meerum Terwogt, J.; ten Bokkel Huinink, W.; Schellens, J.; Schot, M.; Mandjes, I.; Zurlo, M.; Rocchetti, M.; Rosing, H.; Koopman, F.; Beijnen, J. Phase I clinical and pharmacokinetic study of PNU166945, a novel water-soluble polymer-conjugated prodrug of paclitaxel. *Anti-Cancer Drugs* **2001**, *12*, 315–323.
[88] Heath, F.; Haria, P.; Alexander, C. Varying polymer architecture to deliver drugs, *AAPS J.* **2007**, *9*, E235–E240.

[89] Kim, S.; Kim, J. H.; Jeon, O.; Kwon, I.C.; Park, K. Engineered polymers for advanced drug delivery. *Eu. J. Pharm. Biopharm.* **2009**, *71*, 420– 430.
[90] Kotwal, V.; Saifee, M.; Inamdar, N.; Bhise, K.V.; Saifee, M.; Inamdar, N.; Bhise, K. Biodegradable polymers: Which, when and why? *Ind. J. Pharm. Sci.* **2007**, *69*, 616– 625.
[91] Ginty, P.J.; Howdle, S.M.; Rose, F.R.A.J.; Shakesheff, K.M. An assessment of the role of polymers for drug delivery in tissue engineering. In *Polymers in Drug Delivery*, 1st ed; Uchegbu, I. F.; Schatzlein, A.S., Eds.; CRC Press: Boca Raton, **2006**; pp 63– 80.
[92] Jacobs, I.C.; Mason, N.S. Polymer delivery systems concepts. In *Polymeric Delivery Systems—Properties and Applications*; Elnokaly, M.A.; Piatt, D.M.; Charpentier, B.A., Eds.; American Chemical Society: Washington, DC, **1993**; pp 1– 17.
[93] Varma, M.V.S.; Kaushal, A.M.; Garg, A.; Garg, S. Factors affecting mechanism and kinetics of drug release from matrix-based oral controlled drug delivery systems. *Am. J. Drug Delivery* **2004**, *2*, 43–57.
[94] Dash, T.K.; Konkimalla, V.B. Polymeric modification and its implication in drug delivery: Poly-ε-caprolactone (PCL) as a model polymer. *Mol. Pharm.* **2012**, *9*, 2365–2379.
[95] Pillai, O.; Panchagnula, R. Polymers in drug delivery. *Curr. Opin. Chem. Biol.* **2001**, *5*, 447–451.
[96] Nair, L.S., Laurencin, C.T. Polymers as biomaterials for tissue engineering and controlled drug delivery. In: *Tissue Engineering I. Advances in Biochemical Engineering/Biotechnology*; Lee, K.; Kaplan, D., Eds.; Springer, Berlin, Germany, **2005**; 102; pp. 47– 90.
[97] Schreier, H. *Drug Targeting Technology: Physical Chemical Biological Methods*, 1st ed.; CRC Press: Boca Raton, **2001**; pp 12– 270.
[98] G. Rivera-Hernández, M. Antunes-Ricardo, P. Martínez-Morales, M.L. Sánchez. Polyvinyl alcohol based-drug delivery systems for cancer treatment. *Int. J. Pharm.* **2021**, *600*, 120478.
[99] Baker, M.I.; Walsh, S.P.; Schwartz, Z.; Boyan, B.D. A review of polyvinyl alcohol and its uses in cartilage and orthopedic applications. *J. Biomed. Mater. Res. B Appl. Biomater.* **2012**, *100*, 1451–1457.
[100] Saxena, S. Polyvinyl alcohol (PVA). In Chemical and Technical Assessment; FAO: Rome, Italy, **2004**.
[101] Wang, M.; Li, Y.; Wu, J.; Xu, F.; Zuo, Y.; Jansen, J.A. In vitro and in vivo study to the biocompatibility and biodegradation of hydroxyapatite/poly(vinyl alcohol)/gelatin composite. *J. Biomed. Mater. Res. A* **2008**, *85*, 418–426.
[102] Salunkhe, A.B.; Khot, V.M.; Thorat, N.D.; Phadatare, M.R.; Sathish, C.I.; Dhawale, D.S.; Pawar, S.H. Polyvinyl alcohol functionalized cobalt ferrite nanoparticles for biomedical applications. *Appl. Surf. Sci.* **2013**, *264*, 598–604.
[103] Cavalieri, F.; Hamassi, A.E.; Chiessi, E.; Paradossi, G.; Villa, R.; Zaffaroni, N. Ligands tethering to biocompatible ultrasound active polymeric microbubbles surface. *Macromol. Symp.* **2006**, *234*, 94–101.
[104] Yamaoka, T.; Tabata, Y.; Ikada, Y. Comparison of body distribution of poly(vinyl alcohol) with other water-soluble polymers after intravenous administration. *J. Pharm. Pharmacol.* **1995**, *47*, 479–486.
[105] Kaneo, Y.; Hashihama, S.; Kakinoki, A.; Tanaka, T.; Nakano, T.; Ikeda, Y. Pharmacokinetics and biodisposition of poly(vinyl alcohol) in rats and mice. *Drug Metab. Pharmacokinet.* **2005**, *20*, 435–442.
[106] Cerroni, B.; Cicconi, R.; Oddo, L.; Scimeca, M.; Bonfiglio, R.; Bernardini, R.; Palmieri, G.; Domenici, F.; Bonanno, E.; Mattei, M.; Paradossi, G. In vivo biological fate of poly(vinyl alcohol) microbubbles in mice. *Heliyon* **2018**, *4*, e00770.
[107] Brandsch, J.; Piringer, O. Chapter 2 Characteristics of plastic materials; In *Plastic Packaging: Interactions with food and pharmaceuticals*, 2nd ed.; Piringer, O.G.; Bane, A.L., Eds.; Wiley-VCH: Chichester, UK, **2008**; pp. 15–61.
[108] Tharanathan, R.N.; Kittur, F.S. Chitin—The undisputed biomolecule of great potential. *Crit. Rev. Food Sci. Nutr.* **2003**, *43*, 61–87.
[109] Felt, O.; Furrer, P.; Mayer, J.M.; Plazonnet, B.; Buri, P.; Gurny, R. Topical use of chitosan in ophthalmology: Tolerance assessment and evaluation of precorneal retention. *Int. J. Pharm.* **1999**, *180*, 185–193.
[110] Ikinci, G.; Senel, S.; Akincibay, H.; Kas, S.; Ercis, S.; Wilson, C.G.; Hincal, A.A. Effect of chitosan on a periodontal pathogen Porphyromonas gingivalis. *Int. J. Pharm.* **2002**, *235*, 121–127.
[111] Patashnik, S.; Rabinovich, L.; Golomb, G. Preparation and evaluation of chitosan microspheres containing bisphosphonates. *J. Drug Target.* **1997**, *4*, 371–380.

[112] Song, J.; Suh, C.H.; Park, Y.B.; Lee, S.H.; Yoo, N.C.; Lee, J.D.; Kim, K.H.; Lee, S.K. A phase I/IIa study on intra-articular injection of holmium-166-chitosan complex for the treatment of knee synovitis of rheumatoid arthritis. *Eur. J. Nucl. Med.* **2001**, *28*, 489–497.
[113] Chen, Q.; Qi, Y.; Jiang, Y.; Quan, W.; Luo, H.; Wu, K.; Li, S.; Ouyang, Q. Progress in Research of Chitosan Chemical Modification Technologies and Their Applications. *Mar. Drugs* **2022**, *20*, 536.
[114] Inamdar, N.; Mourya, V.K. Thiolated chitosan: Preparation, properties and applications. In *Chitin and Chitosan Derivatives: Advances in Drug Discovery and Developments*; Kim, S.-K., Ed.; CRC Press/Taylor and Francis: Boca Raton, FL, USA, **2013**; pp. 121–150.
[115] Swainson, S.M.E.; Styliari, I.D.; Taresco, V.; Garnett, M.C. Poly (glycerol adipate) (PGA), an enzymatically synthesized functionalizable polyester and versatile drug delivery carrier: A literature update. *Polymers* **2019**, *11*, 1561.
[116] Washington, K.E.; Kularatne, R.N.; Karmegam, V.; Biewer, M.C.; Stefan, M.C. Recent advances in aliphatic polyesters for drug delivery applications. *WIREs Nanomed. Nanobiotechnol.* **2017**, *9*, e1446.
[117] Balla, E.; Daniilidis, V.; Karlioti, G.; Kalamas, T.; Stefanidou, M.; Bikiaris, N.D.; Vlachopoulos, A.; Koumentakou, I.; Bikiaris, D.N. Poly(lactic acid): A versatile biobased polymer for the future with multifunctional properties—From monomer synthesis, polymerization techniques and molecular weight increase to PLA applications. *Polymers* **2021**, *13*, 1822.
[118] Li, Y.; Liao, C.; Tjong, S.C. Synthetic biodegradable aliphatic polyester nanocomposites reinforced with nanohydroxyapatite and/or graphene oxide for bone tissue engineering applications. *Nanomaterials* **2019**, *9*, 590.
[119] Bikiaris, D.; Karavelidis, V.; Karavas, E. Effectiveness of various drug carriers in controlled release formulations of raloxifene HCl prepared by melt mixing. *Curr. Drug Deliv.* **2009**, *6*, 425–436.
[120] Manavitehrani, I.; Fathi, A.; Badr, H.; Daly, S.; Shirazi, A.N.; Dehghani, F. Biomedical applications of biodegradable polyesters. *Polymers* **2016**, *8*, 20–52.
[121] Armentano, I.; Gigli, M.; Morena, F.; Argentati, C.; Torre, L.; Martino, S. Recent advances in nanocomposites based on aliphatic polyesters: Design, synthesis, and applications in regenerative medicine. *Appl. Sci.* **2018**, *8*, 1452.
[122] Briger, I.; Dubernet, C.; Couvreur, P. Nanoparticles in cancer therapy and diagnosis. *Adv. Drug Deliv. Rev.* **2002**, *54*, 631–651.
[123] Couvreur, P.; Vauthier, C. Nanotechnology: Intelligent design to treat complex disease. *Pharm. Res.* **2006**, *23*, 1417–1450.
[124] Bai, Z.; Liu, Y.; Su, T.; Wang, Z. Effect of hydroxyl monomers on the enzymatic degradation of poly (ethylene succinate), poly(butylene succinate), and poly (hexylene succinate). *Polymers* **2018**, *10*, 90.
[125] Qiu, S.; Zhang, K.; Su, Z.; Qiu, Z. Thermal behavior, mechanical and rheological properties, and hydrolytic degradation of novel branched biodegradable poly (ethylene succinate) copolymers. *Polym. Test.* **2018**, *66*, 64–69.
[126] Zhang, K.; Qiu, Z. Miscibility and crystallization behavior of novel branched poly (ethylene succinate)/poly (vinyl phenol) blends. *Chin. J. Polym. Sci.* **2019**, *37*, 1169–1175.
[127] Ishii, N.; Inoue, Y.; Shimada, K.; Tezuka, Y.; Mitomo, H.; Kasuya, K. Fungal degradation of poly (ethylene succinate). *Polym. Degrad. Stab.* **2007**, *94*, 44–52.
[128] Ichikawa, Y.; Washiyama, J.; Moteki, Y.; Noguchi, K. Crystal modification in poly (ethylene succinate). *Polym. J.* **1995**, *27*, 1264–1266.
[129] Tezuka, Y.; Ishii, N.; Kasuya, K.; Mitomo, H. Degradation of poly (ethylene succinate) by mesophilic bacteria. *Polym. Degrad. Stab.* **2004**, *84*, 115–121.
[130] Ueda, A.; Chatani, Y.; Tadokoro, H. Structure studies of polyesters. IV. molecular and structure of poly (ethylene succinate) and poly (ethylene oxalate). *Polym. J.* **1971**, *2*, 387–394.
[131] Papageorgiou, G.Z.; Bikiaris, D.N. Crystallization and melting behavior of three biodegradable poly (alkylene succinates). A comparative study. *Polymer* **2005**, *46*, 12081–12092.
[132] Zhao, J.; Wang, X.; Zhou, W.; Zhi, E.; Zhang, W.; Ji, J. Graphene-reinforced biodegradable poly (ethylene succinate) nanocomposites prepared by in situ polymerization. *J. Appl. Polym. Sci.* **2013**, *130*, 3212–3220.
[133] Carothers, W.H.; Dorough, G.L. Studies on polymerization and ring formation. IV. Ethylene succinates. *J. Am. Chem. Soc.* **1930**, *52*, 711–721.
[134] Chrissafis, K.; Paraskevopoulos, K.; Bikiaris, D. Thermal degradation mechanism of poly (ethylene succinate) and poly (butylene succinate): Comparative study. *Thermochim. Acta* **2005**, *435*, 142–150.

[135] Chrissafis, K.; Paraskevopoulos, K.M.; Bikiaris, D.N. Effect of molecular weight on thermal degradation mechanism of the biodegradable polyester poly (ethylene succinate). *Thermochim. Acta* **2006**, *440*, 166–175.
[136] Bikiaris, D.; Papageorgiou, G.; Achilias, D. Synthesis and comparative biodegradability studies of three poly (alkylene succinate). *Polym. Degrad. Stabil.* **2006**, *91*, 31–43.
[137] Langer, R. New methods of drug delivery. *Science* **1990**, *249*, 1527−1533.
[138] Kamaly, N.; Yameen, B.; Wu, J.; Farokhzad, O. C. Degradable controlled-release polymers and polymeric nanoparticles: mechanisms of controlling drug release. *Chem. Rev.* **2016**, *116*, 2602–2663.
[139] Kim, H.K.; Chung, H.J.; Park, T.G. Biodegradable polymeric microspheres with "open/closed" pores for sustained release of human growth hormone. *J. Control. Release* **2006**, *112*, 167–174.
[140] Webber, W. L.; Lago, F.; Thanos, C.; Mathiowitz, E. Characterization of soluble, salt-loaded, degradable PLGA films and their release of tetracycline. *J. Biomed. Mater. Res.* **1998**, *41*, 18−29.
[141] Fu, Y.; Kao, W.J. Drug release kinetics and transport mechanisms of non-degradable and degradable polymeric delivery systems. *Expert Opin. Drug Delivery* **2010**, *7*, 429−444.
[142] Keraliya, R.A.; Patel, C.; Patel, P.; Keraliya, V.; Soni, T.G.; Patel, R.C.; Patel, M.M. Osmotic drug delivery system as a part of modified release dosage form. *ISRN Pharm.* **2012**, *2012*, 528079.
[143] Uhrich, K. E.; Cannizzaro, S. M.; Langer, R. S.; Shakesheff, K. M. Polymeric systems for controlled drug release. *Chem. Rev.* **1999**, *99*, 3181−3198.
[144] Marin, E.; Briceno, M. I.; Caballero-George, C. Critical evaluation of biodegradable polymers used in nanodrugs. *Int. J. Nanomed.* **2013**, *8*, 3071−3090.
[145] Park, H.; Park, K.; Shalaby, W.S. *Biodegradable Hydrogels for Drug Delivery*; CRC Press, Boca Raton, FL, USA, **1993**; pp 15.
[146] Chen, X.; Ooi, C.P. Effect of ganciclovir on the hydrolytic degradation of poly(lactide-co-glycolide) microspheres. *J. Biomater. Appl.* **2006**, *20*, 287−302.
[147] Rahim, M.A.; Jan, N.; Khan, S.; Shah, H.; Madni, A.; Khan, A.; Jabar, A.; Khan, S.; Elhissi, A.; Hussain, Z.; Aziz, H.C.; Sohail, M.; Khan, M.; Thu, H.E. Recent advancements in stimuli responsive drug delivery platforms for active and passive cancer targeting. *Cancers* **2021**, *13*, 670.
[148] Mura, S.; Nicolas, J.; Couvreur, P. Stimuli-responsive nanocarriers for drug delivery. *Nature Mater.* **2013**, *12*, 991–1003.
[149] Vinchhi, P.; Rawal, S.U.; Patel, M.M. External stimuli-responsive drug delivery systems. In *Drug Delivery Devices and Therapeutic Systems-Developments in Biomedical Engineering and Bioelectronics*; Chappel, E., ed.; Academic Press, **2021**; pp. 267–288.
[150] Fleige, E.; Quadir, M. A.; Haag, R. Stimuli-responsive polymeric nanocarriers for the controlled transport of active compounds: concepts and applications. *Adv. Drug Delivery Rev.* **2012**, *64*, 866−884.
[151] Cheng, R.; Feng, F.; Meng, F.; Deng, C.; Feijen, J.; Zhong, Z. Glutathione-responsive nano-vehicles as a promising platform for targeted intracellular drug and gene delivery. *J. Control. Release* 2011, 152, 2−12.
[152] Xu, H.; Cao, W.; Zhang, X. Selenium-containing polymers: Promising biomaterials for controlled release and enzyme mimics. *Acc. Chem. Res.* **2013**, *46*, 1647−1658.
[153] Wilson, D.S.; Dalmasso, G.; Wang, L.; Sitaraman, S.V.; Merlin, D.; Murthy, N. Orally delivered thioketal nanoparticles loaded with TNF-alpha-siRNA target inflammation and inhibit gene expression in the intestines. *Nat. Mater.* **2010**, *9*, 923−928.
[154] Chen, J.; Ding, J.; Zhang, Y.; Xiao, C.; Zhuang, X.; Chen, X. Polyion complex micelles with gradient pH-sensitivity for adjustable intracellular drug delivery. *Polym. Chem.* **2015**, *6*, 397−405.
[155] Dong, L.; Xia, S.; Wu, K.; Huang, Z.; Chen, H.; Chen, J.; Zhang, J. A pH/enzyme-responsive tumor-specific delivery system for doxorubicin. *Biomaterials* **2010**, *31*, 6309−6316.
[156] Costa, P.; Sousa Lobo, J.M. Modeling and comparison of dissolution profiles. *Eur. J. Pharm. Sci.* **2001**, *13*, 123–133.
[157] Gouda, R.; Baishya, H.; Qing, Z. Application of Mathematical Models in Drug Release Kinetics of Carbidopa and Levodopa ER Tablets. *J. Dev. Drugs* **2017**, *6*, 171.
[158] Panotopoulos, G.P.; Haidar, Z.S. Mathematical modeling for pharmaco-kinetic and -dynamic predictions from controlled drug release nanosystems: a comparative parametric study. *Scientifica* **2019**, *2019*, 9153876.
[159] Dash, S.; Murthy, P.N.; Nath, L.; Chowdhury, P. Kinetic modeling on drug release from controlled drug delivery systems. *Acta Pol. Pharm.* **2010**, *67*, 217–223.
[160] Wakaki, S.; Marumo, H.; Tomioka, K.; Shimizu, G.; Kato, E.; Kamada, H.; Kudo, S.; Fujimoto, Y. Isolation of new fractions of antitumor mitomycins. *Antibiot. Chemother.* **1958**, *8*, 228–240.

[161] Hata, T.; Sano, Y.; Sugawar, R.; Matsumae, A.; Kanamori, K.; Shima, T.; Hosnr, T. Mitomycin, a new antibiotic from Streptomyces. I. *J. Antibiot. (Tokyo)* **1956**, *9*, 141–146.

[162] Hossenlopp, C. Experimental treatment of cancer with mitomycin C alone or in combination with carzinophilin. *The Journal of Antibiotics* **1961**, *14*, 289–297.

[163] Lee, S.J.; Paranhos, A.; Shields, M.B. Does titration of mitomycin C as an adjunct to trabeculectomy significantly influence the intraocular pressure outcome? *Clin. Ophthalmol.* **2009**, *3*, 81**–**87.

[164] Merritt, S.R.; Velasquez, G.; von Recum, H.A. Adjustable release of mitomycin C for inhibition of scar tissue formation after filtration surgery. *Exp. Eye Res.* **2013**, *116*, 9–16.

[165] Beckers, H.J.; Kinders, K.C.; Webers, C.A. Five-year results of trabeculectomy with mitomycin C. *Graefe's Arch. Clin. Exp. Ophthalmol.* **2003**, *241*, 106**–**110.

[166] Crooke, S.T.; Bradner, W.T. Mitomycin C: a review. *Cancer Treat. Rev.* **1976**, *3*, 121–139.

[167] Mizuno, M.; Kawabata, S.; Hamaura, T.; Hashida, M.; Sezaki, H. Characterization of mitomycin C-induced gastrointestinal damage. I. In situ recirculation experiment. *Toxicol. Appl. Pharmacol.* **1989**, *97*, 415–423.

[168] Molyneux, G.; Gibson, F.M.; Gordon-Smith, E.C.; Pilling, A.M.; Liu, K.C.; Rizzo, S.; Sulsh, S.; Turton, J.A. The haemotoxicity of mitomycin in a repeat dose study in the female CD-1 mouse. *Int. J. Exp. Path.* **2005**, *86*, 415–430.

[169] Kojima, T.; Hashida, M.; Muranishi, S.; Sezaki, J. Mitomycin C-dextran conjugate: a novel high molecular weight pro-drug of mitomycin C. *J. Pharm. Pharmacol.* **1980**, *32*, 30–34.

[170] Myers, A.L.; Zhang, Y.P.; Kawedia, J.D.; Zhou, X.; Sobocinski, S.M.; Metcalfe, M.J.; Kramer, M.A.; Dinney, C.P.N.; Kamat, A.M. Solubilization and stability of mitomycin C solutions prepared for intravesical administration. *Drugs R D* **2017**, *17*, 297–304.

[171] Doellman, D.; Hadaway, L.; Bowe-Geddes, L.A.; Franklin, M.; LeDonne, J.; Papke-O'Donnell, L.; Pettit, J.; Schulmeister, L.; Stranz, M. Infiltration and extravasation: update on prevention and management. *J. Infus. Nurs.* **2009**, *32*, 203-211.

[172] Yama, N.; Tsuchida, Y.; Nuka, S.; Kitagawa, S.; Saito, J.; Hyodoh, H.; Hyodoh, K.; Koito, K.; Tamakawa, M.; Akiba, H.; Hareyama, M.; Asai, Y. Usefulness of magnetic resonance imaging for surgical management of extravasation of an antitumor agent: a case report. *Jpn. J. Clin. Oncol.* **2001**, *31*, 122–124.

[173] Onishi, H.; Takahashi, H.; Yoshiyasu, M.; Machida, Y. Preparation and in vitro properties of N-succinyl chitosan– or carboxymethylchitin–mitomycin C conjugate microparticles with specified size. *Drug Dev. Ind. Pharm.* **2001**, *27*, 659–667.

[174] Nomura, T.; Saikawa, A.; Morita, S.; Sakaeda Kakutani, T.; Yamashita, F.; Honda, K.; Takakura, Y.; Hashida, M. Pharmacokinetic characteristics and therapeutic effects of mitomycin C-dextran conjugates after intratumoural injection. *J. Control. Release* **1998**, *52*, 239–252.

[175] Cheung, R.Y.; Ying, Y.; Rauth, A.M.; Marcon, N.; Yu Wu, X. Biodegradable dextran-based microspheres for delivery of anticancer drug mitomycin C. *Biomaterials* **2005**, *26*, 5375–5385.

[176] Xi-Xiao, Y.; Jan-Hai, C.; Shi-Ting, L.; Dan, G.; Xv-Xin, Z. Polybutylcyanoacrylate nanoparticles as a carrier for mitomycin C in rabbits bearing VX2-liver tumor. *Regul. Toxicol. Pharmacol.* **2006**, *46*, 211–217.

[177] Cumming, J.; Allan, L.; Smyth, J.F. Encapsulation of mitomycin C in albumin microspheres markedly alters pharmacokinetics, drug quinone reduction in tumour tissue and antitumour activity: Implications for the drugs' in vivo mechanism of action. *Biochem. Pharmacol.* **1994**, *47*, 1345–1356.

[178] Liu, Y.C.; Li, H.; Shu, X.Z.; Gray, S.D.; Prestwich, G.D. Crosslinked hyaluronan hydrogels containing mitomycin C reduce postoperative abdominal adhesions. *Fertil. Steril.* **2005**, *83*, 1275–1283.

[179] Ishiki, N.; Onishi, H.; Machida, Y. Evaluation of antitumor and toxic side effects of mitomycin C-estradiol conjugates. *Int. J. Pharm.* **2004**, *279*, 81–93.

[180] Sarisozen, C.; Aktaş, Y.; Mungan, A.; Bilensoy, E. Bioadhesive coated poly-epsilon-caprolactone nanoparticles loaded with Mitomycin C for the treatment of superficial bladder tumors. *Eur. J. Pharm. Sci.* **2007**, *32*, S36.

[181] Ekins, S.; Lane, T.R.; Madrid, P.B. Tilorone: a broad-spectrum antiviral invented in the USA and commercialized in Russia and beyond. *Pharm. Res.* **2020**, *37*, 71.

[182] Puhl, A.C.; Fritch, E.J.; Lane, T.R.; Tse, L.V.; Yount, B.L.; Sacramento, C.Q.; Fintelman-Rodrigues, N.; Tavella, T.A.; Maranhão Costa, F.T.; Weston, S.; Logue, J.; Frieman, M.; Premkumar, L.; Pearce, K. H.;

Hurst, B. L.; Andrade, C. H.; Levi, J. A.; Johnson, N. J.; Kisthardt, S. C.; Scholle, F.; Souza, T. M. L.; Moorman, N. J.; Baric, R. S.; Madrid, P. B.; Ekins, S. Repurposing the ebola and marburg virus inhibitors tilorone, quinacrine, and pyronaridine: In vitro activity against SARS-CoV-2 and potential mechanisms. *ACS Omega* **2021**, *6*, 7454–7468.

[183] Fleming, R.W.; Wenstrup, D.L.; Andrews, E.R. Bis-basic ethers and thioethers of fluorenone, fluorenol and fluorene. In: US3592819A, editor.: Aventis Inc; 12/30/1968.

[184] Zhang, J.; Yao, Q.; Liu, Z. An effective synthesis method for tilorone dihydrochloride with obvious IFN-alpha inducing activity. *Molecules* **2015**, *20*, 21458–21463.

[185] Burke, S.M.; Joullie, M.M. New synthetic pathways to tilorone hydrochloride. *Synth. Commun.* **1976**, *6*, 371–376.

[186] Rovó, L.; Madani, S.; Sztanó, B.; Majoros, V.; Smehák, G.; Szakács, L.; Jóri, J. A new thread guide instrument for endoscopic arytenoid lateropexy. *Laryngoscope* **2010**, *120*, 2002–2007.

[187] Madani, S.; Bach, Á.; Matievics, V.; Erdélyi, E.; Sztanó, B.; Szegesdi, I.; Castellanos, P.F.; Rovó, L. A new solution for neonatal bilateral vocal cord paralysis: Endoscopic arytenoid abduction lateropexy. *Laryngoscope* **2017**, *127*, 1608–1614.

[188] Matievics, V.; Bach, A.; Sztano, B.; Bere, Z.; Tobias, Z.; Castellanos, P.F.; Mueller, A.H.; Rovo, L. Functional outcomes of endoscopic arytenoid abduction lateropexy for unilateral vocal cord paralysis with dyspnea. *Eur. Arch. Otorhinolaryngol.* **2017**, *274*, 3703–3710.

[189] Ohno, S.; Hirano, S.; Yasumoto, A.; Ikeda, H.; Takebayashi, S.; Miura, M. Outcome of regenerative therapy for age-related vocal fold atrophy with basic fibroblast growth factor. *Laryngoscope* **2016**, *126*, 1844–1848.

[190] Li, Y.; Xu, W.; Cheng, L.Y. Adipose-derived mesenchymal stem cells accelerate nerve regeneration and functional recovery in a rat model of recurrent laryngeal nerve injury. *Neural. Regen. Res.* **2017**, *12*, 1544–1550.

[191] Sartori, R.; Schirwis, E.; Blaauw, B.; Bortolanza, S.; Zhao, J.; Enzo, E.; Stantzou, A.; Mouisel, E.; Toniolo, L.; Ferry, A.; Stricker, S.; Goldberg, A.L.; Dupont, S.; Piccolo, S.; Amthor, H.; Sandri, M. BMP signaling controls muscle mass. *Nat. Genet.* **2013**, *45*, 1309–1318.

[192] Winbanks, C.E.; Chen, J.L.; Qian, H.; Liu, Y.; Bernardo, B.C.; Beyer, C.; Watt, K.I.; Thomson, R.E.; Connor, T.; Turner, B.J.; McMullen, J.R.; Larsson, L.; McGee, S.L.; Harrison, C.A.; Gregorevic, P. The bone morphogenetic protein axis is a positive regulator of skeletal muscle mass. *J. Cell Biol.* **2013**, *203*, 345–357.

[193] Leppäranta, O.; Tikkanen, J.M.; Bespalov, M.M.; Koli, K.; Myllärniemi, M. Bone morphogenetic protein-inducer tilorone identified by high-throughput screening is antifibrotic in vivo. *Am. J. Respir. Cell Mol. Biol.* **2013**, *48*, 448–455.

[194] Horlock, D.; Kaye, D.M.; Winbanks, C.E.; Gao, X.-M.; Kiriazis, H.; Donner, D.G.; Gregorevic, P.; McMullen, J.R.; Bernardo, B.C. Old drug, new trick: Tilorone, a broad-spectrum antiviral drug as a potential anti-fibrotic therapeutic for the diseased heart. *Pharmaceuticals* **2021**, *14*, 263.

[195] Willson, J. The BMP pathway could curb cachexia. *Nat. Rev. Cancer.* **2021**, *21*, 612.

[196] Geremia, A.; Sartori, R.; Baraldo, M.; Nogara, L.; Balmaceda, V.; Dumitras, G.A.; Ciciliot, S.; Scalabrin, M.; Nolte, H.; Blaauw, B. Activation of Akt-mTORC1 signalling reverts cancer-dependent muscle wasting. *J. Cachexia Sarcopenia Muscle* **2021**, *13*, 648–661.

[197] Smith, R.C.; Lin, B.K. Myostatin inhibitors as therapies for muscle wasting associated with cancer and other disorders. *Curr. Opin. Support Palliat. Care* **2013**, *7*, 352–360.

[198] Saitoh, M.; Ishida, J.; Ebner, N.; Anker, S.D.; von Haehling, S. Myostatin inhibitors as pharmacological treatment for muscle wasting and muscular dystrophy. *JCSM Clinical Reports* **2017**, 2, 1–10.

[199] Suh, J.; Lee, Y.S. Myostatin inhibitors: Panacea or predicament for musculoskeletal disorders? *J. Bone Metab.* **2020**, *27*,151-165.

[200] Rybalka, E.; Timpani, C.A.; Debruin, D.A.; Bagaric, R.M.; Campelj, D.G.; Hayes, A. The failed clinical story of myostatin inhibitors against duchenne muscular dystrophy: Exploring the biology behind the battle. *Cells* **2020**, *9*, 2657.

[201] Barmpalexis, P.; Kanaze, F.I.; Kachrimanis, K.; Georgarakis, E. Artificial neural networks in the optimization of a nimodipine controlled release tablet formulation. *Eur. J. Pharm. Biopharm.* **2010**, *74*, 316–323.

[202] Gelmers, H.J. Calcium-channel blockers in the treatment of migraine. *Am. J. Cardiol.* **1985**, *55*, 139B–143B.

[203] Langley, M.S.; Sorkin, E.M. Nimodipine. A review of its pharmacodynamic and pharmacokinetic properties, and therapeutic potential in cerebrovascular disease. *Drugs* **1989**, *37*, 669–699.

[204] Zhao, Y.; Xin, T.; Ye, T.; Yang, X.; Pan, W. Solid dispersion in the development of a nimodipine delayed-release tablet formulation. *Asian J. Pharm. Sci.* **2014**, *9*, 35–41.

[205] Huang, S.; Huang, Z.; Fu, Z.; Shi, Y.; Dai, Q.; Tang, S.; Gu, Y.; Xu, Y.; Chen, J.; Wu, X.; Ren, F. A novel drug delivery carrier comprised of nimodipine drug solution and a nanoemulsion: preparation, characterization, in vitro, and in vivo studies. *Int. J. Nanomedicine* **2020**, *15*, 1161–1172.
[206] Grunenberg, A.; Keil, B.; Henck, J.O. Polymorphism in binary mixture, as exemplified by nimodipine. *Int. J. Pharm.* **1995**, *118*, 11–21.
[207] He, Z.; Zhong, D.; Chen, X.; Liu, X.; Tang, X.; Zhao, L. Development of a dissolution medium for nimodipine tablets based on bioavailability evaluation. *Eur. J. Pharm. Sci.* **2004**, *21*, 487–491.
[208] Mahmoud, S.H.; Ji, X.; Isse, F.A. Nimodipine pharmacokinetic variability in various patient populations. *Drugs R D* **2020**, *20*, 307–318.
[209] Hernández-Hernández, R.; Coll, T.; Rachitzky, P.; Armas-Hernández, M.J.; Armas-Padilla, M.C.; Velasco, M.; Rizzo, A. Comparison of two nimodipine formulations in healthy volunteers. *J. Hum. Hypertens.* **2002**, *16*, S142–S144.
[210] Krishnaiah, Y.S.; Bhaskar, P.; Satyanarayana, V. Effect of carvone on the permeation of nimodipine from a membrane-moderated transdermal therapeutic system. *Pharmazie* **2003**, *58*, 559–563.
[211] Sun, Y.; Rui, Y.; Wenliang, Z.; Tang, X. Nimodipine semi-solid capsules containing solid dispersion for improving dissolution. *Int. J. Pharm.* **2008**, *359*, 144–149.
[212] Vinge, E.; Andersson, K.E.; Brandt, L.; Ljunggren, B.; Nilsson, L.G.; Rosendal-Helgesen, S. Pharmacokinetics of nimodipine in patients with aneurysmal subarachnoid haemorrhage. *Eur. J. Clin. Pharmacol.* **1986**, *30*, 421–425.
[213] Song, X.; Jiang, Y.; Ren, C.; Sun, X.; Zhang, Q.; Gong, T.; Zhang, Z. Nimodipine-loaded mixed micelles: formulation, compatibility, pharmacokinetics, and vascular irritability study. *Int. J. Nanomedicine* **2012**, *7*, 3689–3699.
[214] Le Daré, B.; Victoni, T.; Bodin, A.; Vlach, M.; Vene, E.; Loyer, P.; Lagente, V.; Gicquel, T. Ethanol upregulates the P2X7 purinergic receptor in human macrophages. *Fundam. Clin. Pharmacol.* **2019**, *33*, 63–74.
[215] Li, J.; Fan, L.; Yuan, M.; Xing, M. Salidroside inhibits lipopolysaccharide-ethanol-induced activation of proinflammatory macrophages via notch signaling pathway. *Curr. Med. Sci.* **2019**, *39*, 526–533.
[216] Schneider, A.C.R.; Gregório, C.; Uribe-Cruz, C.; Guizzo, R.; Malysz, T.; Faccioni-Heuser, M.C.; Longo, L.; da Silveira, T.R. Chronic exposure to ethanol causes steatosis and inflammation in zebrafish liver. *World J. Hepatol.* **2017**, *9*, 418–426.
[217] Soliman, G.M.; Sharma, R.; Choi, A.O.; Varshney, S.K.; Winnik, F.M.; Kakkar, A.K.; Maysinger, D. Tailoring the efficacy of nimodipine drug delivery using nanocarriers based on A2B miktoarm star polymers. *Biomaterials* **2010**, *31*, 8382–8392.
[218] Luca, M.D.; Ioele, G.; Spatari, C.; Ragno, G. Photodegradation of 1,4-dihydropyridine antihypertensive drugs: an updated review. *Int. J. Pharm. Pharm. Sci.* **2018**, *10*, 8–18.
[219] Toth, O.M.; Menyhart, A.; Varga, V.E.; Hantosi, D.; Ivankovits-Kiss, O.; Varga, D.P.; Szabo, I.; Janovak, L.; Dekany, I.; Farkas, E.; Bari, F. Chitosan nanoparticles release nimodipine in response to tissue acidosis to attenuate spreading depolarization evoked during forebrain ischemia. *Neuropharmacology* **2020**, *162*, 107850.
[220] Fieser, L.F. *Experiments in Organic Chemistry*, 2nd ed., **1941**, p. 104.
[221] Sanchez-Chaves, M.; Arranz, F.; Cortazar, M. Poly(vinyl alcohol)functionalized by monosuccinate groups. Coupling of bioactive amino compounds. *Polymer* **1998**, *39*, 2751–2757.
[222] Neises, B.; Steglich, W. Simple Method for the Esterification of Carboxylic Acids. *Angew. Chem. Int. Edn. Eng.* **1978**, *17*, 522–524.
[223] Izunobi, J.U.; Higginbotham, C.L. Polymer molecular weight analysis by 1H NMR spectroscopy. *J. Chem. Educ*. **2011**, *88*, 1098–1104.
[224] Pawcenis, D.; Syrek, M.; Aksamit-Koperska, M.A.; Łojewski, T.; Łojewska, J. Mark-Houwink-Sakurada coefficients determination for molar mass of silk fibroin from viscometric results. SEC-MALLS approach. *RSC Adv*. **2016**, *6*, 38071–38078.
[225] Gupta, B.; Anjum, S.; Ikram, S. Preparation of thiolated polyvinyl alcohol hydrogels. *J. Appl. Polym. Sci.* **2013**, *129*, 815–821.
[226] Matuschek, E.; Brown, D.F.; Kahlmeter, G. Development of the EUCAST disk diffusion antimicrobial susceptibility testing method and its implementation in routine microbiology laboratories. *Clin. Microbiol. Infect.* **2014**, *20*, O255–O266.
[227] Borsagli, M.; Carvalho, I.C.; Mansur, H.S. Amino acid-grafted and N-acylated chitosan thiomers: Construction of 3D bio-scaffolds for potential cartilage repair applications. *Int. J. Biol. Macromol.* **2018**, *114*, 270–282.

[228] Boyer, R.F. A new molecular weight distribution technique for polystyrene. I. Theory. *J. Polym. Sci.* **1952**, *8*, 73–90.
[229] Cornet, C.F.; van Ballegooijen, H. Rapid turbidimetric determinations of θ-conditions. *Polymer* **1966**, *7*, 293.
[230] Janovák, L.; Turcsányi, Á.; Bozó, É.; Deák, Á.; Mérai, L.; Sebők, D.; Juhász, Á.; Csapó, E.; Abdelghafour, M.M.; Farkas, E.; Dékány, I.; Bari, F. Preparation of novel tissue acidosis-responsive chitosan drug nanoparticles: characterization and in vitro release properties of Ca^{2+} channel blocker nimodipine drug molecules. *Eur. J. Pharm. Sci.* **2018**, *123*, 79–88.
[231] Takács, T.; Abdelghafour, M.M.; Deák, Á.; Szabó, D.; Sebők, D.; Dékány, I.; Rovó, L.; Kukovecz, Á.; Janovák, L. Surface wetting driven release of antifibrotic Mitomycin-C drug from modified biopolymer thin films. *Eur. Polym. J.* **2020**, *139*, 109995.
[232] Abdelghafour, M.M.; Deák, Á.; Szabó, D.; Dékány, I.; Rovó, L.; Janovák, L. Use of Self-Assembled Colloidal Prodrug Nanoparticles for Controlled Drug Delivery of Anticancer, Antifibrotic and Antibacterial Mitomycin. *Int. J. Mol. Sci.* **2022**, *23*, 6807.
[233] Zhou, Z.; Xu, W.; He, D.; Fan, J.; Yu, F.; Ren, F. Solid-state grafting of succinic anhydride onto poly(vinyl alcohol). *J. Appl. Polym. Sci.* **2007**,*103*, 848–852.
[234] Tsakos, M.; Schaffert, E.S.; Clement, L.L.; Villadsen, N.L.; Poulsen, T.B. Ester coupling reactions–an enduring challenge in the chemical synthesis of bioactive natural products. *Nat. Prod. Rep.* **2015**, *32*, 605–632.
[235] Bhat, N.V.; Nate, M.M.; Kurup, M.B.; Bambole, V.A.; Sabharwal, S. Effect of γ-radiation on the structure and morphology of polyvinyl alcohol films. *Nucl. Instrum. Methods Phys. Res. B* **2005**, *237*, 585–592.
[236] Stipniece, L.; Salma-Ancane, K.; Rjabovs, V.; Juhnevica, I.; Turks, M.; Narkevica, I.; Berzina-Cimdina, L. Development of functionalized hydroxyapatite/poly (vinyl alcohol) composites. *J. Cryst. Growth* **2016**, *444*, 14–20.
[237] Zhang, B.; Huang, Q.; Luo, F.X.; Fu, X.; Jiang, H.X.; Jane, J.L. Effects of octenylsuccinylation on the structure and properties of high-amylose maize starch. *Carbohydr. Polym.* **2011**, *84*, 1276–1281.
[238] Guan, H.M.; Chung, T.S.; Huang, Z.; Mei, L.C.; Kulprathipanja, S. Poly(vinyl alcohol) multilayer mixed matrix membranes for the dehydration of ethanol-water mixture. *J. Membr. Sci.* **2006**, *268*, 113–122.
[239] Hayashi, T.; Mukamel, S. Vibrational−Exciton couplings for the amide I, II, III, and A modes of peptides. *J. Phys. Chem. B* **2007**, *111*, 11032– 11046.
[240] Uzu, K.; Harada, Y.; Wakaki, S.; Yamada, Y. Studies on Mitomycins, Carcinostatic Antibiotics: Part I. Derivatives and Acid Hydrolysis of Mitomycin A and C Part II. Mitomycinone. *Agric. Biol. Chem.* **1964**, *28*, 388–402.
[241] Stipniece, L.; Salma-Ancane, K.; Rjabovs, V.; Juhnevica, I.; Turks, M.; Narkevica, I.; Berzina-Cimdina, L. Development of functionalized hydroxyapatite/poly (vinyl alcohol) composites. *J. Cryst. Growth.* **2016**, *444*, 14–20.
[242] Asiaei, S.; Smith, B.; Nieva, P. Enhancing conjugation rate of antibodies to carboxylates: Numerical modeling of conjugation kinetics in microfluidic channels and characterization of chemical over-exposure in conventional protocols by quartz crystal microbalance. *Biomicrofluidics* **2015**, *9*, 064115.
[243] Joyner, K.; Song, D.; Hawkins, R.F.; Silcott, R.D.; Duncan, G.A. A rational approach to form disulfide linked mucin hydrogels. *Soft Matter.* **2019**, *15*, 9632–9639.
[244] Cook, S.L.; Bull, S.P.; Methven, L.; Parker, J.K.; Khutoryanskiy, V.V. Mucoadhesion: A food perspective. *Food Hydrocoll.* **2017**, *72*, 281–296.
[245] Korsmeyer, R.W.; Gurny, R.; Doelker, E.; Buri, P.; Peppas, N.A. Mechanisms of solute release from porous hydrophilic polymers. *Int. J. Pharm.* **1983**, *15*, 25–35.
[246] Ritger, P.L.; Peppas, N.A. A simple equation for description of solute release. I. Fickian and non-Fickian release from non-swellable devices in the form of slabs, spheres, cylinders or discs. *J. Control. Release* **1987**, *5*, 23–36.
[247] Kumar, U.; Islam, M.S.; Halder, S.; Rouf, A.S. Assessment of once daily sustained release hydrophilic matrix tablet of carvedilol. *Dhaka. Univ. J. Pharm. Sci.* **2017**, *16*, 43–53.
[248] Sackett, C.K.; Narasimhan, B. Mathematical modeling of polymer erosion: Consequences for drug delivery. *Int. J. Pharm.* **2011**, *418*, 104–114.
[249] Abdelghafour, M.M.; Deák, Á.; Kiss, T.; Budai-Szűcs, M.; Katona, G.; Ambrus, R.; Lőrinczi, B.; Keller-Pintér, A.; Szatmári, I.; Szabó, D.; Rovó, L.; Janovák, L. Self-Assembling Injectable Hydrogel for Controlled Drug Delivery of Antimuscular Atrophy Drug Tilorone. *Pharmaceutics* **2022**, *14*, 2723.
[250] Zhang, Y.; Tao, L.; Li, S.; Wei, Y. Synthesis of multiresponsive and dynamic chitosan-based hydrogels for controlled release of bioactive molecules. *Biomacromolecules* **2011**, *12*, 2894–2901.
[251] Takács, T.; Abdelghafour, M.M.; Lamch, Ł.; Szenti, I.; Sebők, D.; Janovák, L.; Kukovecz, Á. Facile modification of hydroxyl group containing macromolecules provides autonomously self-healing polymers through the formation of dynamic Schiff base linkages. *Eur. Polym. J.* **2022**, *168*, 111086.

[252] Fornaro, T.; Burini, D.; Biczysko, M.; Barone, V. Hydrogen-bonding effects on infrared spectra from anharmonic computations: Uracil–water complexes and uracil dimers. *J. Phys. Chem. A* **2015**, *119*, 4224–4236.
[253] Qi, J.-L.; Xu, W.; Zheng, Y.-Q. Synthesis, crystal structure and magnetic properties of a copper(II) p-formylbenzoate complex. *Z. Für Nat. B* **2012**, *67*, 1185–1190.
[254] Yasmeen, S.; Kabiraz, M.; Saha, B.; Qadir, Md. R.; Gafur, Md. A.; Masum, S. Chromium (VI) ions removal from tannery effluent using chitosan-microcrystalline cellulose composite as adsorbent. *Int. Res. J. Pure Appl. Chem.* **2016**, *10*, 1–14.
[255] Dimzon, I.K.D.; Knepper, T.P. Degree of deacetylation of chitosan by infrared spectroscopy and partial least squares. *Int. J. Biol. Macromol.* **2015**, *72*, 939–945.
[256] Fernandes Queiroz, M.; Melo, K.; Sabry, D.; Sassaki, G.; Rocha, H. Does the use of chitosan contribute to oxalate kidney stone formation? *Mar. Drugs* **2014**, *13*, 41–158.
[257] Zhu, X.; Su, M.; Tang, S.; Wang, L.; Liang, X.; Meng, F.; Hong, Y.; Xu, Z. Synthesis of thiolated chitosan and preparation nanoparticles with sodium alginate for ocular drug delivery. *Mol. Vis.* **2012**, *18*, 1973–1982.
[258] Esquivel, R.; Juárez, J.; Almada, M.; Ibarra, J.; Valdez, M.A. Synthesis and characterization of new thiolated chitosan nanoparticles obtained by ionic gelation method. *Int. J. Polym. Sci.* **2015**, *2015*, 1–18.
[259] Zhao, X.; Wu, H.; Guo, B.; Dong, R.; Qiu, Y.; Ma, P.X. Antibacterial anti-oxidant electroactive injectable hydrogel as self-healing wound dressing with hemostasis and adhesiveness for cutaneous wound healing. *Biomaterials* **2017**, *122*, 34–47.
[260] Vollhardt, K.P.C.; Schore, N.E. *Organic Chemistry: Structure and Function*, 5th ed.; W.H. Freeman: New York, NY, USA, **2005**; pp. 779–784.
[261] Cavalieri, F.; El Hamassi, A.; Chiessi, E.; Paradossi, G. Stable polymeric microballoons as multifunctional device for biomedical uses: Synthesis and characterization. *Langmuir* **2005**, *21*, 8758–8764.
[262] Rajpal, G.; Arvan, P. Disulfide bond formation. In *Handbook of Biologically Active Peptides*, 2nd ed.; Kastin, A.J., Ed.; Academic Press: Boston, MA, USA, **2013**; pp. 1721–1729.
[263] Bernkop-Schnürch, A.; Schwarz, V.; Steininger, S. Polymers with thiol groups: A new generation of mucoadhesive polymers? *Pharm. Res.* **1999**, *16*, 876–881.
[264] Wang, X.; Zheng, C.; Wu, Z.; Teng, D.; Zhang, X.; Wang, Z.; Li, C. Chitosan-NAC nanoparticles as a vehicle for nasal absorption enhancement of insulin. *J. Biomed. Mater. Res. B. Appl. Biomater.* **2009**, *88*, 150–161.
[265] Ways, T.M.; Lau, W.; Khutoryanskiy, V. Chitosan and its derivatives for application in mucoadhesive drug delivery systems. *Polymers* **2018**, *10*, 267.
[266] Tseng, T.C.; Tao, L.; Hsieh, F.Y.; Wei, Y.; Chiu, I.M.; Hsu, S.H. An Injectable, Self-Healing Hydrogel to Repair the Central Nervous System. *Adv.Mater.* **2015**, *27*, 3518–3524.
[267] Balakrishnan, B.; Soman, D.; Payanam, U.; Laurent, A.; Labarre, D.; Jayakrishnan, A. A novel injectable tissue adhesive based on oxidized dextran and chitosan. *Acta Biomater.* **2017**, *53*, 343–354.
[268] Van Tomme, S.R.; Storm, G.; Hennink, W.E. In situ gelling hydrogels for pharmaceutical and biomedical applications. *Int. J. Pharm.* **2008**, *355*, 1–18.
[269] Maiz-Fernández, S.; Pérez-Álvarez, L.; Silván, U.; Vilas-Vilela, J.L.; Lanceros-Méndez, S. Dynamic and self-healable chitosan/hyaluronic acid-based in situ-forming hydrogels. *Gels* **2022**, *8*, 477.
[270] Kondiah, P.J.; Choonara, Y.E.; Kondiah, P.P.; Marimuthu, T.; Kumar, P.; Du Toit, L.C.; Pillay, V. A review of injectable polymeric hydrogel systems for application in bone tissue engineering. *Molecules* **2016**, *21*, 1580.
[271] Poldervaart, M.T.; Wang, H.; van der Stok, J.; Weinans, H.; Leeuwenburgh, S.C.; Öner, F.C.; Dhert, W.J.; Alblas, J. Sustained release of BMP-2 in bioprinted alginate for osteogenicity in mice and rats. *PLoS ONE* **2013**, *8*, e72610.
[272] Singh, N.K.; Lee, D.S. In situ gelling pH- and temperature-sensitive biodegradable block copolymer hydrogels for drug delivery. *J. Control. Release* **2014**, *193*, 214–227.
[273] Dimatteo, R.; Darling, N.J.; Segura, T. In situ forming injectable hydrogels for drug delivery and wound repair. *Adv. Drug Deliv. Rev.* **2018**, *127*, 167–184.
[274] Qu, J.; Zhao, X.; Ma, P.X.; Guo, B. Injectable antibacterial conductive hydrogels with dual response to an electric field and pH for localized "smart" drug release. *Acta Biomaterialia* **2018**, *72*, 55–69.
[275] Qu, X.; Yang, Z. Benzoic-imine-based physiological pH-responsive materials for biomedical applications. *Chem. Asian J.* **2016**, *11*, 2633–2641.

[276] Debnath, T.; Ghosh, S.; Potlapuvu, U.S.; Kona, L.; Kamaraju, S.R.; Sarkar, S.; Gaddam, S.; Chelluri, L.K. Proliferation and Differentiation Potential of Human Adipose-Derived Stem Cells Grown on Chitosan Hydrogel. *PLoS ONE* **2015**, *10*, e0120803.
[277] Numata, K. Silk hydrogels for tissue engineering and dual-drug delivery. In *Silk Biomaterials for Tissue Engineering and Regenerative Medicine*; Kundu, S.C., Ed.; Woodhead Publishing: Sawston, UK, **2014**; pp. 503–518.
[278] Abdelghafour, M.M.; Orbán, Á.; Deák, Á.; Lamch, Ł.; Frank, É.; Nagy, R.; Ádám, A.; Sipos, P.; Farkas, E.; Bari, F.; Janovák, L. The Effect of Molecular Weight on the Solubility Properties of Biocompatible Poly(ethylene succinate) Polyester. *Polymers* **2021**, *13*, 2725.
[279] Billiet, L.; Fournier, D.; Du Prez, F. Step-growth polymerization and 'click' chemistry: The oldest polymers rejuvenated. *Polymer* **2009**, *50*, 3877–3886.
[280] Lin, C.C.; Yu, P.C. The kinetics of polyesterification. II. Succinic acid and ethylene glycol. *J. Polym. Sci. A Polym. Chem*. **1978**, *16*, 1005–1016.
[281] Mitra, T.; Sailakshmi, G.; Gnanamani, A.; Mandal, A.B. Studies on cross-linking of succinic acid with chitosan/collagen. *Mater. Res.* **2013**, *16*, 755–765.
[282] Krishnan, K.; Krishnan, R.S. Raman and infrared spectra of ethylene glycol. *Proc. Indian Acad. Sci.* **1966**, *64*, 111–122.
[283] Phua, Y.; Chow, W.; Ishak, Z.M. The hydrolytic effect of moisture and hygrothermal aging on poly (butylene succinate)/organo montmorillonite nanocomposites. *Polym. Degrad. Stabil.* **2011**, *96*, 1194–1203.
[284] Zhou, S.; Wei, Z.; Sun, Y.; Zhu, Z.; Xie, Z.; Ma, H.; Yin, J.; Wang, J.; Yang, J. Biocompatible linear diamides derivative-nucleated biodegradable poly (ethylene succinate): Tailored crystallization kinetics, aggregated structure and thermal degradation. *Polym. Degrad. Stab.* **2021**, *183*, 109428.
[285] Zeng, J.-B.; Li, Y.-D.; Li, W.-D.; Yang, K.-K.; Wang, X.-L.; Wang, Y.-Z. Synthesis and properties of poly (ester urethane)s consisting of poly (L-lactic acid) and poly (ethylene succinate) segments. *Ind. Eng. Chem. Res.* **2009**, *48*, 1706–1711.
[286] Wong, M.; Hollinger, J.; Kozycz, L.M.; Mccormick, T.M.; Lu, Y.; Burns, D.C.; Seferos, D.S. An apparent size-exclusion quantification limit reveals a molecular weight limit in the synthesis of externally initiated polythiophenes. *ACS Macro Lett.* **2012**, *1*, 1266−1269.
[287] Montgomery, J.R.D.; Lancefield, C.S.; Miles-Barrett, D.M.; Ackermann, K.; Bode, B.E.; Westwood, N.J.; Lebl, T. Fractionation and DOSY NMR as analytical tools: from model polymers to a technical lignin. *ACS Omega* **2017**, *2*, 8466−8474.
[288] Liu, C.; Zeng, J.; Li, S. Improvement of biocompatibility and biodegradability of poly(ethylene succinate) by incorporation of poly(ethylene glycol) segments. *Polymer* **2012**, *53*, 481–489.
[289] Serrano, M.C., Pagani, R., Valletregí, M., Peña, J., Rámila, A., Izquierdo, I., Portolés, M.T. In vitro biocompatibility assessment of poly(epsilon-caprolactone) films using L929 mouse fibroblasts. *Biomaterials* **2004**, *25*, 5603–5611.
[290] Yang, M.; Zhu, S.; Chen, Y.; Chang, Z.; Chen, G.; Gong, Y.; Zhao, N.; Zhang, X. Studies on bone marrow stromal cells affinity of poly (3-hydroxybutyrate-co-3-hydroxyhexanoate). *Biomaterials* **2004**, *25*, 1365–1373.
[291] Webb, K., Hlady, V., Tresco, P.A. Relative importance of surface wettability and charged functional groups on NIH 3T3 fibroblast attachment, spreading, and cytoskeletal organization. *J. Biomed. Mater. Res.* **1998**, *41*, 422–430.
[292] Abdelghafour, M.M.; Orbán, Á.; Deák, Á.; Lamch, Ł.; Frank, É.; Nagy, R.; Ziegenheim, S.; Sipos, P.; Farkas, E.; Bari, F.; Janovák, L. Biocompatible poly(ethylene succinate) polyester with molecular weight dependent drug release properties. *Int. J. Pharm.* **2022**, *618*, 121653.
[293] Morales-Huerta, J.C.; Martínez de Ilarduya, A.; Muñoz-Guerra, S. Modulating the Tg of poly(alkylene succinate)s by inserting bio-based aromatic units via ring-opening copolymerization. *Polymers* **2017**, *9*, 701.
[294] Wolf, B.A. Solubility of polymers. *Pure Appl. Chem.* **1985**, *57*, 323–336.
[295] Morey, D.R.; Tamblyn, J.W. The Fractional Precipitation of Molecular-weight Species from High Polymers. Theories of the Process and Some Experimental Evidence. *J. Phys. Colloid. Chem.***1947**, *51*, 721–746.
[296] Van Krevelen, D.W. *Properties of Polymers*, 4th ed.; Elsevier: Amsterdam, The Netherlands, **2009**.
[297] Seretoudi, G.; Bikiaris, D.; Panayiotou, C. Synthesis, characterization and biodegradability of poly (ethylene succinate)/poly (ε-caprolactone) block copolymers. *Polymer* **2002**, *43*, 5405–5415.
[298] Kasuya, K.-I.; Takagi, K.-I.; Ishiwatari, S.-I.; Yoshida, Y.; Doi, Y. Biodegradabilities of various aliphatic polyesters in natural waters. *Polym. Degrad. Stabil.* **1998**, *59*, 327–332.

[299] Tribedi, P.; Sarkar, S.; Mukherjee, K.; Sil, A.K. Isolation of a novel Pseudomonas sp. from soil that can efficiently degrade polyethylene succinate. *Env. Sci. Pollut. Res.* **2012**, *19*, 2115–2124.
[300] Wilkes, R.A.; Aristilde, L. Degradation and metabolism of synthetic plastics and associated products by Pseudomonas sp.: capabilities and challenges. *J. Appl. Microbiol.* **2017**, *123*, 582–593.
[301] Lee, H.J.; Kim, J.Y.; Park, S.H.; Rhee, Y.S.; Park, C.W.; Park, E.S. Controlled-release oral dosage forms containing nimodipine solid dispersion and hydrophilic carriers. *J. Drug Deliv. Sci. Technol.* **2017**, *37*, 28–37.
[302] Abstiens, K.; Goepferich, A.M. Microfluidic manufacturing improves polydispersity of multicomponent polymeric nanoparticles. *J. Drug Delivery Sci. Technol.* **2019**, *49*, 433–439
[303] Jiang, M.; Braatz, R.D. Designs of continuous-flow pharmaceutical crystallizers: developments and practice. *Cryst. Eng. Comm.* **2019**, *21*, 3534–3551.
[304] Khan, I.U.; Serra, C.A.; Anton, N.; Vandamme, T. Continuous-flow encapsulation of ketoprofen in copolymer microbeads via co-axial microfluidic device: influence of operating and material parameters on drug carrier properties. *Int. J. Pharm.* **2013**, *441*, 809–817.
[305] Serra, C.A.; Cortese, B.; Khan, I.U.; Anton, N.; de Croon, M.H.J.M.; Hessel, V.; Ono, T.; Vandamme, T. Coupling microreaction technologies, polymer chemistry and processing to produce polymeric micro and nanoparticles with controlled size, morphology and composition. *Macromol. React. Eng.* **2013**, *7*, 414–439
[306] Yang, Z.; Foster, D.; Dhinojwala, A. Continuous production of polymer nanoparticles using a membrane-based flow cell. *J. Colloid Interface Sci.* **2017**, *501*, 150–155.
[307] Khadka, P.; Ro, J.; Kim, H.; Kim, I.; Kim, J.T.; Kim, H.; Cho, J.M.; Yun, G.; Lee, J. Pharmaceutical particle technologies: an approach to improve drug solubility, dissolution and bioavailability. *Asian J. Pharm. Sci.* **2014**, *9*, 304–316.
[308] Kumar, A.; Dixit, C.K. Methods for characterization of nanoparticles. In *Advances in nanomedicine for the delivery of therapeutic nucleic acids*; Nimesh, S.; Chandra, R.; Gupta, N., Eds.; Woodhead Publishing: Sawston, UK, **2017**; pp. 43–58.

8. Appendices

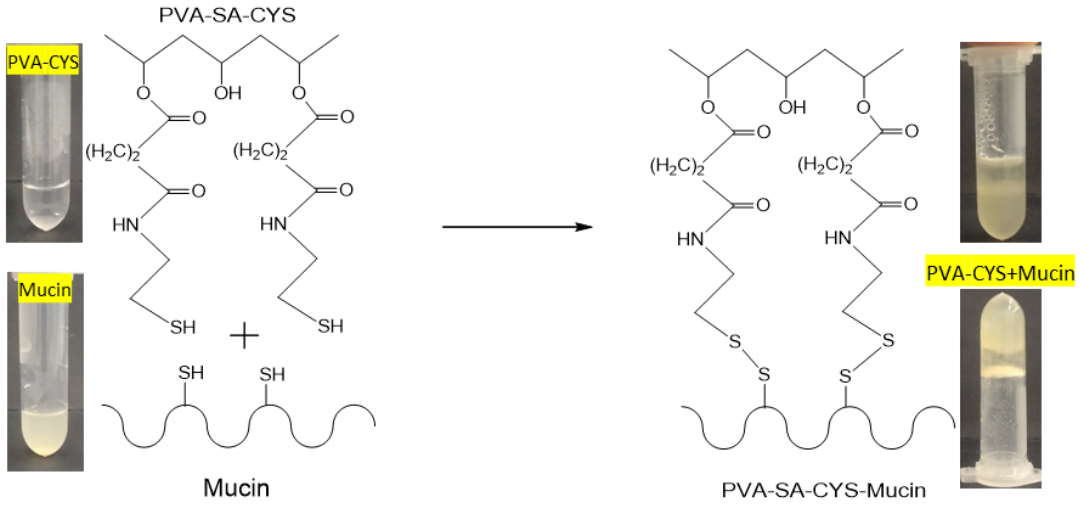

Figure A1. Scheme of the crosslinking of PVA-SA-CYS (1% *w/v*) with Mucin (1% *w/v*) in aqueous solution by the formation of the disulfide bond, and the inserted photo for the formation of hydrogel from the liquid solution of the PVA-SA-CYS and mucin [232].

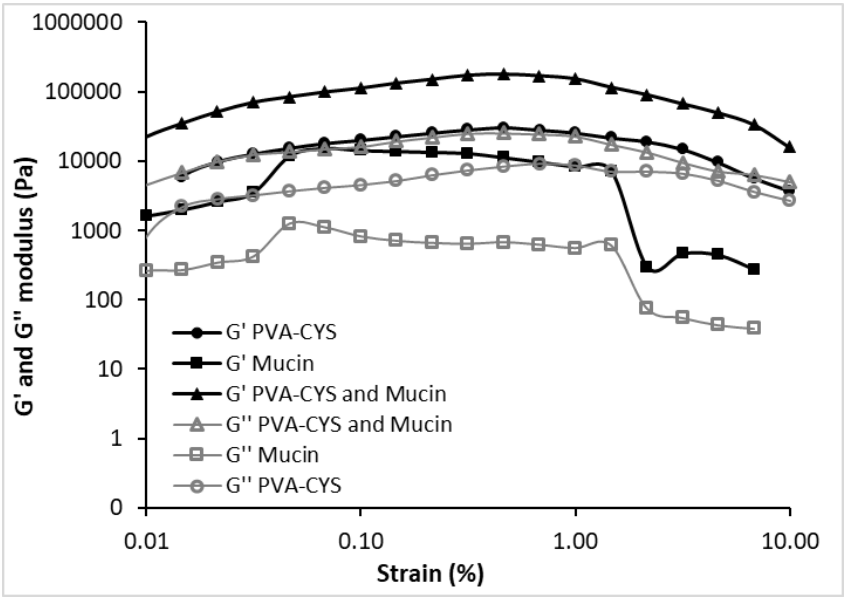

Figure A2. Storage modulus (G') and loss modulus (G") as a function of strain (%) for the PVA-CYS, mucin, and mixture [232].

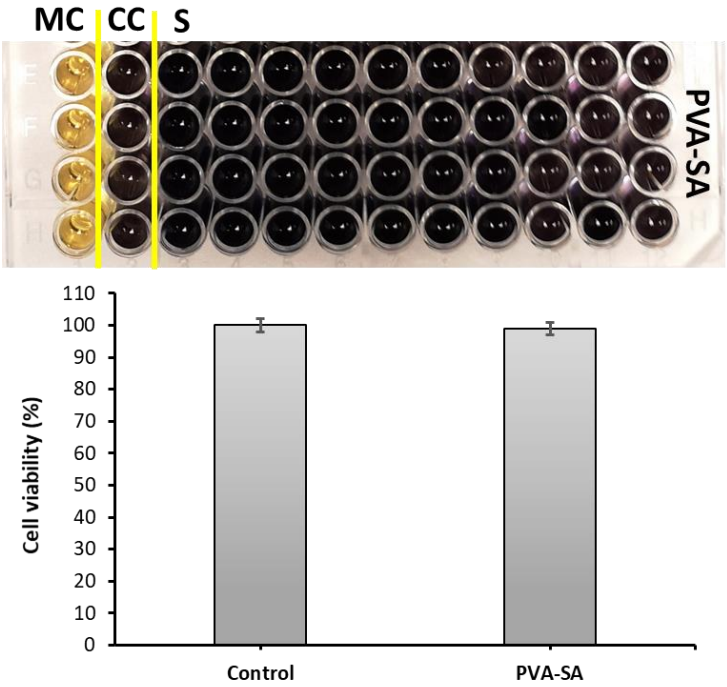

Figure A3. Biocompatibility of the PVA-SA with MRC-5 (human embryonic lung fibroblasts) cells, where MC is medium control, CC is cell control, and S is for PVA-SA sample.

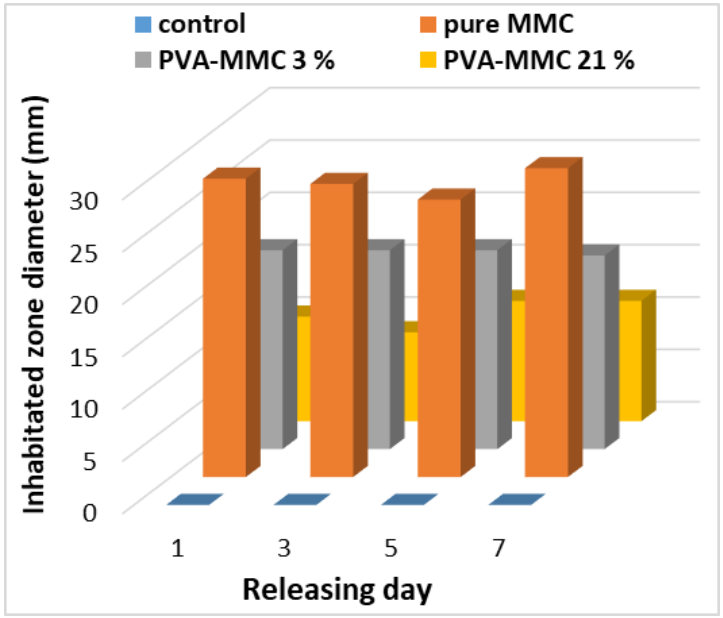

Figure A4. The obtained diameter values of the corresponding specific inhibition zone for 7 days of antibacterial effects of pure MMC and encapsulated forms on *Staphylococcus aureus* (MRSA) test bacteria [232].

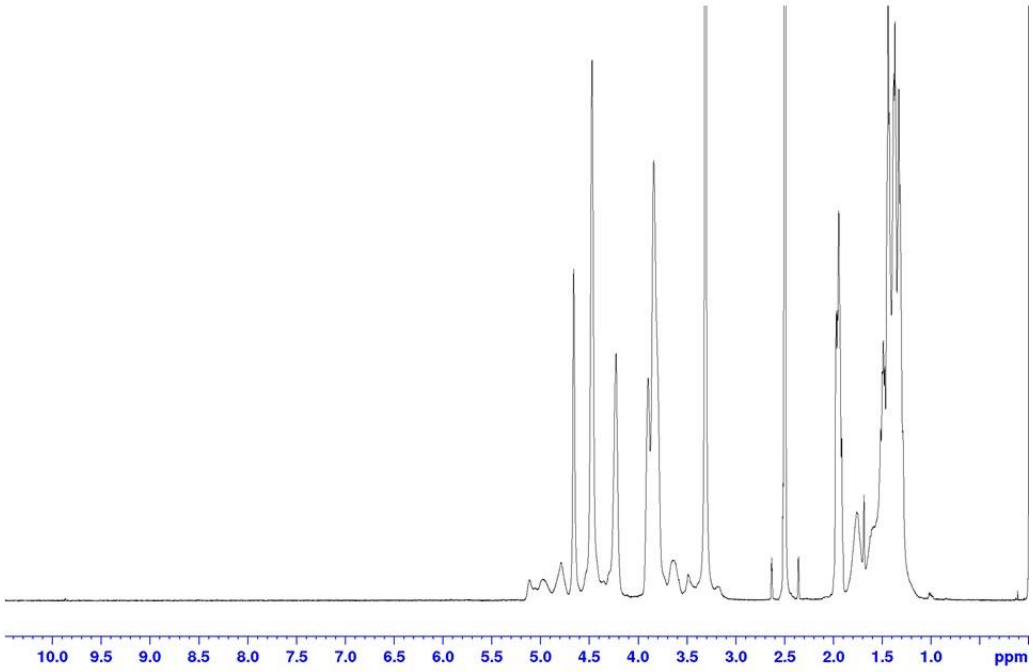

Figure A5. The ^{1}H-NMR spectrum of initial **PVA** [249].

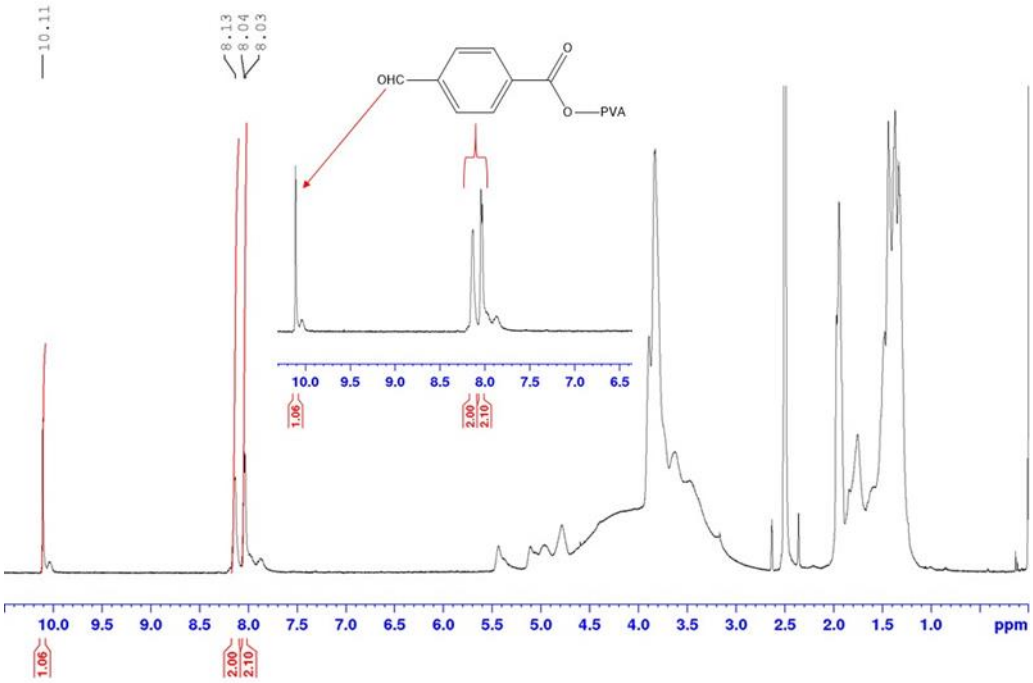

Figure A6. The ^{1}H-NMR spectrum of aldehyde-modified **PVA-CHO** polymer [249].

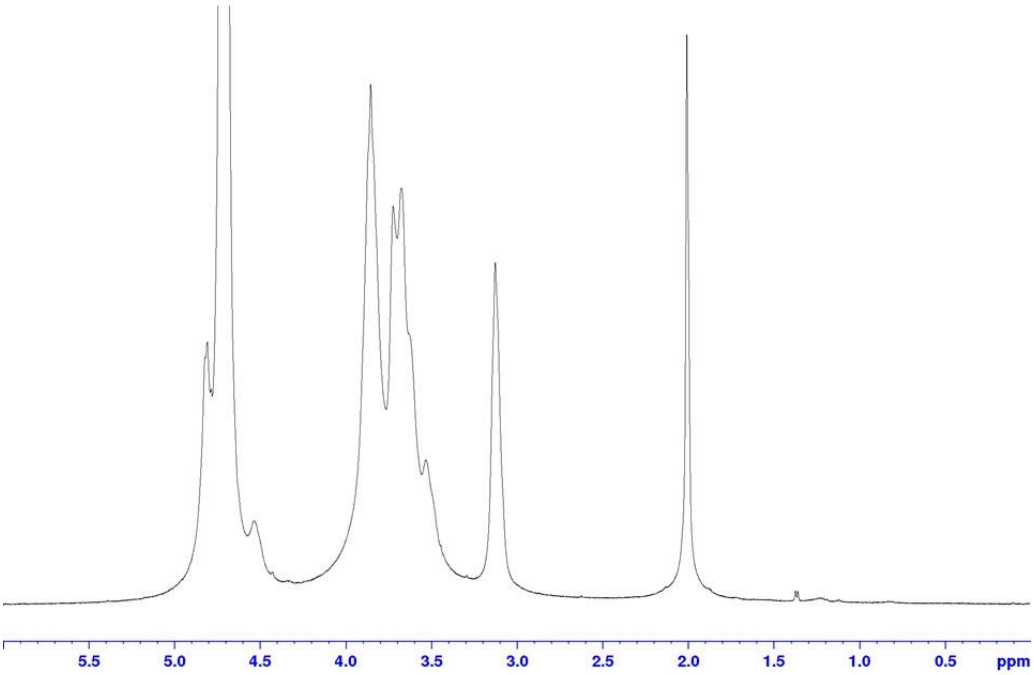

Figure A7. The ^{1}H-NMR spectrum of initial **Chitosan** [249].

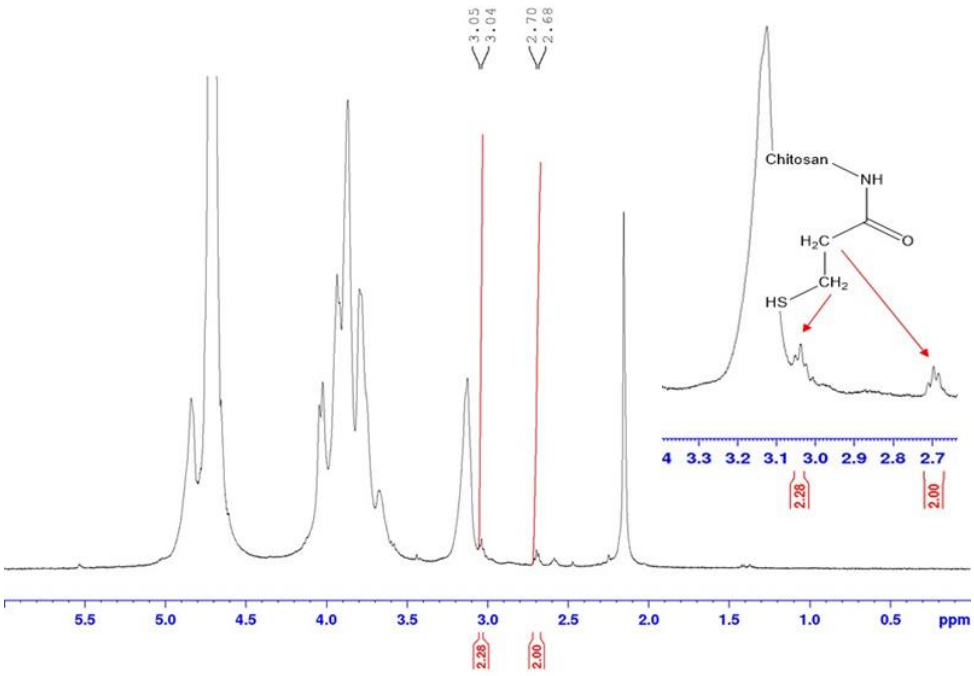

Figure A8. The ^{1}H-NMR spectrum of thiolated chitosan (**CHIT-SH**) [249].

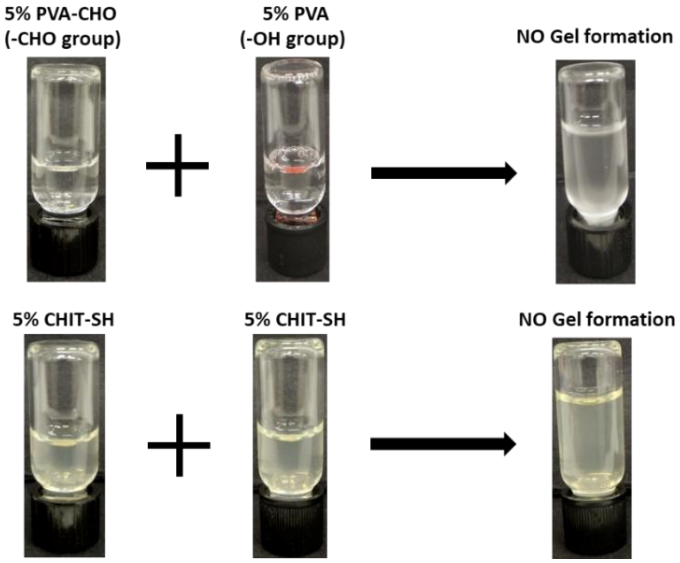

Figure A9. The possibility of bond formation in the hydrogel system; the upper part is the chance of the formation of an acetal bond between CHO of 5% *w/v* PVA-CHO and OH of 5% *w/v* PVA, down part is the formation of the disulfide bond between two SH of 5% *w/v* CH-SH solutions [249].

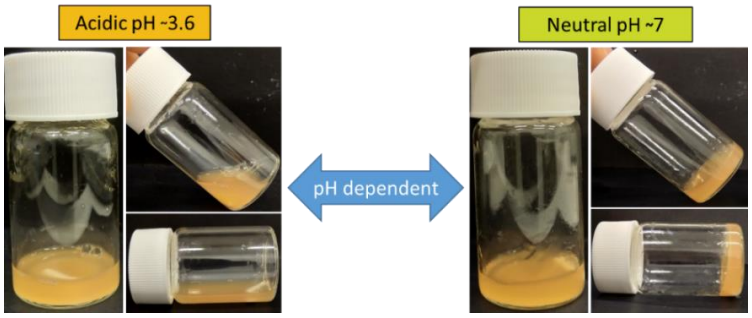

Figure A10. Photos of the PVA-CHIT-Tilorone pH-dependent hydrogel (2% *w/v* polymer concentration with 1.15 mg/mL Tilorone content) [249].

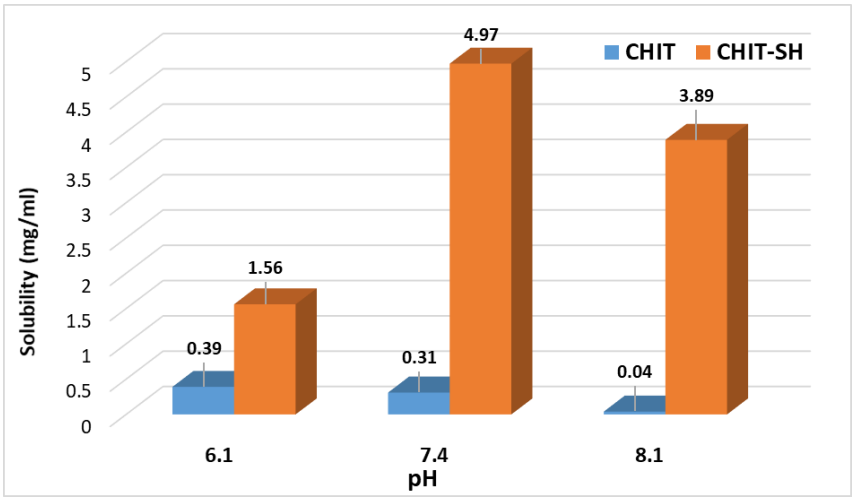

Figure A11. The solubility of initial and modified chitosan with 201.85 ± 12 μmol/g SH content in different pH buffer solutions [249].

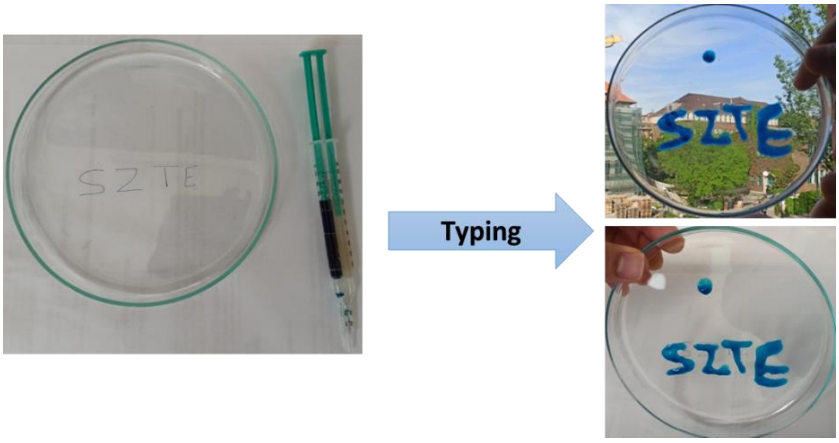

Figure A12. Photos of the static mixing tool between two solutions of PVA-CHO (2% *w/v*) and Chitosan-SH (2% *w/v*) to print the abbreviation name of the University of Szeged [249].

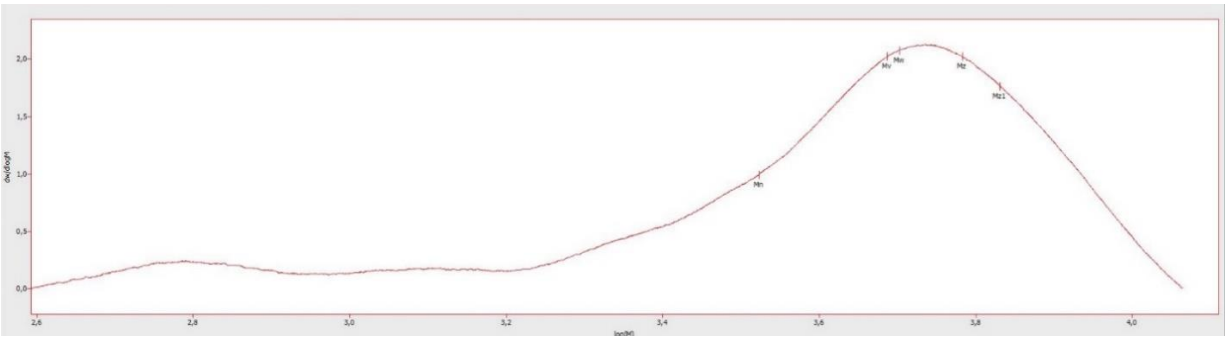

Figure A13. GPC molecular weight distribution curve obtained for polyester with 80 min polycondensation time [292].

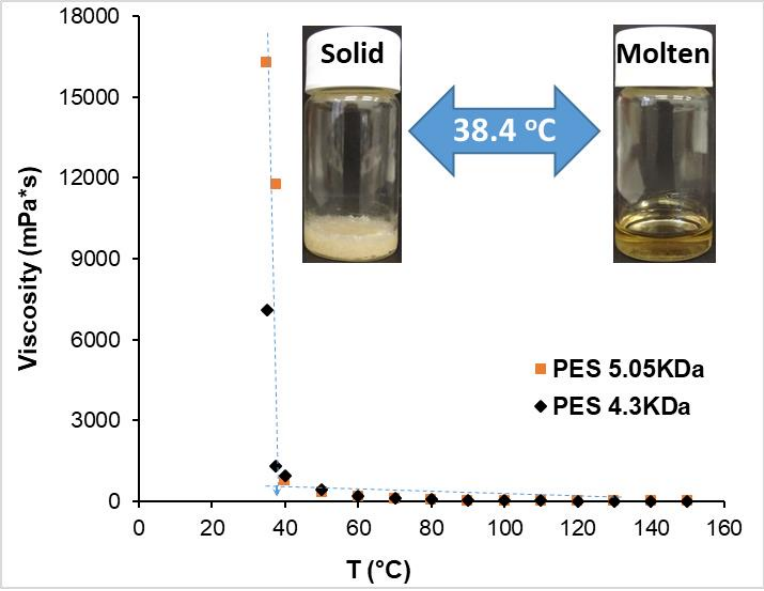

Figure A14. The effect of temperature on the viscosity of PES with two different M_w (5.05 and 4.3 KDa), the insert photos show the solid and molten phase of PES at liquefaction/ solidification temperature (38.4 °C) [292].

Acknowledgments

I would like to convey my sincere thanks to my supervisor, ***Dr. László Janovák*** for his fervent support and continual guidance as well as for helping to develop my skills in scientific research that helped me complete my doctoral studies. Without him, this work would not have been possible.

Also, I am grateful for the Doctoral School of Chemistry at Szeged University. I want to express my gratitude to the head of the Physical Chemistry and Materials Science Department, ***Prof. Ágota Tóth*** for her continuous assistance and support throughout my doctoral studies.

I also owe thanks to ***Dr. Ágota Deák*** for conducting TEM and rheology measurements, ***Dr. Diána Szabó*** for performing the biological measurements, ***Dr. Mária Budai-Szűcs*** for conducting the mucoadhesive measurements (using a TA.XT plus Texture Analyzer), ***Dr. Tamás Kiss*** for conducting Ellman method measurements, ***Dr. Bálint Lőrinczi*** for conducting NMR measurements, and ***Zsuzsanna Hőrits*** for conducting X-ray diffraction (XRD) measurements. I would like to thank all the co-authors of my published articles.

Many thanks to my research group members for their assistance at the beginning of my journey and for the friendly and innovative work environment. I would like to thank all of my friends here in Szeged.

I would like to thank all the members of the Chemistry Department, Faculty of Science, Zagazig University, Egypt.

I acknowledge a scholarship from the Egyptian Ministry of Higher Education and Scientific Research, and I sincerely appreciate the support I have gotten from Egypt's Office for Cultural and Educational Relations in Vienna. I also acknowledge a *Stipendium Hungaricum scholarship* from Tempus Public Foundation.

Finally, I would like to thank my family to whom I owe a great deal. To my brother and my sister for their support. I do not have enough words to express my gratitude to my wife for her constant support and encouragement during my studies. She is a great source of motivation for me. I would like to thank my daughters for inspiring me to give my all. And finally, the one person who has made this all possible has been my mother. She has been a constant source of support and encouragement. She is a great inspiration to me. Hence, great appreciation and enormous thanks are due to her. I thank you all.

Dedication

Dedicated to the memory of my father, Mahmoud, who passed away before I started my doctoral studies and always believed in my ability to be successful in the academic world. You are gone but your belief in me has made this journey possible.

Publications list

Hungarian Scientific Bibliography (MTMT) identifier: 10069798

Publications related to the scientific topic of the dissertation:

1. **Mohamed M. Abdelghafour**, Ágoston Orbán, Ágota Deák, Łukasz Lamch, Éva Frank, Roland Nagy, Adél Ádám, Pál Sipos, Eszter Farkas, Ferenc Bari, and László Janovák. The Effect of Molecular Weight on the Solubility Properties of Biocompatible Poly(ethylene succinate) Polyester. *Polymers*, **2021**, *13*(16), 2725.

   https://doi.org/10.3390/polym13162725 **IF= 4.967**

2. **Mohamed M. Abdelghafour**, Ágoston Orbán, Ágota Deák, Łukasz Lamch, Éva Frank, Roland Nagy, Szilveszter Ziegenheim, Pál Sipos, Eszter Farkas, Ferenc Bari, László Janovák. Biocompatible Poly(ethylene succinate) Polyester with Molecular Weight Dependent Drug Release Properties. *International Journal of Pharmaceutics*, **2022**, *618*, 121653.

   https://doi.org/10.1016/j.ijpharm.2022.121653 **IF= 6.510**

3. **Mohamed M. Abdelghafour**, Ágota Deák, Diána Szabó, Imre Dékány, László Rovó, László Janovák. Use of Self-Assembled Colloidal Prodrug Nanoparticles for Controlled Drug Delivery of Anticancer, Antifibrotic and Antibacterial Mitomycin. *International Journal of Molecular Sciences*, **2022**, *23*, 6807.

   https://doi.org/10.3390/ijms23126807 **IF= 6.208**

4. **Mohamed M. Abdelghafour**, Ágota Deák, Tamás Kiss, Mária Budai-Szűcs, Gábor Katona, Rita Ambrus, Bálint Lőrinczi, Anikó Keller-Pintér, István Szatmári, Diána Szabó, László Rovó, László Janovák. Self-Assembling Injectable Hydrogel for Controlled Drug Delivery of Antimuscular Atrophy Drug Tilorone. *Pharmaceutics*, **2022**,*14(12)*,2723.

   https://doi.org/10.3390/pharmaceutics14122723 **IF= 6.525**

5. László Janovák, László Rovó, Diána Szabó, Imre Dékány, **Mohamed M. Abdelghafour** "Self-ssembled mucoadhesive biopolymer particle release system and preparation method therefor" Filing year (**patent**): **2021**, Filing number: 2130766, Case number: P2100345

Related publications to dissertation: ∑ IF = 24.21

Other publications not related to the scientific topic of the dissertation:

1. László Janovák, Árpád Turcsányi, Éva Bozó, Ágota Deák, László Mérai, Dániel Sebők, Ádám Juhász, Edit Csapó, **Mohamed M. Abdelghafour**, Eszter Farkas, Imre Dékány, Ferenc Bari. Preparation of novel tissue acidosis-responsive chitosan drug nanoparticles: Characterization and in vitro release properties of Ca^{2+} channel blocker nimodipine drug molecules. *European Journal of Pharmaceutical Sciences*, **2018**, *123*, 79-88.

   https://doi.org/10.1016/j.ejps.2018.07.031 **IF= 3.532**

2. **Mohamed M. Abdelghafour**, Ágota Deák, László Mérai, Áron Ágoston, Rita Bélteki, Daniel Sebok, Imre Dekany, Laszlo Janovak. Photocatalytic elimination of interfacial water pollutants by floatable photoreactive composite nanoparticles. *Environmental Pollution*, **2020**, *266*, 115285.

   https://doi.org/10.1016/j.envpol.2020.115285 **IF= 8.071**

3. Tamás Takács, **Mohamed M. Abdelghafour**, Ágota Deák, Diána Szabó, Imre Dékány, László Rovó, Ákos Kukovecz, László Janovák. Prolonged release of antifibrotic mitomycin-C drug from superhydrophobic biopolymer thin films. *European Polymer Journal*, **2020**, *139*, 109995.

   https://doi.org/10.1016/j.eurpolymj.2020.109995 **IF= 4.598**

4. Tamás Takács, **Mohamed M. Abdelghafour**, Łukasz Lamch, Imre Szenti, Dániel Sebők, László Janovák, Ákos Kukovecz, Facile modification of hydroxyl group containing macromolecules provides autonomously self-healing polymers through the formation of dynamic Schiff base linkages. *European Polymer Journal*, **2022**, *168*, 111086.

   https://doi.org/10.1016/j.eurpolymj.2022.111086 **IF= 5.546**

5. Tamás Kiss, Rita Ambrus, **Mohamed M. Abdelghafour**, Scarlett Zeiringer, Atiđa Selmani, Eva Roblegg, Mária Budai-Szűcs, László Janovák, Bálint Lőrinczi, Ágota Deák, Andreas Bernkop-Schnürch, Gábor Katona. Preparation and detailed characterization of the thiomer chitosan–cysteine as a suitable mucoadhesive excipient for nasal powders. *International Journal of Pharmaceutics*, **2022**, *626*,122188.

   https://doi.org/10.1016/j.ijpharm.2022.122188 **IF= 6.510**

6. László Mérai, Ágota Deák, Mohamed A. Harech, **Mohamed M. Abdelghafour**, Dániel Sebők, Áron Ágoston, Szabolcs P. Tallósy, Tamás Szabó, Younes Abouliatim, Mohamed Mesnaoui, Lahbib Nibou, Ákos Kukovecz, László Janovák. Antimicrobial ceramic foam composite air filter prepared from Moroccan red clay, phosphate sludge waste and biopolymer. *Applied Clay Science*, **2022**, *230*, 106703.

   https://doi.org/10.1016/j.clay.2022.106703 **IF= 5.907**

Other publications: ∑ IF = 34.164

All publications: ∑ IF = 58.374

Book Chapter:

Mohamed M. Abdelghafour, Ágota Deák, László Mérai, László Janovák (**2022**). Photoreactive Composite Coatings with Tunable Surface Wetting Properties and Their Application Possibilities. In: Garg, S., Chandra, A. (eds.) *Green Photocatalytic Semiconductors. Green Chemistry and Sustainable Technology*. Springer, Cham.

https://doi.org/10.1007/978-3-030-77371-7_8

Conference lectures and posters related to the dissertation:

Poster:

Mohamed M. Abdelghafour, Diána Szabó, László Rovó, Imre Dékány, László Janovák "*Modified polyvinyl alcohol as versatile prodrug provides self-assembled nanoparticles and hydrogel for biomedical applications*" at Max Bergmann Symposium, on June 9-10, 2022, in Dresden, Germany.

Lecture:

Mohamed M. Abdelghafour, Tamás Takács, Ágota Deák, Diána Szabó, László Rovó, László Janovák "*Preparation of mucoadhesive biopolymer microparticles suitable for the encapsulation and surface immobilization of anticancer agents*" at the EUGLOH Annual Student Research Conference (Global Health Challenges: Diseases of Modern Life), on September 28 – 30, **2020**, Online.

Mohamed M. Abdelghafour, Ágoston Orbán, Ágota Deák, Łukasz Lamch, Eszter Farkas, Ferenc Bari, László Janovák "*Biocompatible and biodegradable aliphatic polyester for drug delivery application*" XLIV. Chemistry Lectures - an international conference for young professionals, on October 26-28, **2021**, in Szeged, Hungary.

Mohamed M. Abdelghafour, Ágota Deák, Tamás Kiss, Mária Budai-Szűcs, Gábor Katona, Rita Ambrus, Anikó Keller-Pintér, Diána Szabó, László Rovó, László Janovák "*Intelligent self-assemble injectable hydrogel as a drug delivery system*" XLV. Chemistry Lectures, Hungarian Chemical Society–Group of Csongrád County, on October 25–27, **2022**, in Szeged, Hungary.

Other conference lectures and posters not related to the dissertation:

Poster:

László Mérai, Ágota Deák, **Mohamed Mahmoud Abdelghafour**, László Janovák, Imre Dékány, Dániel Sebők "*Degradation of organic pollutants by the help of intelligent photoreactive surfaces"* at the EUGLOH Annual Student Research Conference (Global Health Challenges: Diseases of Modern Life) on September 28 – 30, 2020, Online.

László Mérai, **Mohamed M. Abdelghafour**, Ágota Deák, Imre Dékány, László Janovák, *"Stimulus-responsive composite surfaces with magneto- and thermoresponsive wetting characteristics and visible light photoreactivity"* at 11th European Conference on Solar Chemistry and Photocatalysis: Environmental Applications (SPEA), on June 6–10, 2022, in Turin, Italy.

Lecture:

László Janovák, Ágota Deák, László Mérai, **Mohamed M. Abdelghafour**, Imre Dékány "*Functional surfaces with designed wetting and photocatalytic properties*" The 5th International Conference on New Photocatalytic Materials for Environment, Energy and Sustainability (NPM-5) & The 6th International Conference on Photocatalytic and Advanced Oxidation Technologies for the Treatment of Water, Air, Soil and Surfaces (PAOT-6) Szeged, **2021**.05.24.

László Mérai, Ágota Deák, **Mohamed M. Abdelghafour**, Dániel Sebők, Imre Dékány, László Janovák "*Application of photocatalytic filler materials for the preparation of functional composites with designed properties*" The 5th International Conference on New Photocatalytic Materials for Environment, Energy and Sustainability (NPM-5) & The 6th International Conference on Photocatalytic and Advanced Oxidation Technologies for the Treatment of Water, Air, Soil and Surfaces (PAOT-6) Szeged, **2021**.05.24.

Takács Tamás, **Mohamed M. Abdelghafour**, Łukasz Grzegorz Lamch, Szenti Imre, Sebők Dániel, Janovák László, Kukovecz Ákos "*Dinamikus Schiff-bázis kötéseken alapuló, öngyógyító tulajdonságokkal rendelkező polivinil-alkohol*" XLIV. Chemistry Lectures - an international conference for young professionals. October 26–28, **2021**, Szeged.

Tamás Kiss, Rita Ambrus, **Mohamed M. Abdelghafour**, László Janovák, Mária Budai-Szűcs, Ágota Deák, Gábor Katona "*Synthesis and investigation of a mucoadhesive chitosan derivative for intranasal drug delivery".* In: IV. Symposium of Young Researchers on Pharmaceutical Technology, Biotechnology and Regulatory Science, January 19–21, **2022**, Szeged, Hungary.

Tamás Kiss, Rita Ambrus, **Mohamed M. Abdelghafour**, László Janovák, Mária Budai-Szűcs, Ágota Deák, Gábor Katona "*Formulation of levodopa methyl ester containing nasal powder using chitosan-cysteine mucoadhesive thiomer as excipient*" xxv. Spring Wind Conference, May 6–8, **2022**, Pécs, Hungary.